Universidade de Aveiro
2022

Ana Rita Cardoso de Bessa

Macroestruturas à base de grafeno para o tratamento de água contaminada: otimização para uma reutilização mais eficiente da água

Graphene-based macrostructures for the treatment of contaminated water: optimization for a more efficient water reuse

Universidade de Aveiro
2022

Ana Rita Cardoso de Bessa

Macroestruturas à base de grafeno para o tratamento de água contaminada: otimização para uma reutilização mais eficiente da água

Tese apresentada à Universidade de Aveiro para cumprimento dos requisitos necessários à obtenção do grau de Doutor em Nanociências e Nanotecnologia, realizada sob a orientação científica da Doutora Paula Alexandrina de Aguiar Pereira Marques, Investigadora Principal do Departamento Engenharia Mecânica da Universidade de Aveiro e da Professora Eduarda da Cunha Pereira, Professora Associada do Departamento de Química da Universidade de Aveiro

Apoio financeiro da FCT (SFRH/BD/110478/2015)

o júri

Presidente

Doutor João Carlos de Oliveira Matias
Professor Catedrático Universidade de Aveiro

Vogais:

Doutor Tito da Silva Trindade
Professor Catedrático, Universidade de Aveiro

Doutora Cristina Maria Fernandes Delerue Alvim de Matos
Professora Coordenadora Principal, Instituto Superior de Engenharia do Porto

Doutora Paula Alexandrina de Aguiar Pereira Marques (orientadora)
Investigadora Principal, Universidade de Aveiro

Doutora Begoña Espiña Barbeitos
Investigadora Principal, International Iberian Nanotechnology Laboratory (INL)

Doutor Nuno Carlos Lapa dos Santos Nunes
professor auxiliar da Universidade Nova de Lisboa

agradecimentos

I thank Portuguese Science Foundation, I.P., (FCT) for: Ana Bessa PhD grant SFRH/BD/110478/2015. Thanks, are also due for the financial support to the H_2O Value project (PTDC/NAN-MAT/30513/2017) also supported by FCT/MEC through national funds, and the co-funding by the FEDER, within the PT2020 Partnership agreement and Compete 2020 (CENTRO-01-0145-FEDER-030513).

The financial support to TEMA (UIDB/00481/2020 and UIDP/00481/2020), to REQUIMTE (UIDB/50006/2020) and to CESAM (UIDB/50017/2020 and UIDP/50017/2020) is also acknowledge, as well as to CENTRO-01-0145-FEDER-022083.

palavras-chave Tratamento de água, estruturas grafeno, sorção, mercúrio

resumo

Atualmente a contaminação da água é um problema ambiental de impacto crescente em diversos locais do mundo. A água é um recurso finito e a sua contaminação provém tanto de fontes naturais, como da atividade humana. Nos organismos aquáticos, a ação tóxica de contaminantes tais como os metais vestigiais, pode causar a morte das espécies e/ou efeitos bioquímicos nefastos. Os métodos mais tradicionais utilizados no tratamento da água apresentam baixa eficiência na remoção dos metais potencialmente tóxicos, podendo gerar resíduos tóxicos e são métodos dispendiosos. Torna-se assim necessário desenvolver novas tecnologias com custos mais reduzidos, com capacidade regenerativa, com maior eficiência e que não gerem substâncias perigosas. O objetivo deste trabalho é avaliar a remoção de mercúrio da água através da sua sorção em estruturas tridimensionais de grafeno. As estruturas tridimensionais de grafeno utilizadas neste trabalho consistiram em aerogéis de óxido de grafeno funcionalizadas com polietilenoimina (GOPEI) ou quitosano (GOCH). Estas estruturas foram usadas de forma a avaliar a sua eficiência na sorção de mercúrio. Todos estes materiais apresentaram uma excelente performance na remoção de mercúrio em água ultrapura. Em águas reais, o aerogel GOPEI foi o que se apresentou como o mais promissor na remoção deste elemento, tendo sido demonstrada a seletividade deste último para o mercúrio em água mineral usada para consumo humano e na água do mar natural e sintética, contaminadas com mercúrio.

keywords Water treatment, graphene structures, sorption, mercury

abstract

Currently, water contamination is an environmental problem that has high impact in several places of the world. Water is a finite resource, and its contamination comes from both natural sources and human activity. In aquatic organisms, the toxic action of trace metals can cause the death of species and/or harmful biochemical effects. Traditional methods used in water treatment have low efficiency in the removal of these metals, generate toxic residues and are expensive methods. It is therefore necessary to develop new technologies, which with reduced costs and regenerative capacity, have high capacity to remove the toxic metals and do not generate hazardous substances. The objective of this work is to evaluate the removal of mercury through its sorption by three-dimensional graphene structures. The three-dimensional graphene structures used in this work consisted of graphene oxide aerogels functionalized with polyethylene (GOPEI) or chitosan (GOCH). These structures were evaluated in relation with their efficiency in the removal of mercury. All these materials presented excellent performance in the removal of mercury in ultra-pure water. In real waters, the GOPEI aerogel was the one that presented the most promising results in the removal of mercury, and the selectivity of the latter for mercury was demonstrated in mineral water intended for human consumption and in natural and synthetic seawater contaminated with mercury.

Table of Contents

List of Figures

List of Tables

List of abbreviations

3DGON	3DGO with functional nitrogen groups
ATR-FTIR	Attenuated Total Reflectance Fourier Transform Infrared
BET	Brunauer Emmett Teller method
CH	Chitosan
CMA	Maximum permissible concentration
CV-AFS	Cold vapour atomic fluorescence spectroscopy
CVD	Chemical vapor deposition
EQF	Environmental quality standards
GBM	Graphene based materials
GO	Graphene oxide (não estão pela ordem aparece no texto)
GOCH	Graphene oxide aerogels functionalized with chitosan
GOPEI	Graphene oxide aerogels functionalized with polyethyleneimine
Hg	Mercury
LECO© AMA-254	Thermal decomposition atomic absorption spectrometry with gold amalgamation
MA	Average annual value
NQA	Environmental quality standards
PECVD	Plasma-reinforced CVD
PEI	polyethyleneimine
PFO	Pseudo-first order
PSO	Pseudo-second order
PTEs	Potential toxic elements
VLE	Emission limit value
VMA	Maximum permissible value
VMR	Maximum recommended value
XPS	X-ray photoelectron spectroscopy
WHO	World Health Organization

Chapter 1

1. Introduction

The present chapter starts by introducing the motivation and scope of the present work. After, some of the key concepts related to the work performed in this Thesis, together with the state of the art on graphene-based composites for potential toxic trace metals removal from water is presented.
At the end of this chapter is an outline of the chapters and their contents briefly explained.

1.1 Motivation and scope

The global awareness for the long-term human health effects and environmental impacts of metal contamination in water has long been known. The European Parliament revised the environmental quality standards for existing priority substances and stated that these should be considered for the first time in river basin management plans covering the period 2015 to 2021. In this list, cadmium and mercury have been classified as priority hazardous substances with the end of discharges, release and losses by 2020 and lead discharges subject to prior approval with defined limits. Other potentially toxic elements (PTEs) such as arsenic, chromium, lead and nickel have also their strict discharge limits. In the same Directive, it is mentioned that the wastewater treatment can be very costly. In order to facilitate cheaper and more cost-effective treatment, the development of innovative water treatment technologies should be stimulated. Therefore, there is an urgent need to develop alternative robust and cost-effective technologies with higher efficiency.

The booming of nanotechnology and amazing breakthroughs in research on graphene-based materials (GBM) have provided great promise for environmental remediation. Graphene was first isolated and characterised in 2004. It comprises a single layer of carbon atoms arranged in a hexagonal lattice. It was assigned as one of the most promising materials in future due to its extraordinary tensile strength and electrical conductivity. But it has been difficult to produce large quantities of single-layer graphene using existing methods which are also quite costly. This challenge has been overcome by using graphene oxide (GO) which can be produced by graphite exfoliation in laboratory. It

can be composed on a substrate or porous material and can be used as a membrane. Different GBM have been developed for water desalination, sorption and degradation of organic contaminants and the removal of metal ions from polluted waters, as will be reviewed in this Chapter.

Most of the sorption studies of trace metals applying sorbent materials described in literature were done in deionized/distilled water and not in real waters being in most of the cases with only a contaminant, with concentrations that do not correspond to those found in nature. The main objective of this Thesis, was to study the removal of potential toxic trace metals in real waters through GBM, prepared by simple and inexpensive methods and using contaminants at realist concentrations.

1.2 Water contamination problematics

Although earth's crust is mostly covered by water, its salinity makes it unfeasible for human consumption. Also, water distribution is not uniform, which causes several regions to suffer from scarcity of this resource. The rapid population growth in recent decades combined with exponential industrial development and higher urbanization has put a high pressure on obtaining this essential resource. The need for drinking water has increased considerably, while daily contamination leads to its deterioration and, consequently, to a decrease in its availability [1]. It is estimated according to the United Nations that more than 2.7 billion people are expected to suffer from water shortages by 2025 if the planet's consumption does not decrease. This could cause conflicts between nations in the future if the problems of scarcity are not solved. In addition, water is a vital resource for the irrigation of fields, electricity production and other industrial activities that have been increasing annually due to the rapid growth of the world population. Another factor to be taken into account is industrialization and its impact on water quality. The discharge of industrial waste is the main source of water contamination with trace metals and metalloids. Some production processes, including the metallurgical, paint, porcelain and plastics industries, among others, use these potentially toxic elements (PTEs) and ingestion of contaminated water or fish, can lead to serious problems such as nervous system dysfunction and increased incidence of cancer. In aquatic organisms, the toxic action of PTEs can cause the death of species or bioaccumulation, which potentiates the harmful effect of substances through food chains. Water is thus considered a primary

resource for life and necessary for many anthropogenic activities, and so the requalification of water becomes central to sustainability on the planet.

Potentially toxic trace metals can be introduced into aquatic ecosystems in a natural or artificial way. Naturally, through atmospheric entry and rain, releasing them and transporting them from the mother rock or other compartments of the soil where they are present. Artificially, by anthropogenic sources: sewage from urban areas, industrial effluents, agricultural activities and flow rates from mining. Agriculture is also another important anthropogenic source of trace metal for in water bodies. In addition, trace metals released into the soil from this activity are transported to rivers by the flow of surface rainwater, persisting in the aquatic environment because they are in free or ionic form, which facilitates their accumulation in biological tissues mainly in fish.

Trace metals have high chemical reactivity and are bioaccumulative, which means that the body is unable to eliminate them quickly and effectively. Lead, mercury, and cadmium are metals that do not naturally exist in any organism and do not perform nutritional or biochemical functions in microorganisms, plants or animals. For this reason, the presence of these trace metals in living organisms is detrimental in any concentration. Human intake of animals, especially fish, presents an increased risk of contamination, as they are more likely to accumulate harmful products throughout their lives compared to plant products under the same conditions. The usual consumption of water and food - such as fresh water or seafish - contaminated with trace metals endangers health.

1.3 Mercury in the environment

Given the risk that mercury pose to the environment and human health, given their toxicity and carcinogenic potential, in recent years there has been a growing interest in the study of the removal of this element from contaminated water [4]. Mercury is a liquid metal and odorless at room temperature, but when the temperature rises it turns into toxic vapors. This metal has been used in industry and medicine for centuries. This metal may also be present in the form of Hg (I) and Hg (II), which are also toxic. Elemental mercury Hg (0) is characterized by being low water soluble, but very volatile. Along a trophic chain, the increase in the concentration of total mercury also corresponds to the increase of mercury in its organic form, with organic mercury compounds being the most toxic

compared to other compounds formed by this element. Small amounts can cause damage to neurological development as well as damage to the cardiovascular, immune, and reproductive system, and deaths can occur. The exposure of the population to mercury can arise from organic forms of this material: methylmercury (CH_3Hg^+) and ethylmercury ($CH_3CH_2Hg^{+)}$. These compounds can come from the consumption of contaminated fish, dental amalgams, and some vaccines. Contaminated fish are the largest source of methylmercury. The biogeochemical cycle of mercury involves four agents that are connected to each other: atmospheric, terrestrial, aquatic, and biotic. In the terrestrial environment, Hg (II) is associated with soil organic matter. Mercury can be released from natural sources such as volcanic eruptions. It may also originate from human activity, such as gold extraction (South America, Africa, and Asia), mercury mining (Europe and South America) and industrial processes such as the production of caustic soda (Europe, Asia, and North America). Most Hg enters aquatic systems in their inorganic form through anthropogenic discharges, mostly related to chloral-alkaline plants, mining activities or through diffuse sources. Despite the existing restrictions on anthropogenic sources of Hg, historically contaminated sediments can still constitute a source of Hg for the aquatic environment and, consequently, for the biota.

Through the above description it is possible to conclude that it is really necessary to protect the environment and humans from the adverse effects of mercury contamination. In this sense, the world's government institutions have set maximum limits for its level in aquatic systems, as well as for effluent discharges. Also, the scarcity of drinking water is considered one of the biggest problems that humanity will face in the future. Consequently, limits have been set for the discharge of contaminants into the environment and the Europe has identified substances that pose a significant risk, taking into account their human exposure, the amount of effluents discharged and their toxicity (Directive 2000/60/EC). Directive 2008/105/EC established environmental quality standards in the field of water policy (EQF), which aims to control pollution by establishing maximum levels of concentration of certain substances in bodies of water, with a view to protecting human health and the environment.

Hg and Cd have been labelled by the European Union as "hazardous substances" and their emissions should be phased out by 2021 - Decision No 2455/2001/EC of 20 November 2001 of the European Parliament [7]. The limit values for concentrations of

mercury in industrial effluents, irrigation waters and human consumption in accordance with Decree-Law No 236/98 and Directive 2013/39/EU are set out in Table 1.

Table 1 Limit values for mercury concentrations (mg L^{-1}) in accordance with Decree-Law No 236/98 and Directive 2013/39 /EU.

Industrial discharge (mg L^{-1})	**Irrigation (mg L^{-1})**		**Human consumption (mg L^{-1})**	
VLE	VMR	VMA	VMR	VMA
0.05	0.5	2.0	0.0005	0.001

VLE - Emission limit value; VMA - Maximum permissible value; VMR - Maximum recommended value

The limit values for concentrations of mercury in surface waters in accordance with Decree-Law No. 236/98 and environmental quality standards for fresh surface waters and other surface waters, according to Decree-Law No. 218/2015, are presented in Table 2.

Table 2 Limit values for mercury concentrations in surface waters (Decree-Law No. 236/98) and environmental quality standards in accordance with Decree-Law No. 218/2015 for surface fresh water and other surface waters.

Surface waters (µg L^{-1})	**NQA-MA (µg L^{-1}) Surface freshwater**	**NQA-MA (µg L^{-1}) other surface water**	**NQA-CMA (µg L^{-1}) Surface fresh water**	**NQA-CMA (µg L^{-1}) other surface water**
1	0.05	0.05	0.07	0.07

NQA - Environmental quality standards; MA - Average annual value; CMA - Maximum permissible concentration

1.4 Conventional technologies for the removal of potentially toxic trace metals from water

Examples of methods used in removing contaminants from water are precipitation, oxidation-reduction and membrane filtration [8]. The main limitations of these technologies are the generation of secondary waste, its complexity, high cost or inefficiency when contaminants are in low concentration (ppt-ppb), which highlight the need to develop alternative technologies [9].

Sorption is one of the most popular water treatment process, due to its simplicity and efficiency [10] and activated charcoal sorbent is the most relevant one from an

industrial point of view [11]. However, its production cost is high and it cannot be regenerated [12]. The need to treat water contaminated with PTEs remains a major challenge, as a material has not yet been developed that allows rapid sorption and contaminant removal. The main limitations are due to the difficulty in developing a material with high levels of sorbent sites, synthesized without complex chemical processes, easy to implement industrially and at low cost.

Table 3 describes the most common methodologies used for water treatment.

Table 3 Methods for removing potentially toxic elements from waters.

method		description	Advantages	Disadvantages
Chemical precipitation		Formation of insoluble precipitates (reagents + PTES), which can be separated from water by filtration or decanting.	- Simple and inexpensive process - Removal of most metals	- Elimination problems - Waste generation
Membrane filtration	ultrafiltration	- Technique that removes small impurities dissolved or suspended in water using low transmembrane pressures.	- Removes all organic molecules (< 99 %) - Removes viruses and particles - There is no risk of fouling and limited risk of obstruction - Low water and energy consumption	- Almost no removal of low molecular weight ions, gases and organics.
	reverse osmosis	- Use of a semipermeable membrane in which particles circulate from the fluid of highest concentration to the lowest concentration.	- Removes contaminants (ions, bacteria, viruses, particles, colloids, organics). -Low electricity consumption; - Minimal maintenance	- Contaminants are not sufficiently removed to meet type II water requirements; - Membranes can be encrusted and clogged; - High water consumption
	Nanofiltration	- Process equal to ultrafiltration with pores with a nano scale.	- High quality water production -Simplicity of operation and range of use	- Process similar to ultrafiltration, using membranes containing thicker pores than in reverse osmosis and smaller (nano scale) than in ultrafiltration.
Coagulation and flocculation		- Very small particles are aggregated forming flakes so that they can decant.	- Simple and inexpensive process - Stabilization of slands	-High chemical consumption of products
Electrochemical methods		- Use of electrodes capable of altering the toxicity of a chemical species	- Versatility, simplicity of operation, environmentally benign	- High costs and dependence on initial pH and density
Activated carbon sorction		- Large pore surface where potentially toxic elements are adsorbed	- Many metals are removed -High efficiency	- No regeneration -Increase in the price of activated carbon -Efficiency depends on the quality of activated carbon

Other materials used in sorption studies, which were not mentioned in the table above, are biosorbents, which consist of industrial and/or agricultural biological matrix residues, based on live or dead biomass. As examples, we have residues of algae, plants, bacteria, fungi, or the food industry, such as food restored with rice (banana husk). The main advantage of the use of biosorbents is their relative abundance, high number of functional groups, natural origin, and are often considered waste, so biomaterials are not

very expensive. However, the use of biosorbents has as main disadvantage the low sorption capacity when compared to activated carbon.

Recently, much work has been done to investigate the synthesis of 3D graphene macroscopic structures, in general by stacking single graphene oxide (GO) nanosheets, with or without the incorporation of different additives. These different architectures are being explored for water purification, showing very promisors results.

1.5 Sorption process

Sorption process is considered an economical and effective method for removing trace metals from water. The main advantages of sorption, is that it can be applied to a wide variety of contaminants, has a high sorption capacity with fast kinetics and it is a potentially selective process depending on the sorbent. Another advantage of the sorption process is that through it is possible to produce treated water with characteristics suitable for reuse, free of color and odor. The sorption process is also characterized by being sometimes reversible process, being possible to regenerate the sorbent, thus this process is economically viable. For these reasons, the sorption process has become one of the most popular methods for water treatment. The process consists of transferring one or more solutes (sorbate) from a fluid (gas or liquid) to the surface of a solid (sorbent). Interactions that occur between the solute and the solvent result from the existence of attractive unbalanced forces on the sorbent surface. Sorption is also considered a superficial phenomenon, thus being directly linked to the total surface of the sorbent, and the larger the surface, the greater the sorption efficiency. This is the main reason why sorbents with high porosity and surface area are most used in the sorption process. Thus, sorption depends on the size of the pores, their distribution, and the nature of the sorbent surface.

There are two types of sorption: physical sorption (physisorption) and chemical sorption (chemisorption). Physical sorption involves van der Walls bonds, while chemical sorption involves the formation of chemical bonds between sorbate and sorbent. Physisorption is a reversible process in which the sorbed substance remains on the surface of the sorbent and can form molecular layers, where the sorption force decreases as the number of layers increases and there is no chemical change in the sorbed material. On the other hand, in chemical sorption or chemisorption, in which there are chemical bonds between the sorbate and the sorbent surface, leading to the formation of a monolayer of

sorbed molecules, the process is often irreversible. The sorbate-sorbent interaction forces are higher when compared to the forces observed in physical sorption.

Regardless of the type of sorption process, this is characteristic by being a phenomenon of balance, being influenced by several factors. The sorption process is influenced by temperature, sorbent nature, pH of the solution, size of the pores of the sorbent, nature of the solution, contact time between the sorbent and sorbate and by the competition generated between ions present in real waters which compete for the places of binding of the sorbent. The properties of the sorbate that influence sorption are the size of contaminant species and their concentration. With regard to the size of contaminant species, it should not be larger than the size of sorbent pores, since large molecules cause their inactivation, as they decrease the useful energy of sorption. With regard to sorbate concentration, sorption may happen to a greater or lesser extent. It is observed that, at low initial concentrations of sorbate, the removal is higher compared to the high concentrations of sorbate, since at high concentrations of sorbate, the number of sites available in sorbent is limited and once the sorbent is saturated and there is no possibility of greater sorption of the same, even if the amount of sorbate is increased [14,15]. Most studies use high initial concentrations of sorbates, in the order of mg L^{-1}, which is higher when compared to their concentrations in aquatic environment.

In turn, the characteristics of the sorbent that influence sorption are the surface area, porosity, the specific volume of pores, as well as their chemical nature. With regard to the surface area and concentration, the larger the surface area, there will be more places available to favor interaction with sorbate and the larger area of contact with the solution there will be an increase in the sorbate removal capacity by the sorbent [16]. With regard to porosity, the greater the amount of pores present, the greater the efficiency of sorption. The volume and the ideal size of the pores depends on the size of the sorbate. For example, large pores are required for bulky contaminants, but unsuitable for smaller contaminants. The chemical nature of the sorbent is also of great importance, since sorption is also influenced by the functional groups present in the sorbent.

Other factors such as pH and temperature also influence the sorption process. There are many studies that determine that pH is a factor that influences the sorption processes [16] due to the fact that the pH of a solution determines the formation or not of compounds that may have a greater or lower degree of affinity in relation to the sorbent, thus

influencing their sorption. In turn, temperature is a factor that can influence sorption since usually the percentage of sorption of sorbate increases with the increase in temperature, and for high temperatures the phenomenon of desorption can occur, due to the breakdown of sorbent-sorbate bonds.

The presence of other contaminants and/or competitors also influences sorption. Most studies described in the literature are done with only a single contaminant. However, sorption studies should consider real waters, where there are other ions/contaminants present. These contaminants will compete for the sorbent surface, making contaminants with less affinity for the sorbent or at a lower concentration more difficult to sorption. In addition, real water also has dissolved organic matter, such as humic substances. This organic matter has the ability to sorption many contaminants, making its concentration smaller, thus being one of the competitors of sorbents.

Contact time is also a factor that influences sorption. Generally, sorbate removal increases with increasing contact time between sorbate and sorbent until equilibrium is reached.

1.6 Sorption in carbon nanostructures

Nanotechnology is the knowledge and control of matter between 1 and 100 nm in size scales. The physical, chemical and biological properties in nanoscale differ from the properties of primitive materials. Carbon nanostructures have been the target of interest due to their unique structural and physical properties. Carbon is an element that presents allotropia. The term allotrope refers to the different structural changes of a chemical element. It is the property on which certain elements are present in various forms (allotropia), depending on how the atoms of this element are interconnected. Graphene, fullerenes, graphite, carbon and diamond nanotubes are examples of allotropic forms of carbon. Graphene has already been considered, as carbon nanotubes, a highly strategic material with numerous possible real applications.

Graphite - The crystalline structure of graphite consists of hexagonal rings formed by thin parallel plates of graphene (Figure 1). Each carbon atom is covalently bound to three other atoms on the plate (the angle between two bonds is 120°). In graphite, graphene planes are linked to each other by weak forces from Van der Waals. Most of the graphite occurs in the form of flakes and is rarely found in crystalline form. It is also characterized

by being one of the most common allotropic forms of carbon and is the most stable form of carbon under standard conditions.

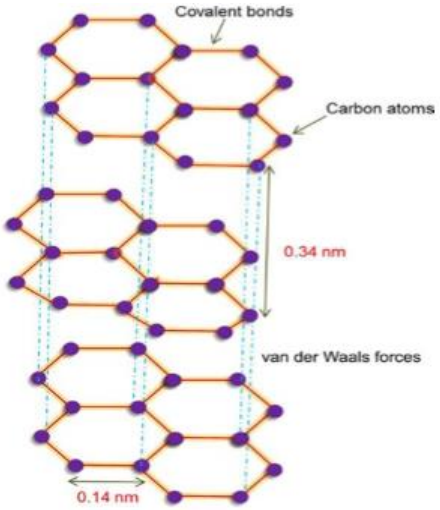

Figure 1 Graphite layered structure [17]

Graphene - Graphene consists of a single atomic layer of carbon atoms with a carbon-carbon bond length of 0.142 nm arranged in a hexagonal lattice. The hexagonal structure of graphene can be seen in Figure 2. It was commonly referred to as the building block of other carbon allotropes, such as carbon nanotubes, graphite and fullerenes before becoming a subject itself. It is characterized by being a monolayer of hybridized carbon atoms sp^2, arranged in a two-dimensional (2D) network, which has attracted enormous attention in recent years due to its exceptional thermal and mechanical properties [18]. It also has a high electrical conductivity. It is one of the strongest materials known, conducts heat better than diamond and can conduct electricity better than silver. Since there are only sp^2 carbon atoms in graphene sheets, graphene can only form Van der Walls bonds with sorbate, so it is not a good sorbent for many types of contaminants, such as trace metal ions. Graphene's sorption capability can be significantly increased by incorporating it with functional groups or other materials.

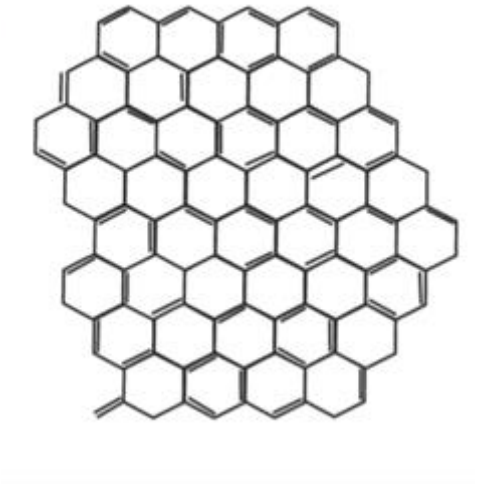

Figure 2 Graphene structure. Adapted from [19].

Graphene oxide (GO) has aroused enormous interest among researchers as it has many of the properties of the pure graphene, but it is easier and cheaper to produce in high quantities and easier to process. One important characteristic of GO, from the chemical point of view, is the high surface area that favors sorption, as well as its significant oxygen content, proving to be very attractive for further functionalization with inorganic and organic chemical structures with interesting properties for water remediation [20][21][22]. GO itself, a chemically derivative of graphene, has many oxygen functional groups in the basal plane and at the end of the sheets in the form of epoxy, hydroxyl and carboxylic groups (Figure 3) [20]. These oxygen groups can bind to trace metal ions by electrostatic interaction [23][24][25].

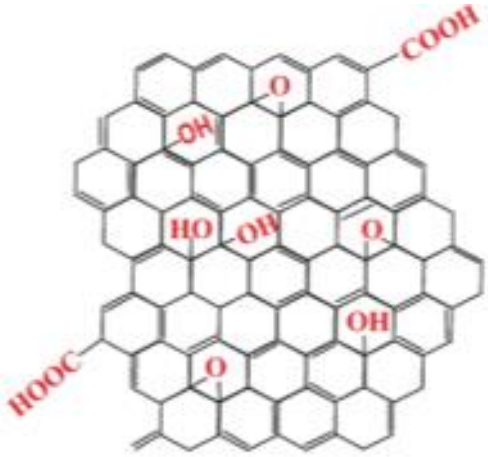

Figure 3 Chemical structure of graphene oxide. Adapted from [19].

GO is mainly synthesized by chemical exfoliation of graphite with strong oxidant reagents using the Brodie, Staudenmaier or Hummers method, or some variations of these methods. Brodie found that the mixture of oxidants ($KClO_4$ + HNO_3) with graphite could form GO [28][27]. Staudenmaier reported the formation of GO when the graphite was heated with H_2SO_4, HNO_3 and $KClO_4^-$. Hummers and Offeman introduced a convenient method to prepare the GO using H_2SO_4 and $KMnO_4$ [27].

1.7 Removal of potential toxic trace metals with graphene-based three-dimensional macrostructures

Graphene-based three-dimensional materials (GBMs) are the combination of micro and macrostructures. 3D graphene structures are referred to as aerogel, hydrogel, sponge or foam depending on the synthesis method. The methods of synthesis of 3D configurations can be done through direct synthesis from carbon sources or by solution-based synthesis. The direct synthesis approach provides control of pore size, density and distribution in the development of 3D structures due to the presence of a porous template where the graphene layers are grown, presenting the disadvantage of being expensive. In turn, solution-based synthesis has some advantages, such as elementary functionalization, scale-up possibility, higher yield, and lower production cost. In direct synthesis methods, such as chemical vapor deposition (CVD), the carbonization of the polymeric structure and plasma-enhanced CVD (PECVD) are used. Chemical vapor deposition (CVD) is a process in which a carbon source is decomposed into a metallic substrate to form a single layer or few layers of graphene sheet. In turn, plasma-reinforced CVD (PECVD) consists of the use of a non-thermal radio frequency plasma to radicalize a monomer, generating reactive chemical species to form coatings and deposit the vertically coated species to build a 3D structure.
In solution-based synthesis, methods such as lyophilization-assisted methods, assisted hydrothermal process, rGO stacking by reduction process, lyophilization and cross-linking are used. The assisted lyophilization model is the process that uses the rapid freezing of an aqueous solution to build a porous 3D structure. The stacking of GO by cross-linking is based on the addition of different chemicals to promote the gelling of dispersion, construction and strengthening of 3D structures through chemical or physical bonding. Chemical additives function as a pore-making agent and introduce new functional groups into the 3D graphene structure [28]. For example, GO-PVA hydrogel was synthesized by a

gelling reversible process, through the alteration of the pH of the system, with gelling at pH < 7 and remaining in the form of a solution at pH > 7, being the GO/PVA hydrogel governed by hydrogen bonds. The GO is known to have a higher hydrophilic character than graphene. In addition, the GO has oxygen atoms with pairs of unshared electrons, which gives them a strong ability to form complexes with metal ions by sharing a pair of electrons. For example, Stiko *et al.* [29] studied the sorption of Zn, Cd, Cu and Pb by GO and demonstrated that the sorption of these metals had increased with the increase of electronegativity of each metal, obtaining good sorption capacities for each of them.

Through the literature it was possible to verify that 3DGO are promising materials in the sorption of trace metals and their performance may vary depending on their composition, the pH of the medium, the temperature at which the sorption process occurs and the concentration of trace metals. Mi *et al.* [30] successfully synthesized a GO aerogel with a unidirectional porous structure. Through synthesized GO aerogels it was possible to obtain a high rate of removal of Cu from water by ion exchange, but it is necessary to control the pH in the application of these materials in wastewater. A pH increase from 2 to 6 resulted in a reduction in the percentage of metal removal (99 to 32.3 %). The authors showed that the GO aerogels take only 15 min to obtain a sorption capacity in the equilibrium, qe=198.1 mg/g, and this value is close to the theoretical maximum qe of activated charcoal (208.8 mg/g) [31]. Other authors have studied the possibility of chemically altering the surface area of 3DGO materials in order to increase their sorption capacity or increase their affinity for a specific contaminant. Henriques *et al.* [32] modified the surface of 3DGO with functional nitrogen groups (3DGON) increasing its removal efficiency for Hg by up to 95 % (Figure 4). These results were obtained only with 10 mg L^{-1} of this material, to achieve a residual concentration of Hg in solution very close to 1 μg L^{-1}, which is the maximum European permissible limit value for human consumption. In this study, they also studied the evaluation of material efficiency under realistic conditions (environmental concentrations of Hg were used in real waters, such as river and sea water), obtaining very promising results.

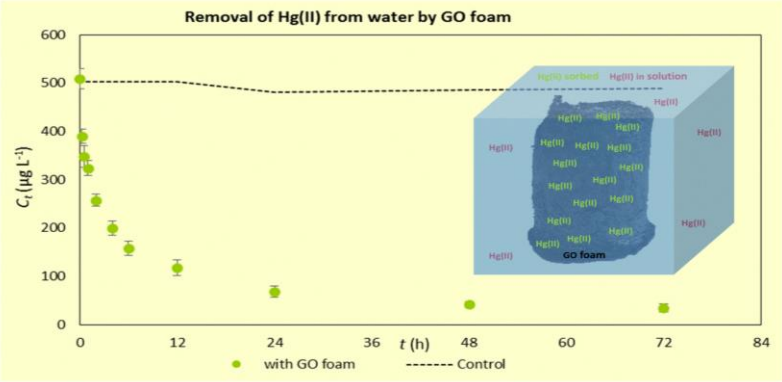

Figure 4 Variation of Hg concentration in solution (CT) with contact time (h) with 10 mg L^{-1} of GO foam [32].

The GO presents high dispersion, which leads to difficulties in separating the GO from the aqueous solution even after sorption of contaminants. The magnetization of GO is a possible solution to solve this problem through an external magnetic field. In addition, magnetic materials have the advantage of separating easily and quickly from the aqueous solution.

Several researchers synthesized metal oxide embedded in GO-based nanocomposites. As examples, we have the material Fe_3O_4/GO developed by Yao *et al.* [33], reduced magnetic GO reported by Bai *et al.* [34] and Li *et al.* [35]), and Mn_3O_4/GO, quoted by Su *et al.* [36]). These materials were applied in the purification of water to remove organic dyes and inorganic toxic metals, and promising results were obtained. These magnetic nanocomposites can have wide applications as they can be easily recovered from aquatic solutions after wastewater treatment processes.

Several organo-functionalized magnetic nanocomposites of GO have also been the subject of study by several authors. As examples we have the alginate encapsulated with GO (MGO) developed by Vu *et al.* [38], the hybrid compound Fe_2O_3 developed by Kang *et al.* [39], Fu *et al.* [40] and Gu *et al.* [41]. These materials were used in trace metal sorption, obtaining very promising results. The material developed by Bong *et al.* [39] (PG-Fe_3O_4) composed of Fe_3O_4 nanoparticles coated in GO layers, as well as the material developed by Gu *et al.* [41] allowed to obtain good sorption capacities for the trace element As. The material developed by Fu *et al.* [40] consisted of a functionalized GO with dithiocarbamate, provided good sorption capacities of the elements Hg, Cu, Cd and Pb due essentially to its large surface area (148m^2 g^{-1}) and the large volume of pores (0.33cm^3 g^{-1}) favoring the sorption of trace metals and obtained a maximum sorption

capacities for each metal of 113.64; 116.28; 147.06 and 181.82 mg/g for Cu, Cd, Pb and Hg, respectively. In turn Sui *et al.* [42], for Ag, Hg and Cu through the use of hybrid gels of GO that were prepared by heating the aqueous mixture of GO and carbon nanotubes with vitamin C without agitation, followed by supercritical drying of CO_2. These gels have shown a great affinity for the metals under study. The desalinator effect caused by this material was also evaluated for concentrations up to 35g L^{-1} of NaCl, and a desalination capacity of 633.3 mg g^{-1} was observed, which compared to other materials already reported is 16 times higher.

Table 4 shows a more extensive literature review of some of the organofunctionalized magnetic GO nanocomposites for trace metal sorption purposes.

Table 4 Nanocomposites of organo-functionalized magnetic graphene oxide for sorption of trace metals.

Sorbent	Trace metal	Sorbent concentration (g L^{-1})	[Metal] (mg L^{-1})	pH	Contact time (h)	Sorption capacity (mg g^{-1})	Removal (%)	Ref.
Glycol-GO	Pb	----	100	2-6	48	146	-----	[43]
Alginate-beads-MGO	Cr	5		As prepared	24			[38]
Polystyrene-MGO	As(III),As (V)	0.1	700	7		As (III):104 As(V):68		[39]
Fe2O3/GO/DCTA	Cu	-------	0.001	8	24	74.05	---	[44]
GO/2-PTSC	Hg	4-12	20	5	0.05	302	86.09	[45]
MCGO	Pb	0.1	-----	5	0.67	79.8		[46]
GO-DPA	Pb; Cd; Ni, Cu	0.008	20	5	0.67	Pb:369.79 Cd:257.20 Ni: 180.89 Cu: 358.82	-----	[47]
Xanthate magnetic-GO	Hg		20	7	3	118.55	97.5	[48]
Amino-magnetic-GO	Cr,Pb, Hg, Cd, Ni	5	5	6-7 Cr(IV):1-3.5		Cr=27.95 Pb:27.83 Hg:23.03 Cd:22.07	Cr:17.29 Pb:27,956 Hg23.03 Cd:27.83	[49]
Zeolite-GO	As (V)	2	0.1	---	2	50	---	[50]
Chitosan-GO	Hg	1	0-500	6	24	397	96	[51]

Table 5 Nanocomposites of organo-functionalized magnetic graphene oxide for sorption of trace metals. (continuation)

EDTA-GO	Cu, Pb	1	0-100	Pb:3 Cu:5	1.5	Pb:454.6 Cu: 108.7	90	[52]
GO Chitosan-MAG Magnetic GO	Hg	0.6	----	7	5	361	88	[53]
Polyaniline-rGO	Hg	2	1000	4	24	1000	94	[54]

Materials resulting from the combination of GO with nitrogen from amines have also been the subject of intense study (NAGOs). These compounds show major improvements in sorption properties that are promising in water treatment, especially for trace metals. Its surface groups, with specific properties and its high surface area contribute to its good performance in water treatment. Examples include alginate/graphene oxide (SAGO) foam reported by Jiao *et al.* [55] obtained with a crosslinking method followed by lyophilization, the PAS-GO material developed by Luo *et al.* [56], the polyethylene in functional cellulose aerogel reported by Li *et al.* [57] and graphene functionalized with tryptophan developed by Tan *et al.* [58]. All these compounds proved to be very efficient in the sorption of trace metals. The material developed by Jiao *et al.* [55] was very efficient in removing Cu and Pb with sorption capacities, respectively, for each of them of 98.0 mg g^{-1} and 267.4 mg g^{-1}. The PAS-GO material, developed by Luo *et al.* [56] and which resulted from cross-linking between the leaves of (GO) and the 3-aminopropiltrietoxylan oligomer (SBP) presented a superior sorption capacity for Pb with 312.5 mg g^{-1}, and an increase in maximum sorption capacity was observed with the increase in temperature. The l-tryptophan reported by Tan *et al.* [58] used in the sorption of Cu and Pb presented a good performance in their sorption. Sorption capacities of 588 mg/g and 222 mg/g were obtained for Cu and Pb, respectively, and the equilibrium was reached after 20 minutes.

Recently Wang *et al.* [59] developed a hybrid graphene/seed fibroin aerogel (GO-SF) and studied the sorption of dyes and trace metals. This aerogel is characterized by being a green sorbent presenting a highly efficient for water treatment. The synthesis of this material consisted of the mixture of GO and SF (fibroin of the seed) and was later lyophilized. The effect of aerogel composition was studied by varying the amount of GO (0.5, 10, 15 and 20 wt % of GO) whose corresponding nomenclature is GO-SF0, GO-SF5, GO-SF10 and GO-SF20, respectively. The maximum sorption capacities obtained for trace

metals using GO-SF0 sorbent were 195.8 mg g^{-1} for Ag,18.6 mg g^{-1} for Zn, 27 mg g^{-1} for Ni and 70.2 mg g^{-1} for Cu. In turn, those obtained using GO-SF20 as sorbent were 161.5 mg g^{-1} for Ag, 72.1 mg g^{-1} for Zn, 13.9 mg g^{-1} for Ni and 834 mg g^{-1} for Cu.

Several studies have been reported on the removal of trace metals and dyes by polyethyleneimine graphene oxide hydrogels/aerogels (GOPEI). As examples we have the studies reported by Guo *et al.* [60] and Singh *et al.* [61]. In the study reported by Guo *et al.*, these authors used 1 mL of GO/PEI hydrogels to study the removal of both methylene blue (MB) and rodamine B (RhB) in deionized water, showing good removal rates for both MB and RhB, reaching almost 100 % sorption for MB and RhB in approximately 4 h, from an initial concentrations of 10 mg L^{-1} and 4 mg L^{-1}, respectively. In turn, GOPEI aerogel developed by Singh [61] showed to be promise in the removal of As (V) and As(III). The maximum sorption capacity obtained was 4.80 mg g^{-1} for As(V) and 4.26 mg g^{-1} for As(III), starting from an initial concentration of As(V)/As(III) of 3 mg L^{-1} ,GOPEI concentration of 0.6 g L^{-1} and room temperature 30 ºC) ,and the equilibrium time was reached for As (III) and As (V) in 35 and 50 min, respectively.

Table 5 presents a review of the broader literature on NAGOS synthesized for the purpose of studying trace metal sorption.

Table 6 Characteristics related to the sorption by NAGOs of trace metals.

Sorbent	Trace metal	Sorbent concentration ($g\ L^{-1}$)	[Metal] ($mg\ L^{-1}$)	pH	Contact time (h)	Sorption capacity ($mg\ g^{-1}$)	Removal (%)	Ref.
PAS-GO	Pb	1		4.9		312.5	---	[56]
GO/PAMAMS	Pb	0.5	200	4.5	1	568.18	---	[62]
LS-GO-PANI	Pb	1.6	---------	5.0	1	216.4	---	[63]
PEI-PD/GO	Pb		50	4.0-5.4	----	197	---	[64]
GO/L-Trp	Pb	0.5		4.0		222	---	[58]
Fe2O3/Cys	Pb	0.5		6.0		459.33	---	[49]
GO-HPEI	Pb	0.1		5.5		438.6	---	[65]
PDA-GO	Pb	0.1				365	---	[66]
HPA-GO	Pb	0.2		5.9		740.7	---	[67]
GO-EDTA	Pb	0.025	20		1.5	454.6	---	[52]
EDTA-Mgo	Pb	2.0		5.1		508.4	---	[68]
EDTA-GO	Pb	0.1		3.0		479	---	[69]
GO/PAMAMS	Cd	0.5		5.0		253.81	---	[62]

Table 7 Characteristics related to the sorption by NAGOs of trace metals. (continuation)

PEI-PD/GO	Hg		50	3.5/4.0		110	---	[64]
MCGS	Hg	0.12	20	7.0	4	361.0	---	[53]
Fe_2O_3-GS	Hg	0.2		6-7	2	23.03	---	[49]
EDTA-mGO	Hg	4.8		4.1		268.4	---	[68]
GOPEI	As(V) e As(III)	0.6	3	As(V)= 4 As(III)= 7	0,97 para As (III) e 0,5 para As (V)	4.80 para As(V) e 0,24 para	---	[61]
CPA_2 (aerogel PEI cellulose)	Cr(VI)	0.02	10–700	1-8		18.7	---	[57]

Although there are several studies on the removal of PTEs from water, most studies still do not address the efficiency of the material under realistic conditions. In fact, most studies focus on removing a single contaminant from synthetic waters, bypassing the complexity of real water and waste water [70]. The multiplicity of different ions present in real waters, interacting and competing for binding sites can affect the efficiency of the removal process. Moreover, concentrations of metal far above realistic values, and large amounts of sorbent material are often used. In general, GO materials have a great sorption capacity for a wide range of PTEs, as well as a very fast sorption kinetics.

1.8 Material desorption and regeneration

An ideal sorbent should not only have a higher sorption capacity, but also a good desorption/regeneration performance. This characteristic translates into a more efficient and economically advantageous material. Therefore, it is important to consider these two factors (sorption and regeneration capacity) in the commercialization of GO and its composites. Some methodologies used in regeneration processes are biological treatment, solvent extraction, and chemical oxidation.

Studies have reported the process of desorption of trace metals from GO and 3DGO structures. For example, Wang *et al.* [71] studied the desorption of Zn from GO through the use of 0.1 mol L^{-1} of HCl and 1 mol L^{-1} of HNO_3, presenting the HCl a superior performance in desorption. Other authors, Juntao Liu *et al.* [72] that studied the sorption of Pb, Cd and Cu using as sorbent 3D graphene/MnO_2 aerogels, found that this material has an excellent regeneration and reuse capacity as well as easy of separation of the solution making these hybrid aerogels ideal candidates for decontamination of water from trace metals. The successive desorption and regeneration processes were used to evaluate the recycling of these aerogels and the desorption was made 0.01 mol L^{-1} HCl for 3 h and subsequently with KOH 0.1 mol L^{-1} to restore the active sites and allowing to regenerate graphene/MnO_2 aerogels for eight cycles. Another regeneration study described by Clemonne *et al.* [69] aimed to study the desorption of Pb from EDTA-GO by decreasing the pH with HCl solution.

It is however very important to note that although these materials can be regenerated and reused again in various sorption cycles, these are always toxic wastes that need to be treated, through safe storage or controlled incineration which carries costs.

1.9 Objectives

The main objective of this thesis was to develop and test graphene-based three-dimensional macrostructures (3DGM) with different surface chemical functionalization for a highly selective and efficient material for the removal of mercury from the waters.

The specific objectives are:

- Prepare 3DGMs by combining graphene oxide with different polymers.
- Control the functionalization of surface chemistry by adding different chemicals containing functional groups with potential affinity with target PTEs during the preparation method.
- Characterize the sorption of mercury by 3DGMs from synthetic waters (kinetics, selectivity, etc.) and optimize operating conditions, comprising the effect of different parameters (pH, ionic force, mass of 3DGMs).
- Evaluate the performance of the 3DGMs selected in real waters.

1.10 Thesis outline

This thesis is divided into 4 chapters. Chapter 1 is the present introduction, where some key concepts for this work are mentioned, followed by a state of the art. Chapter 2 and 3 are based on articles published in peer-reviewed international indexed journals and Chapter 4 presents a brief general discussion of the most relevant results and the general conclusion withdrawn from the work presented in this thesis.

1.11 References

[1] Y. Chen, L. Chen, H. Bai, L. Li, Graphene oxide–chitosan composite hydrogels as broad-spectrum adsorbents for water purification, J. Mater. Chem. A. 1 (2013) 1992–2001. doi: 10.1039/C2TA00406B.

[2] A. Afkhami, R. Moosavi, Adsorptive removal of Congo red, a carcinogenic textile dye, from aqueous solutions by maghemite nanoparticles, J. Hazard. Mater. 174 (2010) 398–403. doi: 10.1016/J.JHAZMAT.2009.09.066.

[3] J. M.-U. W Stum, Aquatic Chemistry Environmental Science and Technology W Stum, J Morgan - USA, 1996.

[4] H. Ali, E. Khan, M. A. Sajad, Phytoremediation of heavy metals—Concepts and applications, Chemosphere. 91 (2013) 869–881. doi: 10.1016/J.CHEMOSPHERE.2013.01.075.

[5] M. Alvand, F. Shemirani, Preconcentration of trace cadmium ion using magnetic graphene nanoparticles as an efficient adsorbent, Microchim. Acta. 181 (2014) 181–188. doi: 10.1007/s00604-013-1094-4.

[6] H. Cheng, Y. Hu, Lead (Pb) isotopic fingerprinting and its applications in lead pollution studies in China: A review, Environ. Pollut. 158 (2010) 1134–1146, May 2010, doi: 10.1016/j.envpol.2009.12.028.

[7] Decision No 2455/2001 / EC, European Parliament on 20 November 2001 establishing the list of priority substances in the field of water policy and amending DIRECTIVE 2000/60 / EC. .

[8] R. Chand Bansal, M. Goyal, Activated carbon adsorption. CRC Press, 2005.

[9] U. Farooq, J. A. Kozinski, M. A. Khan, M. Athar, "Biosorption of heavy metal ions using wheat based biosorbents – A review of the recent literature," Bioresour. Technol. 101 (2010) 5043–5053. doi: 10.1016/J.BIORTECH.2010.02.030.

[10] I. Ali, M. Asim, T. A. Khan, Low cost adsorbents for the removal of organic pollutants from wastewater, J. Environ. Manage. 113 (2012) 170–18. doi: 10.1016/J.JENVMAN.2012.08.028.

[11] F. Ge, M.-M. Li, H. Ye, B.-X. Zhao, Effective removal of heavy metal ions Cd^{2+}, Zn^{2+}, Pb^{2+}, Cu^{2+} from aqueous solution by polymer-modified magnetic

nanoparticles, J. Hazard. Mater. 211 (2012) 366–372. doi: 10.1016/J.JHAZMAT.2011.12.013.

[12] T. A. H. Nguyen, H. H. Ngo, W. S. Guo, J. Zhang, S. Liang, Q. Y. Yue, Q. Li. T. V. Nguyen, Applicability of agricultural waste and by-products for adsorptive removal of heavy metals from wastewater, Bioresour. Technol. 148 (2013) 574–585. doi: 10.1016/J.BIORTECH.2013.08.124.

[13] K. Mahapatra, D. S. Ramteke, L. J. Paliwal, Production of activated carbon from sludge of food processing industry under controlled pyrolysis and its application for methylene blue removal, J. Anal. Appl. Pyrolysis.. 95 (2012) 79–86. doi: 10.1016/j.jaap.2012.01.009.

[14] O. E. Abdel Salam, N. A. Reiad, M. M. ElShafei, A study of the removal characteristics of heavy metals from wastewater by low-cost adsorbents, J. Adv. Res. 2 (2011) 297–303. doi: 10.1016/J.JARE.2011.01.008.

[15] F.-S. Zhang, J. O. Nriagu, H. Itoh, Mercury removal from water using activated carbons derived from organic sewage sludge, Water Res. 39 (2005) 389–395. doi: 10.1016/j.watres.2004.09.027.

[16] M. M. Rao, D. H. K. K. Reddy, P. Venkateswarlu, K. Seshaiah, Removal of mercury from aqueous solutions using activated carbon prepared from agricultural by-product/waste, J. Environ. Manage. 90 (2009) 634–643. doi: 10.1016/J.JENVMAN.2007.12.019.

[17] Z. U. Khan, A. Kausar, H. Ullah, A Review on Composite Papers of Graphene Oxide, Carbon Nanotube, Polymer/GO, and Polymer/CNT: Processing Strategies, Properties, and Relevance, Polym. Plast. Technol. Eng. 55 (2016) 559–58. doi: 10.1080/03602559.2015.1098693.

[18] Y. Lei, F. Chen, Y. Luo, L. Zhang, Synthesis of three-dimensional graphene oxide foam for the removal of heavy metal ions, Chem. Phys. Lett. 593 (2014) 122–127. doi: 10.1016/J.CPLETT.2013.12.066.

[19] S. Priyadarsini, S. Mohanty, S. Mukherjee, S. Basu, M. Mishra, Graphene and graphene oxide as nanomaterials for medicine and biology application, J. Nanostruct Chem. 8 (2018) 123–137. doi.org/10.1007/s40097-018-0265-6

[20] D. R. Dreyer, S. Park, C. W. Bielawski, R. S. Ruoff, The chemistry of graphene oxide,Chem. Soc. Rev. 39 (2010) 228–240. doi: 10.1039/B917103G.

[21] K. Yang, L. Feng, X. Shi, Z. Liu, Nano-graphene in biomedicine: theranostic applications, Chem. Soc. Rev. 42 (2013) 530–547. doi: 10.1039/C2CS35342C.

[22] N. Karousis, S. P. Economopoulos, E. Sarantopoulou, N. Tagmatarchis, Porphyrin counter anion in imidazolium-modified graphene-oxide, Carbon N. Y. 48 (2010) 854–860. doi: 10.1016/J.CARBON.2009.10.039.

[23] S. Park, K.-S. Lee, G. Bozoklu, W. Cai, S. T. Nguyen, R. S. Ruoff, Graphene Oxide Papers Modified by Divalent Ions—Enhancing Mechanical Properties via Chemical Cross-Linking, ACS Nano. 2 (2008) 572–578. doi: 10.1021/nn700349a.

[24] H. Bai, C. Li, X. Wang, G. Shi, On the Gelation of Graphene Oxide, J. Phys. Chem. C. 115 (2011) 5545–5551. doi: 10.1021/jp1120299.

[25] Y. Xu, Q. Wu, Y. Sun, H. Bai, and G. Shi, Three-Dimensional Self-Assembly of Graphene Oxide and DNA into Multifunctional Hydrogels, ACS Nano. 4 (2010) 7358–7362. doi: 10.1021/nn1027104.

[26] Y. Xu, L. Zhao, H. Bai, W. Hong, C. Li, and G. Shi, Chemically Converted Graphene Induced Molecular Flattening of 5,10,15,20-Tetrakis(1-methyl-4-pyridinio)porphyrin and Its Application for Optical Detection of Cadmium(II) Ions, J. Am. Chem. Soc. 131(2009) 13490–13497. doi: 10.1021/ja905032g.

[27] W. S. Hummers, R. E. Offeman, Preparation of Graphitic Oxide, J. Am. Chem. Soc. 80 (1958) 1339–1339. doi: 10.1021/ja01539a017.

[28] H. Bai, C. Li, X. Wang, and G. Shi, A pH-sensitive graphene oxide composite hydrogel, Chem. Commun. 46 (2010) 2376. doi: 10.1039/c000051e.

[29] R. Sitko, E. Turek, B. Zawisza, E. Malicka, E. Talik, J. Heimann, A. Gagor, B. Feista, and R. Wrzalik, Adsorption of divalent metal ions from aqueous solutions using graphene oxide, Dalt. Trans. 42 (2013) 5682. doi: 10.1039/c3dt33097d.

[30] X. Mi, G. Huang, W. Xie, W. Wang, Y. Liu, and J. Gao, Preparation of graphene oxide aerogel and its adsorption for Cu^{2+} ions, Carbon N. Y. 50 (2012) 4856–4864. doi: 10.1016/J.CARBON.2012.06.013.

[31] M. Madhavarao, A. Rames, G. Purnachandrarao, and K. Seshaiah, Removal of copper and cadmium from the aqueous solutions by activated carbon derived from Ceiba pentandra hulls, J. Hazard. Mater. 129 (2006) 123–129. doi: 10.1016/j.jhazmat.2005.08.018.

[32] B. Henriques, G. Gonçalves, N. Emami, E. Pereira, M. Vila, and P. A. A. P.

Marques, Optimized graphene oxide foam with enhanced performance and high selectivity for mercury removal from water, J. Hazard. Mater. 301 (2016) 453–461. doi: 10.1016/J.JHAZMAT.2015.09.028.

[33] V. Chandra, J. Park, Y. Chun, J. W. Lee, I.-C. Hwang, K. S. Kim, Water-Dispersible Magnetite-Reduced Graphene Oxide Composites for Arsenic Removal, ACS Nano. 4 (2010) 3979–3986. doi: 10.1021/nn1008897.

[34] X. Z. Sun, D. X. Li, The Study of Catalytic Oxidation of NOx Using Mn_3O_4/GO/PMS, Adv. Mater. Res. 834 (2013) 458–461. doi: 10.4028/www.scientific.net/AMR.834-836.458.

[35] S. Bai, X. Shen, X. Zhong, Y. Liu, G. Zhu, X. Xu, K. Chen, One-pot solvothermal preparation of magnetic reduced graphene oxide-ferrite hybrids for organic dye removal, Carbon N. Y. 50 (2012) 2337–2346. doi: 10.1016/j.carbon.2012.01.057.

[36] H. Wang, X. Yuan, Y. Wu, H. Huang, X. Peng, G. Zeng, H. Zhong, J. Liang, M. Ren Graphene-based materials: Fabrication, characterization and application for the decontamination of wastewater and wastegas and hydrogen storage/generation, Adv. Colloid Interface Sci. 195 (2013) 19–40. doi: 10.1016/j.cis.2013.03.009.

[37] R. J. Su, M. C. Zhu, X. Z. Sun, and J. Guan, An Environment-Friendly Method to Catalytically Oxidate NO in Waste Water by Supported Manganese Oxide on Graphite Oxide, Appl. Mech. Mater. 768 (2015) 3–9. doi: 10.4028/www.scientific.net/AMM.768.3.

[38] H. C. Vu, A. D. Dwivedi, T. T. Le, S.-H. Seo, E. J. Kim, Y. S. Chang, Magnetite graphene oxide encapsulated in alginate beads for enhanced adsorption of Cr(VI) and As(V) from aqueous solutions: Role of crosslinking metal cations in pH control, Chem. Eng. J. 307 (2017) 220–229. doi: 10.1016/j.cej.2016.08.058.

[39] B. K. Kang, B. S. Lim, Y. Yoon, S. H. Kwag, W. K. Park, Y. H. Song, W. S. Yang , Y. T. Ahn, J. W. Kang, D. H. Yoon, Efficient removal of arsenic by strategically designed and layer-by-layer assembled PS@+rGO@GO@Fe_3O_4 composites, J. Environ. Manage. 201 (2017) 286–293. doi: 10.1016/j.jenvman.2017.05.066.

[40] W. Fu, Z. Huang, .Magnetic dithiocarbamate functionalized reduced graphene oxide for the removal of Cu(II), Cd(II), Pb(II), and Hg(II) ions from aqueous solution: Synthesis, adsorption, and regeneration, Chemosphere. 209 (2018) 449–456. doi: 10.1016/j.chemosphere.2018.06.087.

[41] L. Guo, P. Ye, J. Wang, F. Fu, Z. Wu, Three-dimensional Fe3O4-graphene macroscopic composites for arsenic and arsenate removal, J. Hazard. Mater. 298 (2015) 28–35. doi: 10.1016/J.JHAZMAT.2015.05.011.

[42] Z. Sui, Q. Meng, X. Zhang, R. Ma, B. Cao, Green synthesis of carbon nanotube–graphene hybrid aerogels and their use as versatile agents for water purification, J. Mater. Chem. 22 (2012) 8767. doi: 10.1039/c2jm00055e.

[43] Q. Fang, X. Zhou, W. Deng, Z. Liu, Hydroxyl-containing organic molecule induced self-assembly of porous graphene monoliths with high structural stability and recycle performance for heavy metal removal, Chem. Eng. J. 308 (2017) 1001–1009. doi: 10.1016/j.cej.2016.09.139.

[44] S. Liu, H. Wang, L. Chai, M. Li, Effects of single- and multi-organic acid ligands on adsorption of copper by Fe_3O_4/graphene oxide-supported DCTA, J. Colloid Interface Sci. 478 (2016) 288–295. doi: 10.1016/j.jcis.2016.06.019.

[45] A. Tadjarodi, S. Moazen Ferdowsi, R. Zare-Dorabei, A. Barzin, "Highly efficient ultrasonic-assisted removal of Hg(II) ions on graphene oxide modified with 2-pyridinecarboxaldehyde thiosemicarbazone: Adsorption isotherms and kinetics studies, Ultrason. Sonochem. 33 (2016) 118–128. doi: 10.1016/j.ultsonch.2016.04.030.

[46] Y. Wang, L. Li, C. Luo, X. Wang, H. Duan, Removal of Pb^{2+} from water environment using a novel magnetic chitosan/graphene oxide imprinted Pb^{2+}, Int. J. Biol. Macromol. 86 (2016) 505–511. doi: 10.1016/j.ijbiomac.2016.01.035.

[47] R. Zare-Dorabei, S. M. Ferdowsi, A. Barzin, A. Tadjarodi, Highly efficient simultaneous ultrasonic-assisted adsorption of Pb(II), Cd(II), Ni(II) and Cu (II) ions from aqueous solutions by graphene oxide modified with 2,2′-dipyridylamine: Central composite design optimization, Ultrason. Sonochem. 32 (2016) 265–276. doi: 10.1016/j.ultsonch.2016.03.020.

[48] L. Cui, X. Guo, Q. Wei, Y. Wang, L. Gao, L. Yan, T. Yan, and B. Du, Removal of mercury and methylene blue from aqueous solution by xanthate functionalized magnetic graphene oxide: Sorption kinetic and uptake mechanism, J. Colloid Interface Sci. 439 (2015) 112–120. doi: 10.1016/j.jcis.2014.10.019.

[49] X. Guo, B. Du, Q. Wei, J. Yang, L. Hu, L. Yan, W. Xu, Synthesis of amino functionalized magnetic graphenes composite material and its application to remove

Cr(VI), Pb(II), Hg(II), Cd(II) and Ni(II) from contaminated water, J. Hazard. Mater. 278 (2014) 211–220. doi: 10.1016/j.jhazmat.2014.05.075.

[50] M. Khatamian, N. Khodakarampoor, M. Saket Oskoui, N. Kazemian, Synthesis and characterization of RGO/zeolite composites for the removal of arsenic from contaminated water, RSC Adv. 5 (2015) 35352–35360. doi: 10.1039/C5RA02949J.

[51] G. Z. Kyzas, N. A. Travlou, E. A. Deliyanni, The role of chitosan as nanofiller of graphite oxide for the removal of toxic mercury ions, Colloids Surfaces B Biointerfaces. 113 (2014) 467–476. doi: 10.1016/j.colsurfb.2013.07.055.

[52] I. E. Mejias Carpio, J. D. Mangadlao, H. N. Nguyen, R. C. Advincula, D. F. Rodrigues, Graphene oxide functionalized with ethylenediamine triacetic acid for heavy metal adsorption and anti-microbial applications, Carbon N. Y. 77 (2014) 289–301. doi: 10.1016/j.carbon.2014.05.032.

[53] Y. Zhang, T. Yan, L. Yan, X. Guo, L. Cui, Q. Wei, B. Du, Preparation of novel cobalt ferrite/chitosan grafted with graphene composite as effective adsorbents for mercury ions, J. Mol. Liq. 198 (2014) 381–387. doi: 10.1016/j.molliq.2014.07.043.

[54] R. Li, L. Liu, F. Yang, Preparation of polyaniline/reduced graphene oxide nanocomposite and its application in adsorption of aqueous Hg(II), Chem. Eng. J. 229 (2013) 460–468. doi: 10.1016/j.cej.2013.05.089.

[55] C. Jiao, J. Xiong, J. Tao, S. Xu, D. Zhang, H. Lin, Y. Chen, Sodium alginate/graphene oxide aerogel with enhanced strength–toughness and its heavy metal adsorption study, Int. J. Biol. Macromol. 83 (2016) 133–141. doi: 10.1016/J.IJBIOMAC.2015.11.061.

[56] S. Luo, X. Xu, G. Zhou, C. Liu, Y. Tang, Y. Liu, Amino siloxane oligomer-linked graphene oxide as an efficient adsorbent for removal of Pb(II) from wastewater, J. Hazard. Mater. 274 (2014) 145–155. doi: 10.1016/J.JHAZMAT.2014.03.062.

[57] D.-M. Guo, Q.-D. An, Z.-Y. Xiao, S.-R. Zhai, Z. Shi, Polyethylenimine-functionalized cellulose aerogel beads for efficient dynamic removal of chromium from aqueous solution, RSC Adv. 7 (2017) 54039–54052. doi: 10.1039/C7RA09940A.

[58] M. Tan, X. Liu, W. Li, H. Li, Enhancing Sorption Capacities for Copper(II) and Lead(II) under Weakly Acidic Conditions by Tryptophan-Functionalized Graphene Oxide, J. Chem. Eng. Data. 60 (2015) 1469–1475. doi: 10.1021/acs.jced.5b00015.

[59] S. Wang, H. Ning, N. Hu, K. Huang, S. Weng, X. Wu, L. Wu. J. Liu, Alamusid, Preparation and characterization of graphene oxide/silk fibroin hybrid aerogel for dye and heavy metal adsorption, Compos. Part B Eng. 163 (2019) 716–722. doi: 10.1016/j.compositesb.2018.12.140.

[60] H. Guo, T. Jiao, Q. Zhang, W. Guo, Q. Peng, X. Yan, Preparation of Graphene Oxide-Based Hydrogels as Efficient Dye Adsorbents for Wastewater Treatment, Nanoscale Res. Lett. 10 (2015) 272. doi: 10.1186/s11671-015-0931-2.

[61] D. K. Singh, V. Kumar, V. K. Singh, S. H. Hasan, Modeling of adsorption behavior of the amine-rich GOPEI aerogel for the removal of As from aqueous media, RSC Adv. 6 (2016) 56684–56697. doi: 10.1039/C6RA10518A.

[62] F. Zhang, B. Wang, S. He, R. Man, Preparation of Graphene-Oxide/Polyamidoamine Dendrimers and Their Adsorption Properties toward Some Heavy Metal Ions, J. Chem. Eng. Data, 59 (2014) 1719–1726. doi: 10.1021/je500219e.

[63] X. Feng, C. Liang, J. Yu, X. Jiang, Facile fabrication of graphene oxide-polyethylenimine composite and its application for the Cr (VI) removal, Sep. Sci. Technol. 53 (2018) 2376–2387, 2018, doi: 10.1080/01496395.2018.1458880.

[64] Z. Dong, F. Zhang, D. Wang, X. Liu, J. Jin, Polydopamine-mediated surface-functionalization of graphene oxide for heavy metal ions removal, J. Solid State Chem. 224 (2015) 88–93. doi: 10.1016/j.jssc.2014.06.030.

65] Y. Liu, L. Xu, J. Liu, X. Liu, C. Chen, G. Li Y. Meng, Graphene oxides cross-linked with hyperbranched polyethylenimines: Preparation, characterization and their potential as recyclable and highly efficient adsorption materials for lead (II) ions, Chem. Eng. J. 285 (2016) 698–708. doi: 10.1016/j.cej.2015.10.047.

[66] C. Cheng, S. Li, J. Zhao, X. Li, Z. Liu, L. Ma, X. Zhang, S. Sun, C. Zhao, Biomimetic assembly of polydopamine-layer on graphene: Mechanisms, versatile 2D and 3D architectures and pollutant disposal, Chem. Eng. J. 228 (2013) 468–481. doi: 10.1016/j.cej.2013.05.019.

[67] L. Hu, Z. Yang, L. Cui, Y. Li, H. H. Ngo, Y. Wang, Q. Wei, H. Ma, L.Yan, B. Du, Fabrication of hyperbranched polyamine functionalized graphene for high-efficiency removal of Pb(II) and methylene blue, Chem. Eng. J. 287 (2016) 545–556. doi: 10.1016/j.cej.2015.11.059.

[68] L. Cui, Y. Wang, L. Gao, L. Hu, L. Yan, Q. Wei, B. Du, EDTA functionalized magnetic graphene oxide for removal of Pb(II), Hg(II) and Cu(II) in water treatment: Adsorption mechanism and separation property, Chem. Eng. J. 281 (2015) 1–10. doi: 10.1016/j.cej.2015.06.043.

[69] C. J. Madadrang, H. Y. Kim, G. Gao, N. Wang, J. Zhu, H. Feng, M. Gorring, M. L. Kasner, S. Hou, Adsorption behavior of EDTA-graphene oxide for Pb (II) removal, ACS Appl. Mater. Interfaces. 4 (2012) 1186–1193. doi: 10.1021/am201645g.

[70] F. Pagnanelli, A. Esposito, F. Vegliò, Multi-metallic modelling for biosorption of binary systems, Water Res. 36 (2002) 4095–4105. doi: 10.1016/S0043-1354(02)00112-4.

[71] H. Wang, X. Yuan, Y. Wu, H. Huang, G. Zenga, Y. Liua, X. Wang, N. Lin, Y. Qi, Adsorption characteristics and behaviors of graphene oxide for Zn(II) removal from aqueous solution, Appl. Surf. Sci. 279 (2013) 432–440. doi: 10.1016/j.apsusc.2013.04.133.

[72] J. Liu, X. Ge, X. Ye, G. Wang, H. Zhang, H. Zhou, Y. Zhang, H. Zhao, D graphene/δ-MnO_2 aerogels for highly efficient and reversible removal of heavy metal ions, J. Mater. Chem. A. 4 (2016) 1970–1979. doi: 10.1039/C5TA08106H.

[73] Q. Fang, Y. Shen, B. Chen, Synthesis, decoration and properties of three-dimensional graphene-based macrostructures: A review, Chem. Eng. J. 264 (2015) 753–771. doi: 10.1016/J.CEJ.2014.12.001.

[74] Y. Shen, Q. Fang, B. Chen, Environmental applications of three-dimensional graphene-based macrostructures: adsorption, transformation, and detection," Environ. Sci. Technol. 49 (2015) 67–84. doi: 10.1021/es504421y.

[75] S. Nardecchia, D. Carriazo, M. L. Ferrer, M. C. Gutiérrez, F. del Monte, Three dimensional macroporous architectures and aerogels built of carbon nanotubes and/or graphene: synthesis and applications, Chem. Soc. Rev. 42 (2013) 794–830. doi: 10.1039/C2CS35353A.

[76] K. C. Kemp, H. Seema, M. Saleh, N. H. Le, K. Mahesh,V. Chandra, K. S. Kim, Environmental applications using graphene composites: water remediation and gas adsorption, Nanoscale, 5 (2013) 3149. doi: 10.1039/c3nr33708a.

[77] H. Vijwani, M. N. Nadagouda, V. Namboodiri, S. M. Mukhopadhyay, Hierarchical hybrid carbon nano-structures as robust and reusable adsorbents: Kinetic studies

with model dye compound, Chem. Eng. J. 268 (2015) 197–207. doi: 10.1016/J.CEJ.2015.01.027.

[78] S. Lagergren, About the theory of so-called adsorption of soluble substances, K. Sven. Vetenskapsakademiens Handl. 24 (1898) 1–39.

Chapter 2

2. Graphene Oxide/Polyethyleneimine aerogel for high-performance mercury sorption from natural waters

This chapter correspond to the following published article:

Chemical Engineering Journal 398 (2020) 125587

Contents lists available at ScienceDirect

Chemical Engineering Journal

journal homepage: www.elsevier.com/locate/cej

Graphene oxide/polyethyleneimine aerogel for high-performance mercury sorption from natural waters

Ana Bessa[a,b], Bruno Henriques[b], Gil Gonçalves[a], Gonzalo Irurueta[a], Eduarda Pereira[b], Paula A.A.P. Marques[a,*]

[a] TEMA, Mechanical Engineering Department, University of Aveiro, 3810-193 Aveiro, Portugal
[b] CESAM & LAQV-REQUIMTE, Department of Chemistry, University of Aveiro, 3810-193, Portugal

2.1 Abstract

The development of effective sorbent materials to remove mercury (Hg) from real waters is a challenge. Here, we report the simple preparation of high-performance GOPEI aerogel for Hg remediation by self-assembly of high branched polyethyleneimine (PEI) with elevated molecular weight (Mw = 750k) and graphene oxide (GO) under acidic conditions (pH<3). Our studies revealed that the improved dimensional stability of GOPEI aerogels, critical for their use as sorbent materials, was obtained for a ratio GO:PEI 3:1. A small amount (10 mg L^{-1}) of GOPEI proved a highly efficiency for Hg removal from natural waters (tap (91%), river (90%) and sea (81%)) under realistic environmental concentrations (50 µg L^{-1}), where the existence of co-ions and different Hg-speciation are usually inhibitory factors of a good removal efficiency. This excellent performance was attributed to the synergistic effect resultant from the interactions between GO and PEI, giving a high content of N-rich groups and negative zeta potential over a wide pH range (from 2 to 12). Kinetic modelling pointed to differences on the main mechanisms behind the Hg removal by GOPEI in ultrapure *vs* natural waters. In ultrapure water pseudo-first order, usually associated with physical sorption, showed to be the best fit according to Akaike's Information Criterion (99.8% of probability), while in natural waters pseudo-second order model performed better (51.5% to 99.9% of probability), suggesting that the sorption is likely to rely on chemical interactions between Hg ions and the functional groups of GOPEI. Furthermore, GOPEI showed to be easily regenerated, keeping its high removal performance after 3 successive sorption-desorption cycles.

Keywords: graphene oxide-based aerogels, high molecular weight branched polyethyleneimine, wastewater, removal of Hg, real waters.

2.2 Introduction

Mercury (Hg) is currently ranked the third most toxic element to human health [1] with water (river, estuaries, lakes and sea) driving one of the major human exposure route [2] as it is well expressed in the Mercury in Europe's Environment Report [3]. Once in the food chain, Hg can bioaccumulate and bioamplificate causing adverse effects [4,5] With legislation in the water field becoming increasingly restrictive (e.g. the European Union seeks to ban the presence of Hg in wastewater discharges after 2021) [6], it becomes imperative to develop new methodologies to remove Hg from contaminated water that are more efficient than the ones currently available. Those innovative methodologies should be effective even when Hg is present at relatively low concentrations in water bodies, i.e., going beyond the previous allowable value in residual waters (50 μg L^{-1}) [7].

Nanotechnology has gained wide attention due to the possibility of producing engineered nanomaterials that are promising for full scale water treatment [8,9]. Lately, a new generation of graphene-based three dimensional (3D) macrostructures with superior sorption ability for hazard organic molecules and trace metals is being proposed [10–14]. Graphene oxide (GO), a graphene derivative, is composed of planar graphene-like aromatic areas with random size sp^3-hybridized carbons domains [15] shows an amphiphilicity, negatively charged nature and multi oxygen-containing groups on its surface (hydroxyl, epoxy and carboxyl groups), allowing a vast range of chemical interactions with molecules or ions [16,17]. Therefore, the self-assembly of 2D GO nanosheets in the presence of polymers through the establishment of chemical and/or physical bonds result in the formation of stable hydrogel [13,18].

For the preparation of GO-polymer aerogels with an intrinsic high sorption capacity for different ions and/or molecules, amine rich polymers are a natural choice due to the high affinity between amine groups and the oxygen functional groups of GO [19], enabling this combination with a synergistic performance for sorption of several contaminants from water [20,21]. Therefore, polyethyleneimine (PEI), that owns a high density of primary, secondary and tertiary amine groups, which allows the instantaneous formation of cross-linked hydrogels with GO, is one of the most explored cross-linking agents for water remediation purposes [19]. One of the first reports about the preparation of 3D GOPEI porous materials describes a simple methodology consisting in the mixture of a GO

dispersion (10 mg mL^{-1}) and an aqueous PEI solution (30 mg mL^{-1}, Mw = 800). The resultant aerogel showed light weight (0.02 – 0.03 g cm^{-3}), large specific surface area (476 m^2 g^{-1}) and hierarchically porous structure, showing an excellent adsorption performance for dyes and CO_2 adsorption [22]. Lately, different variations of this composition and methodology have been investigated for trace metal sorption showing great affinity for As (III) and As(V) [19], Pb(II) [23], U(VI) [24], Cu(II), Cd(II) and Pb(II) [25], and Cr(VI) ions. Although some authors used crosslinkers to promote the GO to PEI linkage such as oxalyl chloride [23], the majority of the studies report a facile, cost-effective and eco-friendly one-step method to create the hydrogel [19,24,26]. Though different GOPEI-based materials have been proposed in the literature, their application has been limited to simple case studies, such as distilled/ultrapure water containing one contaminant, mostly under unrealistic high concentrations. Furthermore, the efficiency of GOPEI aerogels towards water Hg remediation was not explored yet [27].

In a previous work [28], we reported the higher efficiency of a GO aerogel doped with nitrogen groups comparatively to GO aerogel doped both sulphur and nitrogen on Hg sorption from river water. However, that material showed clear limitations in waters with high ionic strength by removing only 42% of Hg in seawater. Therefore, the objective of this work was to develop and test a GO-based aerogel by the self-assembly of GO with a hyperbranched PEI with a higher Mw (750k) than other previously reported. The high amine-rich groups content is expected to act as active sorption sites for Hg, providing this aerogel with a better performance for Hg removal in natural waters (tap, river and sea). From the best of our knowledge, this is one the first nanocomposite materials reported so far, that presents a high Hg sorption performance simultaneously for three natural water matrices. Furthermore, we confirmed that the GOPEI presents the possibility for regeneration, with a small decrease in its performance. Since the preparation of GOPEI is cost-effective and easily scalable, this material has a high potential to reach the market of water remediation systems.

2.3 Materials and methods

2.3.1 Material synthesis

Polyethyleneimine (PEI) (analytical standard solution 50% (w/v) in water, Mw ~750k from Sigma Aldrich) solution with a concentration of 5 mg mL^{-1} was prepared in distilled water. Graphene oxide water dispersion (0.4 wt% concentration, from Graphenea) was used as received. The pH of both, PEI solution and GO suspension, was individually adjusted at 2 using 0.1 mol dm^{-3} HCl or NaOH solutions, before mixing, with a ratio of 25 wt% (PEI/GO), and rapidly hand shaken for 10 s to form a stable hydrogel. These experimental conditions were adapted from previous authors work [29]. The hydrogel was freeze-dried (Telstar LyoQuest HT-40, Beijer Electronics Products AB, Malmoe, Sweden) and a 3D porous aerogel was obtained. This aerogel was then immersed in ultrapure water (Milli-Q, 18 MΩ/cm) for 12 h to remove acidic residues and un-reacted species and freeze-dried again. The same methodology was adopted to prepare an aerogel using a PEI with a Mw of 800. This was done for comparative studies in order to confirm the influence of the PEI Mw in the mercury removal efficiency.

2.3.2 Material characterization

XPS spectra were acquired in an ultra-high vacuum (UHV) system with a base pressure of 2 x 10^{-10} mbar. High resolution spectra were recorded at normal emission take-off angle and with a pass-energy of 20 eV, which provides an overall instrumental peak broadening of about 0.5 eV. XPS spectra were calibrated in binding energy by referencing to the first component of the C 1s core level at 284.5 eV (C sp^2). Complementary, the chemical structure of the GOPEI was analysed via Attenuated Total Reflectance Fourier Transform Infrared (ATR-FTIR) in a Bruker Tensor 27 FT-IR spectrometer (Bruker Corporation, Massachusetts, USA). The spectra were recorded between 400 and 4000 cm^{-1}, with a resolution of 4 cm^{-1} and 256 scans. The microstructure was evaluated using a scanning electron microscope (FEG-SEM HITACHI S4100). The zeta potential of GOPEI, GO and PEI were measured at different pH values using a Zetasizer Nano-ZS (Model

Malver). The specific surface area was measured on a Gemini Micromeritics apparatus using the Brunauer Emmett Teller (BET) method.

2.3.3 Mercury sorption studies

The sorption of Hg on GOPEI was studied through batch experiments, where 10 mg of material was kept in contact with 1 L of Hg contaminated water for 24 h, in Schott glass bottles, under constant magnetic stirring (700 rpm). A certified standard solution of Hg (1001 ± 2 mg L^{-1} of Hg(II) in HNO_3 0.5 mol L^{-1}, from Merck) was used to contaminate ultrapure, tap, river, and sea waters to obtain the concentration of 50 µg L^{-1}, which corresponds to the old maximum permissible value for Hg in wastewaters discharges (Directive 84/156/EEC).

River water was collected in the Vouga river (40°40′42″ N, 08°22′18″ W), sea water on the coast of Aveiro (40°32′58″ N 8°46′31″ W) and tap water in the University of Aveiro, all in Portugal. At the laboratory, waters were filtered through 0.45 µm pore size filters and stored in dark at 4 ºC, until use. A brief characterization of all waters in terms of pH, conductivity, salinity and major and minor elements concentration was performed.

After spiking with Hg, solutions were left to pre-equilibrate during 24 h before the addition of GOPEI, which corresponded to the start of experiment. The sorption kinetics was followed by collecting 5 mL of water at defined periods of time, which was immediately centrifuged at 5000 rpm for 3 min. The supernatant liquid was collected and acidified to pH ≤ 2 using Suprapur© HNO_3 (65% v/v) [28].

The quantification of Hg was performed by cold vapour atomic fluorescence spectroscopy (CV-AFS), using a PSA 10.025 Millennium Merlin Hg analyser and $SnCl_2$ (2% m/v in HCl 10% v/v) as a reducing agent.[30] All assays were conducted in duplicate. A control experiment, corresponding to Hg contaminated water in absence of GOPEI, was always run in parallel.

2.3.4 Effect of pH

The effect of water pH (2, 4, 7 and 9) on Hg removal by GOPEI was studied for an initial concentration of 50 μg L^{-1} Hg in ultra-pure water. The pH was adjusted with HNO_3 (65%) or NaOH (1M) solution. Experiments were carried out as described previously.

2.3.5 Mercury sorption/desorption cycles study

The potential regeneration and reuse of GOPEI was investigated by conducting 3 consecutive Hg sorption-desorption cycles, in ultrapure and tap waters. After Hg sorption, GOPEI loaded with Hg was placed in contact with 40 ml of HNO_3 (v/v) for 6 h, freeze-dried for 24 h, and reused in Hg sorption, as described previously. In order to evaluate the success of the regeneration, after each desorption cycle with the eluent, the Hg content of the material was analysed by thermal decomposition atomic absorption spectrometry with gold amalgamation, using a LECO© AMA-254 [6].

2.3.6 Analysis of sorption data

The performance of GOPEI was evaluated in terms of percentage of Hg removed from the solution (*R*, %), using the following equation:

$$R(\%) = \frac{C_0 - C_t}{C_0} \times 100 \quad (1)$$

where C_0 is the initial Hg concentration in solution (μg L^{-1}) and C_t is the Hg concentration at time *t* (μg L^{-1}). Assuming that all Hg removed from the solution was retained by GOPEI, it was possible to estimate the Hg concentration in the material at time *t*, q_t (μg g^{-1}):

$$q_t = \frac{(C_0 - C_t)}{m} \times V \quad (2)$$

where V (L) represents the volume of the solution and m (g) the mass of GOPEI. When equilibrium is attained, $t = t_e$ (time of equilibrium), $q_t = q_e$ (concentration of Hg in the material at equilibrium) and $C_t = C_e$ (residual concentration of Hg in solution) [28].

The kinetics of Hg sorption on GOPEI was studied by applying three widely accepted reaction models in their non-linear forms [31] to the experimental data, namely, the

Lagergren pseudo-first-order model [32], the Ho's pseudo-second-order model [33] and the Elovich model [34] (Table S2.1). In addition to the reaction models, two widely known diffusion-based models, Boyd's film-diffusion [35] and Webber's pore-diffusion [36], were used.

Equilibrium data were fitted using 5 different models in their non-linear forms: the two-parameter Langmuir, Freundlich, Dubinin–Radushkevich and Temkin isotherm models and the three-parameter Sips or Langmuir-Freundlich isotherm model [37] (Table S2.2).

2.4 Results and discussion

2.4.1. Chemical and structural analysis of GOPEI

GOPEI hydrogel was originated from the simple mixture of GO and PEI aqueous solutions at pH 2. The formation and stability of the hydrogel is extremely dependent of the acidic medium that maximizes the electrostatic interactions and hydrogen bonding between GO and PEI. The effect of the pH of the medium on the hydrogel formation is illustrated in Figure S2.1 (SI). After freeze drying, the lightweight GOPEI aerogel preserved the characteristic brown colour of GO (Figure 5a), suggesting that GO preserves a high concentration of oxygen functional groups in the final macrostructure [38]. The SEM analysis (Figure 5b) shows a microporous 3D network with a large interconnected channel structure resulting from the self-assembly between PEI polymer chains and GO nanosheets, which is important to enable the fast diffusion of the adsorbate inside the aerogel. The porous nature of the GOPEI aerogel was further examined by microCT (Figure 5c) giving and estimation of a total porosity of 76.9 %.

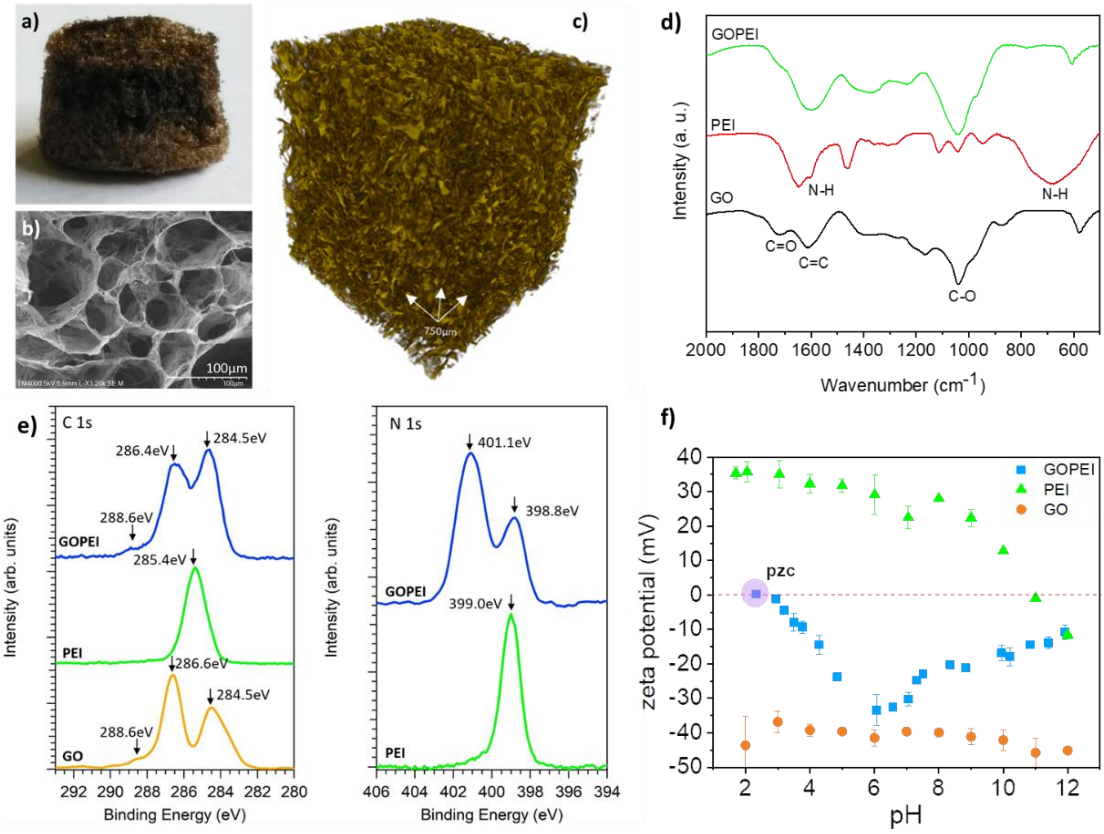

Figure 5 a) photograph of GOPEI aerogel; b) SEM image of GOPEI cross section; c) micro-CT image reconstruction of GOPEI aerogel d) FTIR of GO, PEI and GOPEI aerogel; e) HR-XPS spectra for C1s of GO, PEI and GOPEI aerogel and for N1s of PEI and GOPEI aerogel; and GOPEI aerogel; and f) Zeta potential of GO, PEI and GOPEI aerogel in function of pH.

The value of specific surface area (BET) obtained for this aerogel was of 61.93 m^2/g and the estimated pore volume of 0.07 cm^3/g. We consider that the overlapping of GO sheets, the high degree of oxidation and the adsorbed water on the surface of the aerogel can contribute to the low ability of nitrogen to adsorb into the oxidized surface of GO and consequently contribute to the low values of BET determined [39]. In a previous work, we showed that GO aerogels usually presents isotherms with a H3-type hysteresis loop that corresponds to slit-shaped pores and aggregates of plate-like particles [40]. This category of isotherms did not reach a plateau at saturation pressure (P/P_0 = 0.99), representing unrestricted multilayer adsorption in large mesopores and macropores, which difficult a

reliable estimation of the pore volume values. Thus, we consider that the determined BET value for the present aerogel is underestimated.

FTIR analysis of the individual components (GO and PEI) used to prepare the GOPEI aerogel and of the GOPEI are shown in Figure 5d. The spectrum of GO revealed its characteristic absorption bands at 1726 cm^{-1} (C=O), 1620 cm^{-1} (C=C) and 1046 cm^{-1} (C-O), [41] and the typical absorption bands of branched PEI at 1592 cm^{-1} and 770 cm^{-1} assigned to N-H vibrations [42] were visualized in the PEI spectrum. The FTIR analysis of GOPEI exhibited simultaneously the N-H (1596 cm^{-1}) bands attributed to PEI and C=O (1736 cm^{-1}) and C-O (1052 cm^{-1}) from GO, indicating an appropriate integration of the polymer with the carbon nanophase.

High resolution XPS of GO, PEI and GOPEI aerogel was conducted to determine the chemical composition of the aerogel as well as the interactions between GO and PEI (Figure 5e). C 1s core level of GO could be described by three main components, the first centred at a binding energy (BE) of 284.5 eV was ascribed to Csp^2/Csp^3 of the graphene sheets [42], the second at 286.6 eV was assigned to C-O, while the broad shoulder at higher BEs (around 288.6 eV) was attributed to other minor oxygen functional groups such as C=O and COOH [42], also present at GO nanosheets surface. On the other hand, C1s of PEI presented a single component at a BE of 285.4 eV in good agreement with the literature [43]. Thereby, C1s spectra of GOPEI was obtained by the convolution between GO and PEI spectra. It presented three main components, one broad peak at 284.5 eV ascribed to Csp^2/Csp^3 and C from PEI, and the two others at 286.4 eV (C-O) and 288.6 eV (C=O/COOH) attributed to the presence of oxygen functional groups from GO nanosheets [16,29,42].

Complementary, N1s spectra of PEI showed a single peak centred at 399.9 eV ascribed to nitrogen groups of the polymeric chains (Figure 5e) [43]. However, it is important to notice that after the formation of the aerogel, N1s split into two main components. The first component at 398.8 eV (30 at%) could be attributed to the unchanged nitrogen functional groups, as previously observed for PEI alone, while the new component at 401.1 eV (70 at%) was attributed to the formation of positively charged nitrogen groups interacting with the oxygen functional groups of GO [26]. These findings indicated the establishment of electrostatic interactions between the negatively charged oxygen functional groups at GO

nanosheets surface and the nitrogen functional groups on branched PEI chains, being responsible for the formation of structurally stable GOPEI aerogels.

Surface zeta (ζ) potential of the aerogel was measured at different pH values (between 2 – 12) to study the possible influence of the surface charge on the sorption capacity (Figure 5f) [19]. Remarkably, GOPEI displayed negative ζ potential values all over the working pH range, showing a point of zero charge (pzc) at ~ pH 2.6. The lowest ζ potential values were observed in the pH interval of 4 – 10, with values ranging from -15 to -30 mV. To help to clarify this result, the individual ζ potential curves for GO and hyperbranched PEI were also determined (Figure 5f). GO displayed a persistent high negative surface charge all over the pH range with values between -39 and -45 mV. For PEI, positive ζ potential values of around +35 mV were measured in the pH range 2 – 8, after that, a fast decreasing was verified with a pzc at pH 11. These results suggested that, in the present GOPEI aerogel, there was no full compensation of the negative surface charges from GO by the positive surface charges from PEI. Although the GO was in excess with respect to PEI (3:1), PEI had a very high Mw (750k) and consequently a higher contribution from the nitrogen functional groups (-NH-, -N<, NH_2) for the net surface charge would be expected. However, the GO's negative surface charge was compensated by the PEI positive charge only at pH < 2.6. Previous works citing the use of GOPEI-based materials for metal ion removal reported positive mean ζ potential values attributed to the protonation of amine groups. For example, X. Feng *et al.* [44] prepared GOPEI aerogels for Cr (VI) removal with a GO:PEI relation of 1:1 using PEI Mw from 600 to 10k reporting positive mean ζ potential values in the pH range from 2 to 7, with the mean surface potential increasing as the pH decreased. In a recent study, a set of GOPEI hydrogels were synthesized with PEI of several Mw (600, 1.8k, 10k and 70k) and different GO:PEI ratios (1:1, 1:2 and 1:3), also tested for Cr (VI) removal [26]. In this case, the higher pzc value of 9.8 was obtained for the conditions PEI 70k and GO:PEI = 1:2 and the lowest of 5.8 for PEI 600 and GO:PEI = 1:1, signifying that the pzc decreases as the GO:PEI ratio increases and Mw decreases. These findings were supported by Wang *et al.*[24] that prepared a GOPEI, for uranium removal, using a large excess of GO with respected to PEI (~ 23:1). Their findings revealed a pzc around 3, together with a continuous decrease of ζ potential values with increasing pH (the PEI Mw was not mentioned).

To mention also, in our study, the observed inflection of the ζ potential curve trend for GOPEI at around pH 6 in Figure 5f. This means that other factors should be playing a role for this conduct, rather than just simple charge compensation. The answer can be tentatively attributed to the hyperbranched PEI conformation, which is pH-dependent according to Kim *et al.* [45] who studied the pH dependent conformations for hyperbranched PEI (25k) from All-Atom Molecular Dynamics (MD) simulations. Based on their findings, we may postulate that PEI molecules in GOPEI could be adopting different conformations depending on the pH of the medium, presenting a more rounded conformation at neutral pH, and thus hiding the amine groups, or elongating at low and high pH values, thus exposing the amine groups.

2.4.2 Mercury sorption studies

Figure 6 displays the time-evolution of Hg concentration in different water matrixes (ultra-pure water (a); tap water (b); river water (c) and sea water (d)) in the presence and absence of GOPEI. Relatively constant concentrations of Hg in solution were observed in sorbent-free experiments over the whole experimental period, indicating that potential losses due to adsorption in glass walls or to volatilization were negligible. In the presence of the GOPEI, a marked decrease in normalized concentrations of Hg, C_t/C_0, was observed in the first 2 h of contact, from 1.0 to < 0.1 in ultrapure water (Figure 6a), and from 1.0 to 0.28 in tap water (Figure 6b). These results reveal a strong interaction between the Hg and the surface of the material, which is initially free of metal, and thus a high concentration gradient existed between the solution and the material. After the initial abrupt descent, a steady state was reached in ultrapure water at t = 2 h, from which the removal process reached the equilibrium. In tap water, Hg sorption extended up to 6 h, albeit at a slower rate, as the driving force decreased. In river and sea waters (Figure 6c and 6d, respectively) GOPEI kept its high performance, probably due to its high content in N groups, and lower ζ potential, as discussed before. The loss of efficiency with increasing matrix complexity underscored the need of studies on real water, which continues to be a hiatus in most works that focus only on ideal systems, leading to misjudgements of the actual potential of the proposed materials.

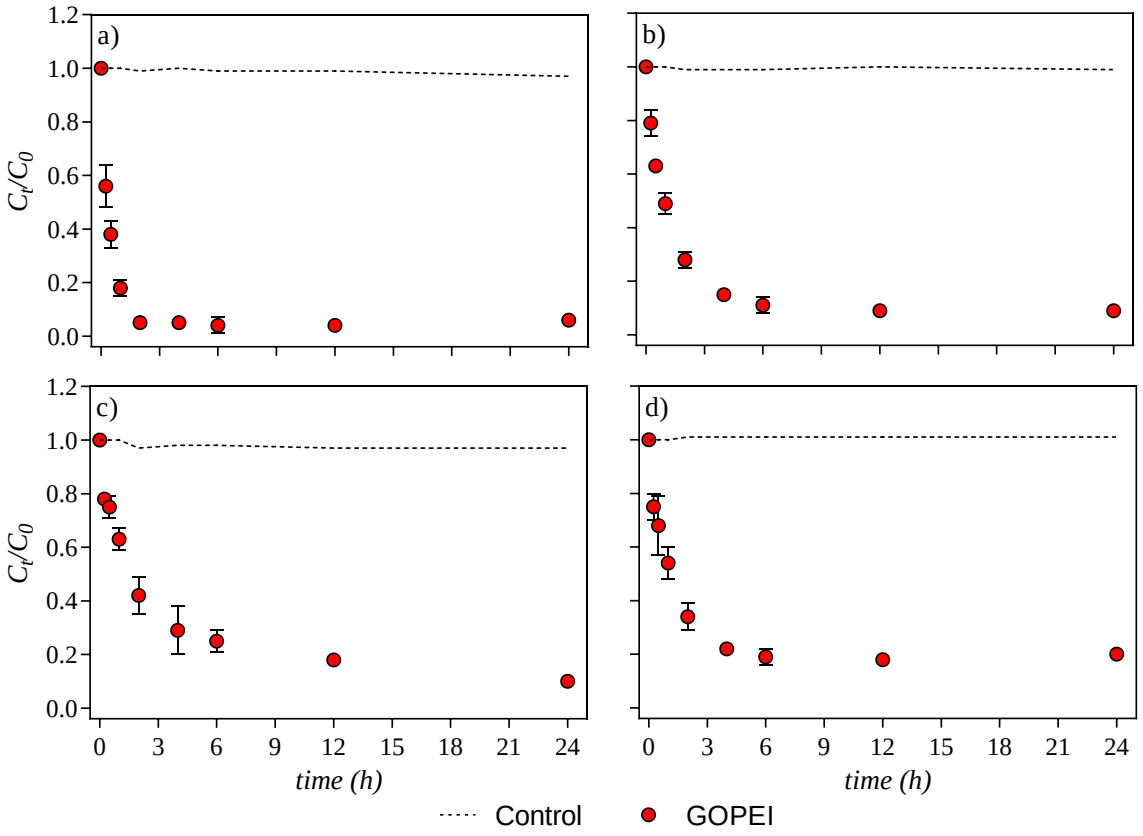

Figure 6 Normalized concentration of Hg in solution (C_t/C_0) during the contact time (h) with 10 mg L-1 of GOPEI in different water matrixes spiked with Hg: a) ultra-pure water; b) tap water; c) river water and d) sea water. The dotted line corresponds to the control (Hg spiked water in the absence of sorbent). Initial concentration of Hg 50 µg L^{-1}. Results correspond to mean ± amplitude of 2 replicates.

The effectiveness of GOPEI (Figure 7) was analysed considering the maximum removal percentage at equilibrium, the time required to reach the equilibrium and the residual concentration of Hg in water, which was compared with legal criteria concerning the presence of this priority hazardous substance in water intended for human consumption [46–48]. Sorption kinetics showed to be fast, which is very promising for a practical application [27]. Removal took from 1 to 6 h, excluding the removal of Hg from river water by GOPEI that lasted 24 h, probably because less Hg was readily available in the water column due to metal binding to dissolved organic matter, which content is greater when comparing to the other natural water matrixes [49]. Nevertheless, GOPEI achieved 90% of Hg removal in river water, leading to a residual concentration of 5 µg L^{-1}, much alike that obtained in tap water, 4.5 µg L^{-1}, being closer but higher than the European

guideline for drinking water, 1 µg L^{-1} (Directive 98/83/EC) [46]. Nevertheless, according to the World Health Organization (WHO), those values are below the guideline for inorganic mercury, 6 µg L^{-1}, assuming a 60-kg adult drinking 2 litres of water per day and allocating 10% of the total daily intake (TDI) to drinking-water [50].

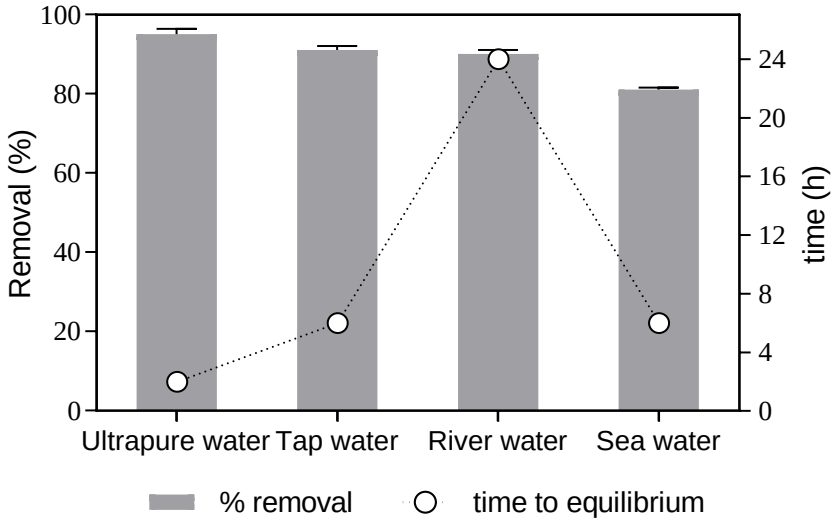

Figure 7 Removal percentage of Hg by GOPEI from ultrapure, tap, river and sea waters (showed values are Hg removed at equilibrium and time required to achieve equilibrium). Initial concentration of Hg 50 µg L^{-1}; amount of GO-based material of 10 mg L^{-1}. Results correspond to mean values of 2 replicates.

It is important to notice that, although GOPEI aerogel was able to decrease Hg concentrations in different contaminated waters studied down to values close to the European requirements for water intended to human consumption, 1 µg L^{-1}, in just 2 h, equilibrium concentration in sea water was obtained for values higher than 9 µg L^{-1}.

The relevance of the PEI Mw on the performance of the aerogel is highlighted by the comparative study the aerogels prepared with a PEI with a Mw 800 and 750000. The mercury sorption test performed in ultra-pure water under the same experimental conditions ([Hg] = 50 µg L^{-1} and sorbent doses 10 mg L^{-1}) showed that the maximum removal percentage achieved with GOPEI (Mw =800) was 17% after 2 h, against 95% removal for GOPEI (Mw=750000) (Figure S2.2).

Overall, results highlighted GOPEI as a promising alternative for the removal of Hg from water. Additional assays conducted with this material at different water pH values

(2, 4, 7 and 9) that may be considered representative of most real cases also point out that GOPEI has a wide range of application (Figure 8). The major differences were observed for pH = 2 (performance loss) that is below the point of pzc of GOPEI, (as discussed before), where GOPEI surface charge was positive, not favouring the removal of cationic species of Hg.

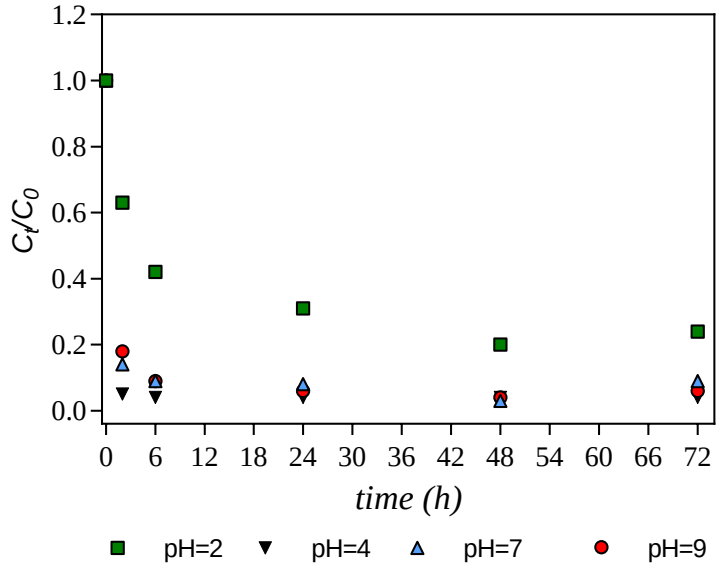

Figure 8 Normalized concentration of Hg (C_t/C_0) in ultra-pure water during the contact time (h) for 10 mg L^{-1} of GOPEI at different initial water pH values, 2, 4, 7 and 9. Initial concentration of Hg 50 µg L^{-1}. Controls were omitted for clarity.

Further, to assess the potential of GOPEI for real applications we decided to perform a comparative study, under the same experimental conditions, with one of the most used materials for water purification so far, activated carbon (*Chemviron* Carbon). The results obtained (Figure S2.3) point out that after 2 h, the activated carbon reached a maximum removal capacity of ~10% in comparison with GOPEI which presents a removal efficiency of 95% for the same time interval. Furthermore, activated carbon reach the equilibrium, when still a high concentration of mercury remains in solution (~45 µg L^{-1}), while GOPEI allows to reach the legal limit threshold of European guideline for drinking water (<1 µg L^{-1}).

2.4.2.1. Sorption isotherms

Figure 9 shows the fittings accomplished by the selected isotherm models, in their nonlinear forms, for the equilibrium data corresponding to the Hg sorption by GOPEI in ultrapure water. Estimated parameters and goodness of fit are summarized in Table 6.

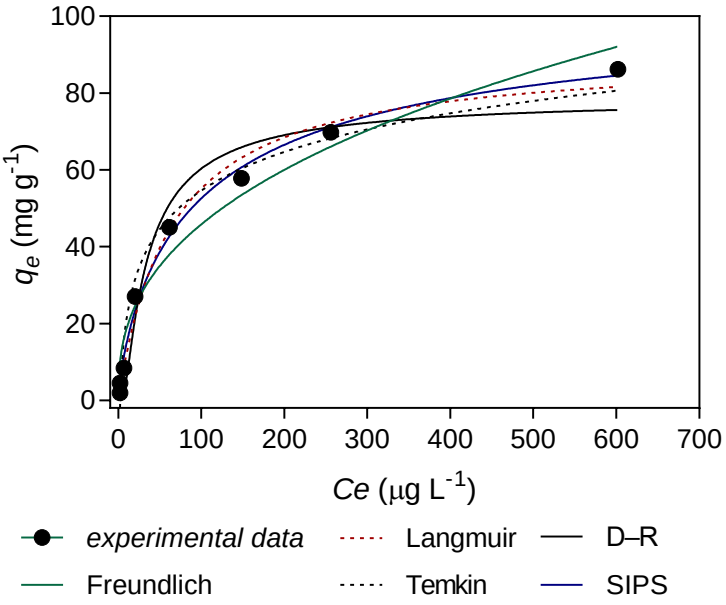

Figure 9 Fittings to the experimental data accomplished by Freundlich, Langmuir, Temkin, Dubinin–Radushkevich and SIPS sorption isotherms models, for the Hg – GOPEI system (21 ± 1 °C). Concentration of GOPEI in ultrapure water 10 mg L^{-1}; and of Hg 0, 25, 50, 100 300, 500, 750 e 1500 μg L^{-1}.

For the conditions assessed, all isotherms models described quite well the experimental data, although Dubinin–Radushkevich and Freundlich performed worse, especially for higher sorbate concentrations (Figure 9). The higher value of R^2 (0.9934) and lower value of Sy.x (3.086) indicated that SIPS isotherm model achieved the best fitting. Nevertheless, the analysis using Akaike's Information Criterion (AIC) [31] which is a robust method to compare models with different degrees of freedom, indicated Langmuir as the preferred model, with a 91% probability to be correct (against 9% of SIPS). Also, the heterogeneity index derived from the SIPS isotherm, 1/n = 0.78 ± 0.10, was relatively close to the unit, condition where this model is reduced to the Langmuir isotherm, assuming a monolayer adsorption. The dimensionless separation factor, R_L, calculated using the Langmuir constant, b_L ($RL=1/(1+b_L\ C_0)$) varied between 0.71 and 0.040 for initial concentrations of Hg in solution, C_0, ranging from 25 to 1500 μg L^{-1}, which was indicative of favourable adsorption ($0 < R_L < 1$) [51].

The mean free energy of adsorption, E (kJ mol^{-1}) calculated by Dubinin–Radushkevich isotherm model ($E=1/\sqrt{-2B}$) was in the interval 11 – 19 kJ mol^{-1}, which supported that chemical forces were dominant in the binding between Hg and GOPEI [51–53].

Table 8 Best fit values and goodness of fit obtained from the adjustments of Freundlich Langmuir and SIPS models to the experimental data (sorption of Hg onto GOPEI).

Isotherm model	Best fit values		Goodness of fit	
Freundlich	K_F ± SD (µg g^{-1})	7.64 ± 1.99	R^2	0.961
	1/n ± SD	0.389 ± 0.0941	Sy.x	6838
Langmuir	q_m ± SD (µg g^{-1})	90.3 ± 4.47	R^2	0.988
	b_L ± SD (L μg^{-1})	0.0157 ± 0.00273	Sy.x	3791
Temkin	B ± SD (J mol^{-1})	171 ± 27.0	R^2	0.976
	K_t ± SD (L μg^{-1})	0.433 ± 0.160	Sy.x	5349
Dubinin–Radushkevich	q_m ± SD (µg g^{-1})	79.1 ± 13.5	R^2	0.957
	B ± SD ($mmol^2/J^2$)	0.00549 ± 0.00282	Sy.x	7220
SIPS	q_m ± SD (µg g^{-1})	106 ± 11.6	R^2	0.993
	1/n ± SD	0.781 ± 0.100	Sy.x	3086
	b_S ± SD	0.00990 ± 0.00349		

The maximum Hg sorption capacity, q_m, according to Langmuir and SIPS isotherms was within the interval 90.3 – 106 mg g^{-1}, which was higher than the value of 35.0 ± 1.95 mg g^{-1} obtained under the same experimental conditions, in previous work using a nitrogen-doped GO macrostructure [28], evidencing the great potential of this material as the basis of a new water treatment technology. Although a small set of materials has maximum theoretical capacities superior to that obtained for GOPEI (Table

S2.3), it should be noted that those studies deal with unrealistically high concentrations of Hg and sorbents, much higher than those of the present work. An example of this, is the work of Yap *et al.* [54] where a material made of GO covalently attached to cysteamine molecules showed a maximum sorption capacity of 169 mg g^{-1} at a pH 5 using also 10 mg L^{-1} of adsorbent, but with higher initial Hg concentration of 1.5 mg L^{-1}. In the present study, 0.05 mg L^{-1} initial Hg concentration was used, value corresponding to the legal limit of Hg discharge in the environment established in the Directive 84/156/EEC. It is important to refer that in water treatment, theoretically, the higher the concentration of the contaminant in solution, the greater the maximum amount of Hg bound per unit of sorbent mass. Also, the sorbents removal efficiency is conditioned when using concentrations as lower as the ones used in our study, which highlights the efficiency of our GOPEI.

2.4.2.2 Kinetic modelling

Figure 10 shows the amount of Hg sorbed onto GOPEI over time, q_t (µg g^{-1}) *vs t*, along with the adjustments achieved by the selected sorption kinetic models. The parameters estimated by the models as well as coefficient of determination (R^2) and the standard deviation of residuals ($S_{y.x}$) were calculated as refereed in a previous article [28].

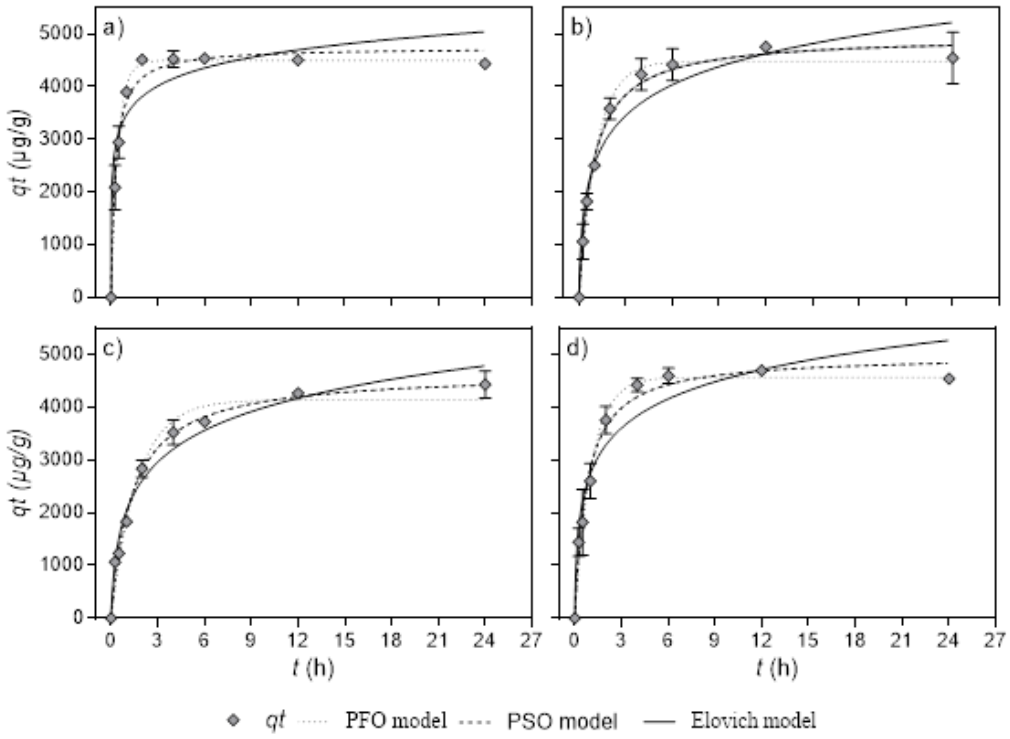

Figure 10 Fittings of pseudo-first order (PFO), pseudo-second order (PSO) and Elovich models to experimental data concerning the sorption of Hg onto GOPEI over time: a) ultrapure water; b) tap water; c) river water and d) sea water. Concentration of GOPEI and Hg in water of 10 mg L^{-1} and 50 µg L^{-1}, respectively.

Overall, the mathematical models studied showed to be suitable to describe the sorption kinetics ($0.903 < R^2 < 0.989$). Nevertheless, in ultrapure water the PFO model showed to be the best according to AIC (99.8% of probability), and the only one capable of correctly describing the transition between the initial ascendant step and the plateau that corresponds to equilibrium (Figure 6). In addition, this model, which is usually associated with physical sorption, obtained the best estimate of the value of q_e at 24 h.

In the cases where the experimental points are better fitted by PFO, the surface of the sorbent is said to be homogeneous and, theoretically, only one binding mechanism will occur [55]. So, we can assume that for the system GOPEI-Hg in ultrapure water, there was no limitation of surface area and binding sites, and then the adsorption approaches a homogeneous process.

In natural waters, the evaluation between models by using AIC indicated that the kinetics followed PSO model (with a probability ranging from 51.5% to 99.9%), which suggested that the sorption was likely to rely on chemical interactions between Hg ions and the functional groups of GOPEI. The fact that *qt vs t* followed different kinetics (PFO *vs* PSO), indicated that probably the main mechanisms behind the removal of Hg by GOPEI in ultrapure *vs* natural waters will be different. Despite the best performance of PSO, this model did not accurately predict the value of *qe* for t = 24 h in tap and sea waters (Figure 10).

The piecewise linear regression (PLR) of data (Table 7) revealed a first linear segment from Boyd film-diffusion fitting (R^2= 0.9995) whose intercept confidence interval (95 % confidence level) included the zero, suggesting that the sorption was not controlled by film-diffusion [55].

Table 9 Parameters of the adjustments achieved by Boyd's film-diffusion and Webber' s intraparticle-diffusion models to the experimental data of Hg sorption by GOPEI.

Stage	**Boyd's film-diffusion**		**Webber' s intraparticle-diffusion**		
	intercept	R^2	Breakpoint (min)	K_i (µg g^{-1} $min^{-1/2}$)	R^2
1st	-0.08839 [-0.30568; 0.12891]	0.9995 (n=3)	82.5	0.4635	0.9955 (n=3)
2nd	-	-	-	-0.0032	0.7580 (n=5)

Webber's intraparticle-diffusion´s fitting (Figure 11) showed multiple linear segments, corresponding to different diffusion stages. However, evidence ratio from AIC analysis showed that the hypothesis of two steps diffusion was 1.15×10^{11} times more likely to be the correct than the one comprising three stages. The breakpoint was found to be at 82.5 min, from which the intra-particle diffusion began to slow down as Hg concentration in solution decreased.

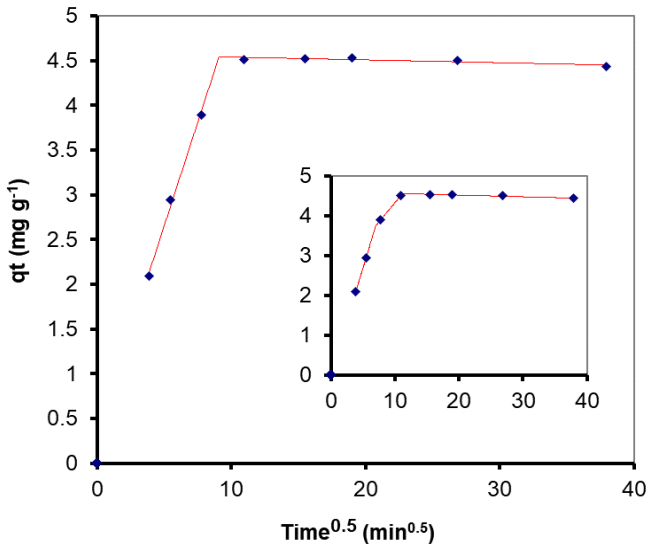

Figure 11 Kinetic modelling of the sorption process of Hg onto GOPEI by Webber' s intraparticle-diffusion model.

2.4.2.3. Removal mechanisms

The sorption process of most of the GO-based sorbents is mainly governed by the ability to establish different soft chemical interactions with the ionic species in solution. Here the performance of GOPEI aerogel was studied in detail by monitoring the chemical interfacial behaviour after the Hg water exposure. For that purpose, the sorbent performance was accessed by the exposure to several batch of Hg contaminated ultrapure water at different pHs. Figure 12 plots the maximum removal percentage together with the ζ potential values (previously shown in section 3.1). Importantly, the results showed that the former removal efficiency was constant (>95%) and independent of the pH, except for values below the pzc (<2) of the aerogel.

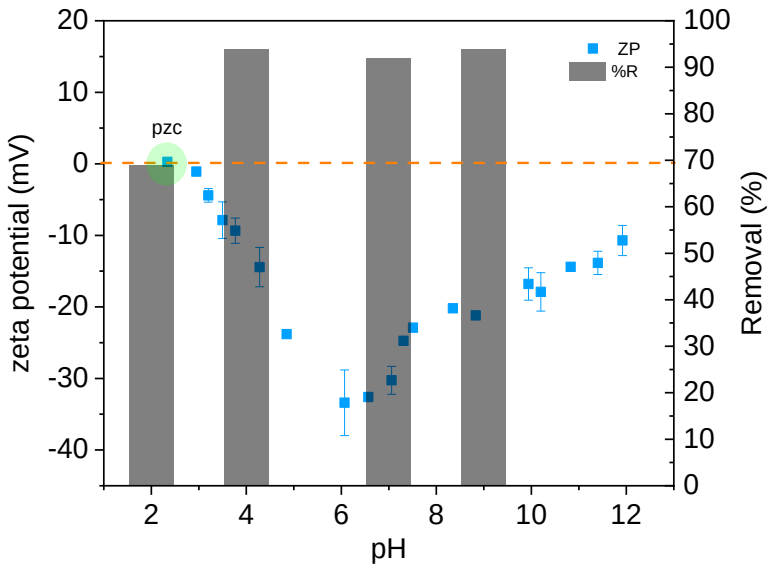

Figure 12 Graphical representation of the zeta potential in function of pH, together with the maximum removal percentage (R%) of Hg by GOPEI aerogel measured at different pHs.

XPS analysis of the GOPEI after the Hg removal was done and compared with the XPS results before Hg contact, for deeper understanding of the adsorption mechanism of Hg by GOPEI. Comparing both XPS survey spectra, the appearance of Hg peak on XPS

spectra of GOPEI after adsorption was observed (Figure S2.4). The high resolution XPS spectra of N1s highlighted remarkable changes on the shape of this peak after adsorption, which revealed the participation of the nitrogen functional groups on the global sorption process (Figure 13a). The comparative results provided relevant evidence about the strong launch of interactions with Hg species by the decrease of the relative peak intensity at 401.1 eV (32 at%) due to positively charged nitrogen groups and the correspondent increase of the peak at 399.3 eV assigned to -NH_2 groups (68 at%).[26] In fact, these results revealed that the positively charged nitrogen functional groups, resultant from the interactions with oxygen functional groups during the self-assembly of GOPEI, can be restored by the establishment of interactions with the mercury species in solution as schematized in Figure 9b. The speciation studies of mercury in ultrapure water (pH = 4) showed that the main species in solution were: 93.0% non-charged species $Hg(OH)_2$, plus a small contribution of positive ions 5.5% $(Hg(OH))^+$ and 1.5% Hg^{2+} (determined by Visual MINTEQ 3.1). In summary, considering the results of mercury speciation and the XPS N1s results, we suggest that the regeneration of nitrogen functional groups observed for GOPEI after the adsorption was mainly governed by the establishment of hydrogen bonds with $Hg(OH)_2$ species (Figure 13b). Previous XPS studies performed with different GOPEI-based aerogels showed an inverse trend of nitrogen functional groups nature after removal of chromium [26]. In the referred study, the N1s peak showed an increase of the component assigned to the presence of positively charged nitrogen species in detriment of free amine groups. However, in that case most chromium ionic species in water are positively charged (Cr^{3+} and $Cr(OH)^{2+}$), so the nitrogen functional groups can act as electron donors for the reduction of chromium ionic species to Cr(0). These evidences suggested that the sorption process occurred preferentially by a charge transfer from N to Hg, that N groups were the main sorption sites and their protonation controlled sorption efficacy [56]. Indeed, the Hard Soft Acid Base (HSAB) theory, establishes that the soft acid mercury ions has a strong affinity for amine soft bases, forming metal-chelate complex [57].

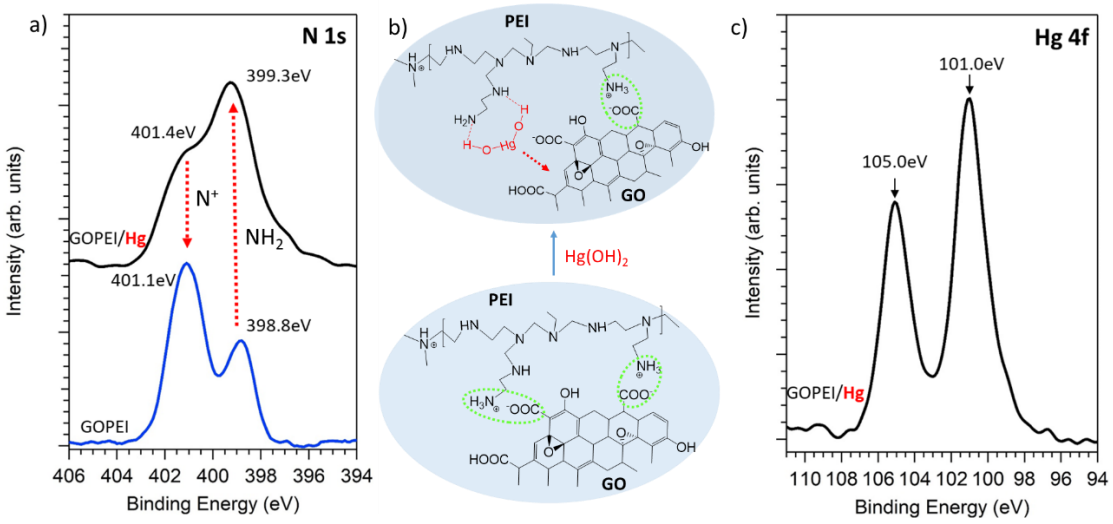

Figure 13 High resolution Ns1 spectra of GOPEI before and after Hg adsorption a). Schematic representation of the sorption mechanism of $Hg(OH)_2$ by the GOPEI aerogel b). High resolution Hg 4f spectra after sorption to GOPEI aerogel c).

Nevertheless, it is important to emphasize that, although no significant changes on C1s and O1s peaks were detected by XPS after Hg exposure (Figure S2.3) the contribution of these elements for the total sorption process cannot be neglected. In fact, in a previous work, we showed the important contribution of oxygen functional groups on the removal mechanism of Hg species from ultrapure waters [28].

Regarding the high-resolution XPS spectra of Hg4f (Figure 13c), two main components at around 101.0 eV ($Hg4f_{7/2}$) and 105.0 eV ($Hg4f_{5/2}$) were detected. These results are in agreement with the speciation studies for Hg in ultrapure water by showing the predominance of oxidized forms $Hg(OH)_2$ and $(Hg(OH))^+$in solution at pH 4.

The high resilience of negative charges on GOPEI surface may justify the higher affinity obtained for Hg species in river water (pH 4.2) where a high content of other ions and/or organic matter was present, which may directly compete with Hg for the sorbent active sites. The branched structure of the high Mw PEI used in this work showed to play an important role on the sorption mechanism, providing higher density of nitrogen functional groups able to stablish atomic spatial rearrangements and avoiding steric effects during the complexation of Hg species. This was confirmed by the poor Hg removal efficiency of the GOPEI prepared with PEI of Mw 800 (17% removal against 95% in 2 h). The relevance of the GOPEI chemical structure was even more pronounced for its sorption performance in

sea water. GOPEI presented a negative ζ potential at the pH of seawater (7.8) which allowed the removal of 85% of Hg.

The elemental composition of the natural waters under study was analysed by ICP before and after Hg removal by GOPEI (Table S2.4). In general, the major elements Ca, Na, K and Mg were not removed by the aerogel. Regarding the minor elements analysed, it was observed that in tap water, GOPEI decreased the concentration of Al, Fe and Zn. In river water only Fe and Pb concentrations diminished, while in sea water Al and Zn were removed by GOPEI. The higher content in cations in seawater, particularly Na, Mg, K and Ca, as well as the high concentration of Cl^- may also interfere with Hg sorption due to the competition for binding sites at the macrostructure surface, or due to changes in the speciation and mobility of Hg (e.g. formation of chlorine complexes with Hg). Results demonstrated that this inhibitory effect was not pronounced (81% Hg removal in sea water), which may be attributed to the high density of N functional groups in the prepared GOPEI. Moreover, the branched structure of the selected PEI may allow atomic spatial rearrangements in order to avoid steric effects during the complexation of mercury species.

2.4.3 GOPEI regeneration and reuse

The regeneration is an important aspect for a sorbent, since it enables an economic and environmentally sustainable long-term water purification technology [58]. Figure 14 shows that, even after three consecutive sorption-desorption cycles, using HNO_3 2% (v/v) as eluent, GOPEI kept its high Hg removal efficiency in ultrapure water (94 – 96%), while a low decrease on the performance was observed for tap water (from 90 to 81 %). These findings highlight the high potentiality of GOPEI to be used in industrial scale applications.

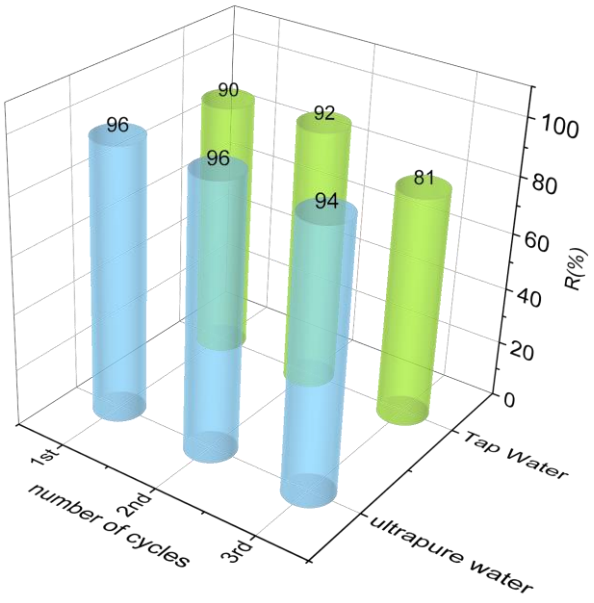

Figure 14 Efficiency of Hg removal by GOPEI, from ultrapure and tap waters, after 3 consecutive regeneration cycles. Concentration of GOPEI and Hg in water of 10 mg L^{-1} and 50 µg L^{-1}, respectively. Eluent HNO_3 2% (v/v).

2.5. Conclusions

In the present study, high Mw (750k) branched PEI and GO nanosheets (1:3 ratio) were used to produce a hydrogel in aqueous acidic medium by a simple stirring method, easy to scale-up. This hydrogel was freeze-dried providing an aerogel (GOPEI) which demonstrated a high efficiency and selectivity for Hg removal from different natural waters under an extended pH range which was attributed to the persistent negative ζ potential of this particular material in the same pH interval.

Due to a systematic XPS characterization study we were able to confirm a dynamic character of the nitrogen functional groups from GOPEI suggesting the establishment of hydrogen bonds between nitrogen groups and the mercury species in solution.

Moreover, the applied kinetics models suggested that in natural waters the sorption of Hg presents a chemical nature. The residual concentrations of Hg in water were in accordance with World Health Organization (WHO), except for sea water. Furthermore, in most cases, the sorption kinetics showed to be very fast, with Hg removal by GOPEI always taking from 1 to 6 h. That relevant features under realist conditions make GOPEI aerogels a very sustainable approach for a practical application.

2.6 References

[1] L. Therese, L. Casteleyn, Mercury pollution in modern times and its socio-medical consequences, Sci. Total Environ. 654 (2019) 720–734. https://doi.org/10.1016/j.scitotenv.2018.10.408.

[2] C. T. Driscoll, R. P. Mason, H. M. Chan, D. J. Jacob, N. Pirrone, Mercury as a Global Pollutant: Sources, Pathways, and Effects, Environ. Sci. Technol. 47 (2013) 4967–4983. https://x.doi.org/10.1021/es305071v.

[3] European Environment Agency, Mercury in Europe's environment - A priority for European and global action, (2018) 1–72. https://doi.org/10.2800/558803.

[4] P. Govind, S. Madhuri, Heavy metals causing toxicity in animals and fishes, Res. J. Anim. Vet. Fish. Sci. 2 (2014) 17–23.

[5] G. Bjørklund, M. Dadar, J. Mutter, J. Aaseth, The toxicology of mercury : Current research and emerging trends, Environ. Res. 159 (2017) 545–554. https://doi.org/10.1016/j.envres.2017.08.051.

[6] B. Henriques, A. Teixeira, P. Figueira, A.T. Reis, J. Almeida, C. Vale, E. Pereira, Simultaneous removal of trace elements from contaminated waters by living Ulva lactuca, Sci. Total Environ. 652 (2019) 880–888. https://doi.org/10.1016/j.scitotenv.2018.10.282.

[7] Commission regulation, Directive 84/156/EEC (1984). Council Directive 84/156/EEC of 8 March 1984 on limit values and quality objectives for mercury discharges by sectors other than the chlor- alkali electrolysis industry, Off. J. Eur. Communities. 74 (1984) 29. https://eur-lex.europa.eu/LexUriServ/LexUriServ.do?uri=CONSLEG:2006R1881:20100701:EN:PDF.

[8] A. S. Adeleye, J. R. Conway, K. Garner, Y. Huang, Y. Su, A. A. Keller, Engineered nanomaterials for water treatment and remediation : Costs, benefits, and applicability, Chem. Eng. J. 286 (2016) 640–662. https://doi.org/10.1016/j.cej.2015.10.105.

[9] X. Qu, P. J. J. Alvarez, Q. Li, Applications of nanotechnology in water and wastewater treatment, Water Res. 47 (2013) 3931–3946.

https://doi.org/10.1016/j.watres.2012.09.058.

[10] S. I. Siddiqui, S. A. Chaudhry, A review on graphene oxide and its composites preparation and their use for the removal of As^{3+} and As^{5+} from water under the effect of various parameters : Application of isotherm , kinetic and thermodynamics, Process Saf. Environ. Prot. 119 (2018) 138–163. https://doi.org/10.1016/j.psep.2018.07.020.

[11] J. Xu, Z. Cao, Y. Zhang, Z. Yuan, Z. Lou, X. Xu, X. Wang, Chemosphere A review of functionalized carbon nanotubes and graphene for heavy metal adsorption from water : Preparation , application , and mechanism, Chemosphere. 195 (2018) 351–364. https://doi.org/10.1016/j.chemosphere.2017.12.061.

[12] B. Yang, K., Wang, J., Chen, X., Zhao, Q., Ghaffar, A., & Chen, Application of graphene-based materials in water purification: from the nanoscale to specific devices, Environ. Sci. Nano. 5 (2018) 1264–1297. https://doi.org/10.1039/C8EN00194D.

[13] Z. Niu, L. Liu, L. Zhang, X. Chen, Porous Graphene Materials for Water Remediation, Small. 10 (2014) 3434–3441. https://doi.org/10.1002/smll.201400128.

[14] N. Yousefi, X. Lu, M. Elimelech, N. Tufenkji, Environmental performance of graphene-based 3D macrostructures, Nat. Nanotechnol. 14 (2019) 107–119. https://doi.org/10.1038/s41565-018-0325-6.

[15] G. Goncalves, P. A. A. P. Marques, C.M. Granadeiro, H.I.S. Nogueira, M.K. Singh, J. Gr, Surface Modification of Graphene Nanosheets with Gold Nanoparticles : The Role of Oxygen Moieties at Graphene Surface on Gold Nucleation and Growth, Chem. Mater. 21 (2009) 4796–4802. https://doi.org/10.1021/cm901052s.

[16] D. R. Dreyer, S. Park, W. Bielawski, R. S. Ruoff, The chemistry of graphene oxide, Chem. Soc. Rev. 39 (2010) 228–240. https://doi.org/10.1039/b917103g.

[17] J. Shao, W. Lv, Q. Yang, Self-Assembly of Graphene Oxide at Interfaces, Adv. Mater. 26 (2014) 5586–5612. https://doi.org/10.1002/adma.201400267.

[18] S. Kabiri, D. N. H. Tran, S. Azari, D. Losic, J. Accepted, Graphene-diatom silica aerogels for efficient removal of mercury ions from water, ACS Appl. Mater. Interfaces. 7 (2015) 11815–11823. https://doi.org/10.1021/acsami.5b01159.

[19] D. K. Singh, V. Kumar, V. K. Singh, S. H. Hasan, Modeling of adsorption behavior of the amine-rich GOPEI aerogel for the removal of As (III) and As (V) from

aqueous media, RSC Adv. 6 (2016) 56684–56697. https://doi.org/10.1039/C6RA10518A.

[20] Y. Li, L. Yang, X. Zhu, J. Hu, H. Liu, Post-synthesis modification of porous organic polymers with amine : a task-specific microenvironment for CO 2 capture, Int. J. Coal Sci. Technol. 4 (2017) 50–59. https://doi.org/10.1007/s40789-016-0148-8.

[21] B. Yameen, Design of Polymer-Brush-Grafted Magnetic Nanoparticles for Highly Efficient Water Remediation, ACS Appl. Mater. Interfaces. 5 (2013) 3784−3793.

[22] Z. Sui, Y. Cui, J. Zhu, B. Han, Preparation of Three-Dimensional Graphene Oxide – Polyethylenimine Porous Materials as Dye and Gas Adsorbents, ACS Appl Mater Interfaces. 5 (2013) 9172–9179. https://doi.org/10.1021/am402661t.

[23] Y. Liu, L. Xu, J. Liu, X. Liu, C. Chen, G. Li, Y. Meng, Graphene oxides cross-linked with hyperbranched polyethylenimines: Preparation, characterization and their potential as recyclable and highly efficient adsorption materials for lead (II) ions, Chem. Eng. J. 285 (2016) 698–708. https://doi.org/10.1016/j.cej.2015.10.047.

[24] X. Wang, Q. Liu, J. Liu, R. Chen, H. Zhang, R. Li, Z. Li, J. Wang, 3D self-assembly polyethyleneimine modified graphene oxide hydrogel for the extraction of uranium from aqueous solution, Appl. Surf. Sci. Jou. 426 (2017) 1063–1074.

[25] D. Pakulski, S. Witomska, A. Aliprandi, V. Patroniak, A. Ciesielski, Graphene oxide-branched polyethylenimide foams for efficient removal of toxic cations from water, J. Mater. Chem. A. 6 (2018) 9384–9390. https://doi.org/10.1039/C8TA01622D.

[26] J. Geng, Y. Yin, Q. Liang, Z. Zhu, H. Luo, Polyethyleneimine cross-linked graphene oxide for removing hazardous hexavalent chromium: Adsorption performance and mechanism, Chem. Eng. J. 361 (2019) 1497–1510. https://doi.org/10.1016/j.cej.2018.10.141.

[27] N. K. Gupta, A. Gupta, 2D and 3D carbon-based adsorbents for an efficient removal of HgII ions: A review, Flat Chem. 11 (2018) 1–14. https://doi.org/10.1016/J.FLATC.2018.11.002.

[28] B. Henriques, G. Gonçalves, N. Emami, E. Pereira, M. Vila, Optimized graphene oxide foam with enhanced performance and high selectivity for mercury removal from water, J. Hazard. Mater. 301 (2016) 453–461. https://doi.org/10.1016/j.jhazmat.2015.09.028.

[29] A. F. Girão, G. Gonçalves, K. S. Bhangra, J. B. Phillips, J. Knowles, G. Irurueta, M.K. Singh, I. Bdkin, A. Completo, P.A.A.P. Marques, Electrostatic self-assembled graphene oxide-collagen scaffolds towards a three-dimensional microenvironment for biomimetic applications, RSC Adv. 6 (2016) 49039–49051. https://doi.org/10.1039/c6ra10213a.

[30] B. Henriques, L. S. Rocha, C. B. Lopes, P. Figueira, R. J. R. Monteiro, A. C. Duarte, M. A. Pardal, E. Pereira, Study on bioaccumulation and biosorption of mercury by living marine macroalgae: Prospecting for a new remediation biotechnology applied to saline waters, Chem. Eng. J. 281 (2015) 759–770. https://doi.org/10.1016/j.cej.2015.07.013.

[31] M. I. El-Khaiary, G. F. Malash, Common data analysis errors in batch adsorption studies, Hydrometallurgy. 105 (2011) 314–320. https://doi.org/DOI 10.1016/j.hydromet.2010.11.005.

[32] S. Lagergren, About the theory of so-called adsorption of soluble substances, K. Sven. Vetenskapsakademiens Handl. 24 (1898) 1–39.

[33] Y. S. Ho, G. McKay, Pseudo-second order model for sorption processes, Process Biochem. 34 (1999) 451–465. https://doi.org/Doi 10.1016/S0032-9592(98)00112-5.

[34] M. J. D. Low, Kinetics of Chemisorption of Gases on Solids, Chem. Rev. 60 (1960) 267–312. https://doi.org/Doi 10.1021/Cr60205a003.

[35] G. E. Boyd, A. W. Adamson, L.S. Myers, The Exchange Adsorption of Ions from Aqueous Solutions by Organic Zeolites, J. Am. Chem. Soc. 69 (1947) 2836–2848. https://doi.org/Doi 10.1021/Ja01203a066.

[36] W. J. Weber, J. C. Morris, Kinetics of adsorption on carbon from solution, J. Sanit. Eng. Div. 89 (1963) 31–60.

[37] A. Gunay, E. Arslankaya, I. Tosun, Lead removal from aqueous solution by natural and pretreated clinoptilolite: Adsorption equilibrium and kinetics, J. Hazard. Mater. 146 (2007) 362–371. https://doi.org/DOI 10.1016/j.jhazmat.2006.12.034.

[38] J. Wang, E. Caliskan, Š. Lidija, Green reduction of graphene oxide using alanine, Mater. Sci. Eng. C. 72 (2017) 1–6. https://doi.org/10.1016/j.msec.2016.11.017.

[39] M. A. Worsley, P.J. Pauzauskie, T.Y. Olson, J. Biener, J.H. Satcher, T.F. Baumann, Synthesis of Graphene Aerogel with High Electrical Conductivity, Eur. J. Chem. 24 (2018) 15903–15911. https://doi.org/10.1021/ja1072299.

[40] C .D. Alejandro Borrás, Gil Gonçalves, Gregorio Marban, Stefania Sandoval, Susana Pinto, Paula A. A. P. Marques, Julio Fraile, Gerard Tobias, Ana M. López-Periago, Preparation and Characterization of Graphene Oxide Aerogels: Exploring the Limits of Supercritical CO_2 Fabrication Methods, Chem Eur J. 24 (2018) 15903–15911. https://doi.org/10.1002/chem.201803368.

[41] G. Gonçalves, J. Borme, I. Bdkin, A. González-Mayorga, G. Irurueta, H.I.S. Nogueira, M. C. Serrano, P. Alpuim, P. Marques, Reductive nanometric patterning of graphene oxide paper using electron beam lithography, Carbon N. Y. 129 (2018) 63–75. https://doi.org/10.1016/j.carbon.2017.11.067.

[42] S. Wen, F. Zheng, M. Shen, X. Shi, Surface modification and PEGylation of branched polyethyleneimine for improved biocompatibility, J. Appl. Polym. Sci. 128 (2013) 3807–3813. https://doi.org/10.1002/app.38444.

[43] P. Louette, F. Bodino, J.-J. Pireaux, Poly(ethylene imine) (PEI) XPS Reference Core Level and Energy Loss Spectra, Surf. Sci. Spectra. 12 (2005) 54–58. https://doi.org/10.1116/11.20050911.

[44] X. Feng, C. Liang, J. Yu, X. Jiang, Facile fabrication of graphene oxide-polyethylenimine composite and its application for the Cr(VI) removal, Sep. Sci. Technol. 53 (2018) 2376–2387. https://doi.org/10.1080/01496395.2018.1458880.

[45] I. Kim, T. A. Pascal, S. J. Park, M. Diallo, W. A. Goddard, Y. Jung, PH-Dependent Conformations for Hyperbranched Poly(ethylenimine) from All-Atom Molecular Dynamics, Macromolecules. 51 (2018) 2187–2194. https://doi.org/10.1021/acs.macromol.7b02573.

[46] Council Directive 98/83/EC, Council Directive 98/83/EC of 3 November 1998 on the quality of water intended for human consumption., J. Eur. Communities. 330 (1998) 32–54.

[47] Directive 2013/39/EU, Directive 2013/39/EU of the European Parliament and of the Council of 12 August 2013 amending Directives 2000/60/EC and 2008/105/EC as regards priority substances in the field of water policy, 226 (2013) 1–17.

[48] Decree-Law No. 236/98, Decree-Law No. 236/98 of the Portuguese Ministry of the Environment of 1 August establishing water quality standards, 176 (1998) 3676–3722.

[49] D. S. Tavares, C .B. Lopes, A. L. Daniel-da-Silva, C. Vale, T. Trindade, M. E.

Pereira, Mercury in river, estuarine and seawaters – Is it possible to decrease realist environmental concentrations in order to achieve environmental quality standards?, Water Res. 106 (2016) 439–449. https://doi.org/10.1016/j.watres.2016.10.031.

[50] B. Yan, Z. Hiew, L. Yee, X. Jiat, S. Thangalazhy-gopakumar, S. Gan, S. Shee, G. Pan, T.C. Yang, Review on synthesis of 3D graphene-based configurations and their adsorption performance for hazardous water pollutants, Process Saf. Environ. Prot. 116 (2018) 262–286. https://doi.org/10.1016/j.psep.2018.02.010.

[51] I. T. A. Gunay, E. Arslankaya, Lead removal from aqueous solution by natural and pretreated clinoptilolite : Adsorption equilibrium and kinetics, J. Hazard. Mater. 146 (2007) 362–371. https://doi.org/10.1016/j.jhazmat.2006.12.034.

[52] N. Kumar, A. Sengupta, A. Gupta, J. Ravindra, Journal of Environmental Chemical Engineering Biosorption-an alternative method for nuclear waste management : A critical review, J. Environ. Chem. Eng. 6 (2018) 2159–2175. https://doi.org/10.1016/j.jece.2018.03.021.

[53] K. Vijayaraghavan, T.V.N. Padmesh, K. Palanivelu, M. Velan, Biosorption of nickel (II) ions onto Sargassum wightii : Application of two-parameter and three-parameter isotherm models, 133 (2006) 304–308. https://doi.org/10.1016/j.jhazmat.2005.10.016.

[54] D.L. Pei Lay Yap, S. Kabiri, Di. N.H. Tran, Multifunctional Binding Chemistry on Modified Graphene Composite for Selective and Highly Efficient Adsorption of Mercury, ACS Appl. Mater. Interfaces. 11 (2019) 6350–6362. https://doi.org/10.1021/acsami.8b17131.

[55] H. Qiu, L. Lv, B. Pan, Q. Zhang, W. Zhang, Q. Zhang, Critical review in adsorption kinetic models, J. Zhejiang Univ. Sci. A. 10 (2009) 716–724. https://doi.org/10.1631/jzus.A0820524.

[56] L. Dambies, C. Guimon, S. Yiacoumi, E. Guibal, Characterization of metal ion interactions with chitosan by X-ray photoelectron spectroscopy, Colloids Surfaces A. 177 (2001) 203–214.

[57] F. S. Awad, K. M. Abouzeid, W. M. A. El-maaty, A. M. El-wakil, Efficient Removal of Heavy Metals from Polluted Water with High Selectivity for Mercury (II) by 2-Imino-4-Thiobiuret Partially Reduced Graphene Oxide (IT-PRGO), ACS Appl. Mater. Interfaces. 9 (2017) 34230−34242.

https://doi.org/10.1021/acsami.7b10021.

[58] P. L. Yap, T. T. Tung, S. Kabiri, N. Matulick, D. N. H. Tran, D. Losic, Polyamine-modified reduced graphene oxide: A new and cost-effective adsorbent for efficient removal of mercury in waters, Sep. Purif. Technol. 238 (2020) 116441. https://doi.org/10.1016/J.SEPPUR.2019.116441.

2.7. Supplementary material of chapter 2

Figures

Figure S2.5 Photographs of the mixtures of the solutions of GO and PEI at pH below and above 3. The image shows that the formation of stable hydrogel between GO and PEI only occur for pH values lower than 3, where the electrostatic interactions are maximized.

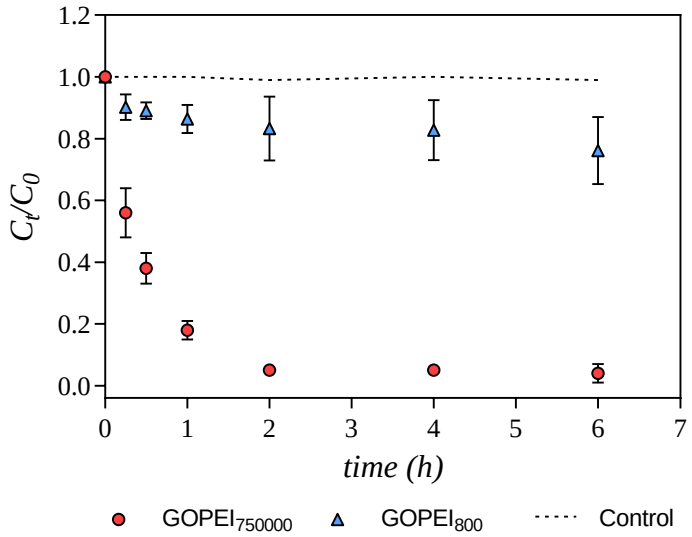

Figure S2.6 Normalized concentration of Hg in solution (C_t/C_0) during the contact time (h) with 10 mg L^{-1} of GOPEI (MW=800 (orange) or 750 000(blue)) in ultrapure water spiked with Hg.

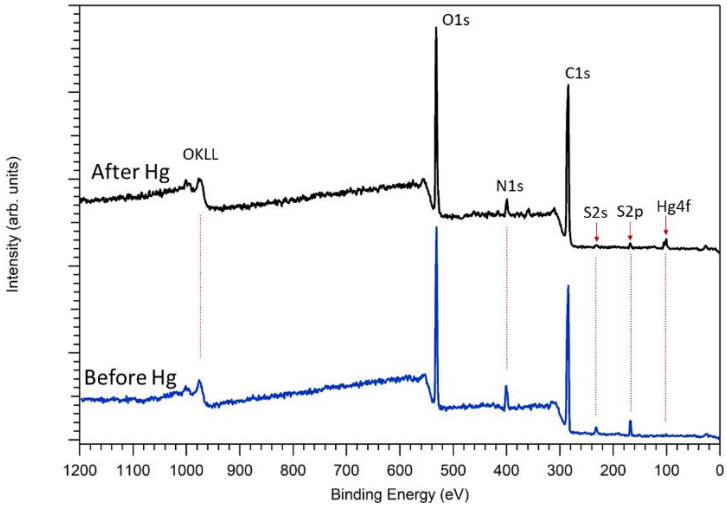

Figure S2.7 Survey XPS spectra of GOPEI before (blue) and after (black) Hg exposure.

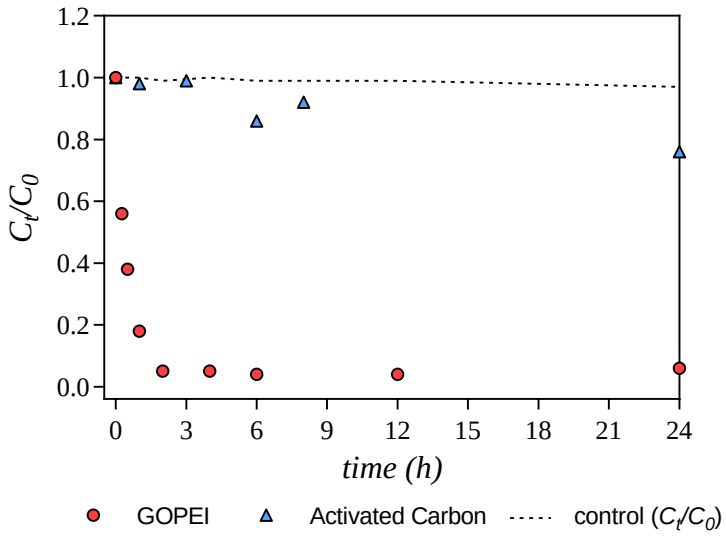

Figure S2.8 Normalized concentration of Hg in solution (C_t/C_0) during the contact time (h) with 10 mg L^{-1} of GOPEI and Activated Carbon in ultrapure water spiked with Hg.

Tables

Table S2.5 Sorption reaction kinetic models.

Kinetic model	Equation	References
Pseudo-first-order (Lagergren)	$q_t = q_e(1-e^{-k_1 t})$	(1)
Adsorption capacity Pseudo-second-order (Ho)	$q_t = \frac{q_e^2 k_2 t}{1+q_e k_2 t}$	(2)
Elovich	$q_t = \frac{1}{\beta}\ln(1+\alpha\beta t)$	(3)

Where q_t is the amount of metal sorbed per gram of at time t (μmol g^{-1}), q_e amount of metal sorbed per gram of materials at equilibrium (μmol g^{-1}), k_1 rate constant of pseudo-first order (h^{-1}), k_2 rate constant of pseudo-second order (g μmol^{-1} h^{-1}), α initial sorption rate (μmol g^{-1} h^{-1}), β desorption constant (g μmol^{-1}).

Table S2.6 Equilibrium data models.

Equilibrium model	Equation	References
Langmuir isotherm	$q_e = \frac{q_m b_L C_e}{1+b_L C_e}$	(4)
Freundlich isotherm	$q_e = K_F C_e^{1/n}$	(5)
Dubinin-Radushkevich	$qe = \frac{RT}{bT} lnATCe$	(6)
Temkin	$qe = (qs)exp(-k_{ad}\varepsilon^2)$	(7)
Sips	$q_e = \frac{q_m (b_S C_e)^{1/n}}{1+(b_S C_e)^{1/n}}$	(8)

where, q_m is the maximum sorption capacity (μg g^{-1}), b_L is the Langmuir constant related to the free energy of adsorption (L μg^{-1}), C_e is the concentration of metal sorbed in the equilibrium μg. L^{-1}, K_F is a constant related to the adsorption capacity of the sorbent ($\mu g^{1-1/n}$ $L^{1/n}$ g^{-1}) and n is the adsorption intensity or the heterogeneity of the sorbent, b_S is the Sips constant related to the energy of adsorption (L $\mu g^{-1})^{1/n}$

Table S2.7 Amount of Hg(II) sorbed per unit of sorbent mass (qm or qe*) for some materials reported in the literature. Experimental conditions used are also presented when available.

Sorbent	$[Hg)]_{initial}$ (mg L^{-1})	Sorbent dose (mg L^{-1})	pH	qm/qe* (mg g^{-1})	Reference
GOPEI aerogel	**0.025 – 1.5**	**10**	**4 - 9**	**90.3 - 106**	***This study***
Activated carbon	20 - 240	2000	-	147	(9)
Coal	4.8	10000	-	38.8	(10)
Cassia seeds	50 - 700	10-50	6	135	(11)
Banana peel	0.01 - 5	12500	-	0.65	(12)
Reed (Phragmites australis)	10	-	6	0.0369	(13)
Activated carbon obtained from furfural	10 - 40	200	5.5	174	(14)
Pepper Biochars: BP300 BP450 BP600	1 - 50	2000	6	 24.2 18.8 15.1	(15)
ITPRGO	500	1000-3500	1 - 6	624	(16)
Thiol-functionalized magnetite/GO	100	10	-	289.9	(17)
HT-rGO-N CM-rGO-N	1.5 - 11	0.125	5 - 9	63.8 59.9	(18)
CFA-derived Ag0-nanocomposite	10 - 550	5000	2.0	20.5 - 22.3	(19)
CFA-derived zeolite	10	100000	2.5	0.3	(20)
Mesoporous Silica–Gelatin Aerogels	0.030 - 1.0	320	6.0	209	(21)
d-MoS_2/Fe_3O_4 nanosheets	200	200	5	425.5	(22)
Magnetic Fe_3O_4@C	200	50	-	83.1	(23)

Table S2.8 Elemental analysis of natural waters before and after Hg removal studies by GOCH and GOPEI.

Water source	**Tap**		**River Conductivity = 33.1 µS/m**		**Sea Salinity = 34.7**	
	Initial	GOPEI	Initial	GOPEI	Initial	GOPEI
pH	7.13	7.21	4.20	4.11	7.80	7.87
Major elements ($mg\ L^{-1}$)						
Ca	33	33	1.3	1.1	411	398
Na	8.5	8.0	5.5	5.1	> 1000	> 1000
K	1.9	1.9	0.5	0.5	> 500	> 500
Mg	2.0	2.0	0.5	0.5	> 2000	> 2000
Minor elements ($\mu\ L^{-1}$)						
B	10	6.5	4.3	4.2	5346	5300
Al	34	9	54	50	178	11.6
Cr	0.7	0.6	< 0.5	< 0.5	16.8	16.6
Fe	54	<10	12	<5	351	350
Co	< 0.1	<0.1	< 0.1	<0.2	< 40	<40
Ni	< 1	< 1	< 1	< 1	< 20	< 20
Cu	2.7	< 1	< 1	< 1	< 20	< 20
Zn	76	12	7.8	6	1120	830
As	< 2	< 2	< 2	< 2	< 100	< 100
Se	< 2	< 2	< 2	< 2	185	185
Sr	21	24	7	5	9338	9300
Cd	<0.1	< 0.1	0.21	< 0.1	< 40	< 40
Sb	< 0.1	< 0.1	< 0.1	< 0.1	< 2	< 2
Ba	6.1	5.3	2.3	2.0	160	155
Pb	< 0.1	< 0.1	2.2	< 0.2	< 80	< 80

2.7.1 References

[1] S, Lagergren, About the theory of so-called adsorption of soluble substances, K. Sven. Vetenskapsakademiens Handl. 24 (1898) 1–39.

[2] Y. S. Ho, G. McKay, Pseudo-second order model for sorption processes. Process Biochem. 34 (5) (1999) 451–465. https://doi.org/Doi 10.1016/S0032-9592(98)00112-5.

[3] M. J. D. Low, Kinetics of Chemisorption of Gases on Solids. Chem. Rev. 60 (3), (1960) 267–312. https://doi.org/10.1021/Cr60205a003.

[4] I. Langmuir, The adsorption of gases on plane surfaces of glass, mica and platinum. J Am Chem Soc. 40(9) (1918) 1361-403.

[5] D. Cho, E. Kim, Y. Hung, Heavy metal removal by microbial biosorbents. In: Wang LK, Tay J-H, Tay STL, Hung Y-T, eds. Environmental Bioengineering: Humana Press 2010, p. 375-402.

[6] H. Demiral, E. Demiral, F. Tumsek, B. Karabacakoglu, Adsorption of chromium(VI) from aqueous solution by activated carbon derived from olive bagasse and applicability of different adsorption models. Chem. Eng. J. 144 (2008) 188-196. https://doi.org/10.1016/j.cej.2008.01.020.

[7] O. Hamdaoui, E. Naffrechoux, Modeling of adsorption isotherms of phenol and chlorophenols onto granular activated carbon: Part I. Two-parameter models and equations allowing determination of thermodynamic parameters J. Hazard. Mater. 147 (2007) 381-394. https://doi.org/10.1016/j.jhazmat.2007.01.021.

[8] R. Sips Combined form of Langmuir and Freundlich equations. J Chem Phys. 16 (1948) 490-495.

[9] J. N. Sahu, J. Acharya, B. C. Meikap, Optimization of production conditions for activated carbons from Tamarind wood by zinc chloride using response surface methodology. Bioresour. Technol. 101(6) (2010) 1974–1982. https://doi.org/10.1016/j.biortech.2009.10.031.

[10] T. Wajima, K. Sugawara, Adsorption behaviors of mercury from aqueous solution using sulfur-impregnated adsorbent developed from coal. Fuel Process. Technol. 92(7) (2011) 1322–1327. https://doi.org/10.1016/j.fuproc.2011.02.008.

[11] V Singh, S. K Singh, S. Maurya, Microwave induced poly(acrylic acid) modification of Cassia javanica seed gum for efficient Hg(II) removal from solution. Chem. Eng. J. 160(1) (2010) 129–137. https://doi.org/10.1016/j.cej.2010.03.020.

[12] E. Fabre, C. B. Lopes, C. Vale, E. Pereira, C. M. Silva, Valuation of banana peels as an effective biosorbent for mercury removal under low environmental concentrations. Sci. Total Environ. 709 (2020) 135883. https://doi.org/10.1016/j.scitotenv.2019.135883.

[13] P. C. Soto-Ríos, M. A. León-Romero, O. Sukhbaatar, O. Nishimura, Biosorption of mercury by reed (Phragmites australis) as a potential clean water technology. Water, Air, Soil Pollut. 229(10) (2018) 328. https://doi.org/10.1007/s11270-018-3978-8.

[14] M. F. Yardim, T. Budinova, E. Ekinci, N. Petrov, M. Razvigorova, V. Minkova, Removal of mercury (II) from aqueous solution by activated carbon obtained from furfural. Chemosphere. 52(5) (2003) 835–841. https://doi.org/10.1016/S0045-6535(03)00267-4.

[15] X. Dong, L. Q. Ma, Y. Zhu, Y. Li, B. Gu, Mechanistic investigation of mercury sorption by brazilian pepper biochars of different pyrolytic temperatures based on x-ray photoelectron spectroscopy and flow calorimetry. Environ. Sci. Technol. 47(21) (2013) 12156–12164. https://doi.org/10.1021/es4017816.

[16] F. S. Awad, K. M. Abouzeid, W. M. A. El-maaty, A. M. El-wakil, Efficient removal of heavy metals from polluted water with high selectivity for mercury (II) by 2-Imino-4-thiobiuret partially reduced graphene oxide (IT-PRGO). ACS Appl. Mater. Interfaces. 9 (2017) 34230−34242. https://doi.org/10.1021/acsami.7b10021.

[17] J. Bao, Y. Fu, Z. Bao, Thiol-functionalized magnetite/graphene oxide hybrid as a reusable adsorbent for Hg^{2+} removal. Nanoscale Res Lett. 8(1) (2013) 486. https://doi.org/10.1186/1556-276X-8-486.

[18] P. L. Yap, T. T. Tung, S. Kabiri, N. Matulick, D. N. H. Tran, and D. Losic. polyamine-modified reduced graphene oxide: A new and cost-effective adsorbent for efficient removal of mercury in waters, Sep. Purif. Technol. 238 (2020) 116441, https://doi.org/10.1016/j.seppur.2019.116441.

[19] Z. Tauanov, J. Lee, V. J. Inglezakis, Mercury reduction and chemisorption on the surface of synthetic zeolite silver nanocomposites: Equilibrium studies and

mechanisms. J. Mol. Liq. 305 (2020) 112825. https://doi.org/10.1016/j.molliq.2020.112825.

[20] M. Attari, S. S. Bukhari, H. Kazemian, S. Rohani, A low-cost adsorbent from coal fly ash for mercury removal from industrial wastewater. J. Environ. Chem. Eng. 5(1) (2017) 391–399. https://doi.org/10.1016/j.jece.2016.12.014.

[21] P. Herman, I. Fábián, J. Kalmár, Mesoporous silica–gelatin aerogels for the selective adsorption of aqueous Hg(II). ACS Appl. Nano Mater. 3(1) (2020) 195–206. https://doi.org/10.1021/acsanm.9b01903.

[22] Y. Song, M. Lu, B. Huang, D. Wang, G. Wang, L. Zhou, Decoration of defective MoS_2 nanosheets with Fe_3O_4 nanoparticles as superior magnetic adsorbent for highly selective and efficient mercury ions (Hg^{2+}) removal. J. Alloys Compd. 737 (2018) 113–121. https://doi.org/10.1016/j.jallcom.2017.12.087.

[23] Z. Chen, Z. Geng, Z. Zhang, L. Ren, T. Tao, R. Yang, Z. Guo, Synthesis of Magnetic Fe_3O_4 @C Nanoparticles modified with -SO_3H and -COOH Groups for fast removal of Pb^{2+}, Hg^{2+}, and Cd^{2+} Ions. Eur. J. Inorg. Chem. 20 (2014) 3172–3177. https://doi.org/10.1002/ejic.201301500.

Chapter 3

3. Green graphene-chitosan sorbent materials for mercury water remediation

This chapter correspond to the following published article:

nanomaterials

MDPI

http://www.mdpi.com/journal/nanomaterials

Article

Green Graphene–Chitosan Sorbent Materials for Mercury Water Remediation

Ana Bessa [1,2], Gil Gonçalves [1], Bruno Henriques [2,3], Eddy M. Domingues [1], Eduarda Pereira [3] and Paula A. A. P. Marques [1,*]

1 Centro de Tecnologia Mecânica e Automação (TEMA), Mechanical Engineering Department, University of Aveiro, 3810-193 Aveiro, Portugal; arcb@ua.pt (A.B.); ggoncalves@ua.pt (G.G.); eddy@ua.pt (E.M.D.)

2 Centro de Estudos do Ambiente e do Mar (CESAM) & Department of Chemistry, University of Aveiro, 3810-193 Aveiro, Portugal; brunogalinho@ua.pt

3 Laboratório Associado para a Química Verde-Rede de Química e Tecnologia (LAQV-REQUIMTE) & Department of Chemistry, University of Aveiro, 3810-193 Aveiro, Portugal; eduper@ua.pt

* Correspondence: paulam@ua.pt

Received: 18 June 2020; Accepted: 24 July 2020; Published: 28 July 2020

check for updates

3.1 Abstract

The development of new graphene-based nanocomposites able to provide synergistic effects for the adsorption of toxic heavy metals in realistic conditions (environment) is of higher demand for future applications. This work explores the preparation of a green nanocomposite based on self-assembly of graphene oxide (GO) with chitosan (CH) for the remediation of Hg(II) in different water matrices, including ultrapure and natural waters (tap water, river water and seawater). Starting at a concentration of 50 μg L^{-1}, the results showed that GO-CH nanocomposite have an excellent adsorption capacity of Hg (II) using very small doses (10 mg L^{-1}), in ultrapure water, with a removal percentage (% R) of 97 %, after only 2h of contact time. In case of tap water % R was of 81.4% after 4 h contact time. In the case of river and seawater, the GO-CH nanocomposite showed a limited performance due the high complexity of the water matrices, leading to the residual removal of Hg(II). The obtained residual concentration of Hg(II) at equilibrium in river and seawater for GO-CH was 13% R and 7% R, respectively. Our studies conducted with different mimicked sea waters, revealed that the removal of mercury is not affected by the presence of NO_3^- and Na^+ (> 90% R of Hg(II)), however in the presence of Cl^- the mercury removal was virtually non-existent (1% R of Hg(II)), most likely because of the formation of very stable chloro-complexes of Hg(II) with less affinity towards GO-CH.

Keywords: Removal of Hg, Real waters, Chitosan, Graphene Oxide-based nanocomposites

3.2 Introduction

Water pollution is one of the most severe problem our planet faces, and managing water resources sustainably under climate change, population growth and economic development poses novel challenges in the 21st century, termed the Century of the Environment [1,2]. Heavy metals are an extreme hazardous class of non-biodegradable and bio-accumulative elements that present a serious threat to all forms of life, even at trace levels concentrations [3]. Among the heavy metals, the United States (US) Government Agency for Toxic Substances and Disease Registry mercury ranks mercury (Hg) as the third most toxic elements to human health [4]. Aquatic ecosystems are an important part of the global biogeochemical cycle of Hg. Inorganic Hg can convert to a toxic methyl Hg form (CH_3Hg) in water (river and sea) driving one of the main human exposure path by the consumption of fish, particularly if caught in the sea [5]. Once it reaches the food chain, Hg tends to bioaccumulate, ultimately causing harmful effects to human health [6,7]. Therefore, Hg presents a significant risk to both the global environment and human health as well expressed in Europe's environment report [8].

In this context, there is a high demand to develop advanced green materials and technologies with high performance for water remediation. Nanotechnology has earned wider attention and the use of engineered nanomaterials show promise for global water treatment [9,10]. One can find many examples in the literature of natural based materials used as sorbents for several prejudicial metal(oid)s, such as a myriad of tree leaves, agricultural biowaste, or even banana peels [11–13].

Recently, new graphene-based three dimensional (3D) macrostructures with enhanced sorption capability towards hazardous organic molecules and heavy metal(oid)s have been proposed [14–18]. Graphene consists in a single atomic layer of graphite with bond length between carbon-carbon of 0.142 nm and like graphite, the atoms in graphene are arranged in a hexagonal lattice. As there are only sp^2 carbon atoms on the graphene sheets, pristine graphene can only provide van der walls force to bind adsorbates, so it is not a good adsorbent for many types of contaminations, such as metal ions. Graphene oxide (GO), sparked huge interest among researchers as it retains plenty of the properties of the highly valued pristine graphene, but it is much easier, and cheaper, to make in bulk

quantities and easier to process. It is composed of planar graphene-like aromatic domains (sp^2) of random size separated by sp^3-hybridized carbons decorated by hydroxyl, epoxy and carboxyl groups [19]. GO is amphiphilic, has a negative charge and surface comprising multi oxygen-containing groups. This multitude of oxygen functional groups allows an incredible variety of chemical interactions with other molecules. For example, hydrogen bonds between hydroxyl groups from GO and other hydroxyl-rich molecules; electrostatic interactions between the negatively ionized carboxyl groups located at the edges and positive charged species; π-π interactions with other π-conjugated materials due to the delocalized electrons over sp^2-hybridized carbon atom domains [20]. The chemical composition and molecular structure make GO behave like a polymer [21]. Therefore, the self-assembly of 2D GO nanosheets in the presence of natural polymers into 3D macrostructures is possible due to the establishment of previously described chemical and/or physical bonds and can result in the formation of a hydrogel [17]. This is a relatively simple method which can be easily scale-up for commercial or industrial use [18]. Recently, our group developed the 3D GO structures by chemically modifying the surface GO with nitrogen functional groups (3DGON) increasing its removal efficiency towards Hg up to 95% [22].

A sensible polymer selection for the development of the above-mentioned GO-based 3D macrostructures would focus on the presence of amine functional groups due to the high affinity these groups and the oxygen functional groups from GO. Additionally, these polymers type show a natural high sorption ability for different pollutants [23], thus this combination may result in a synergistic behaviour for improved adsorption of several pollutants in water. A widely accessible natural biopolymer obtained from the alkaline deacetylation of chitin, chitosan (CH), is hydrophilic, environmentally friendly and non-toxic and has been used as agent for the removal of dyes and heavy metals from contaminated waters [24]. For the specific case of heavy metal(oid)s, the adsorption onto GO-CH based materials has been studied for the removal of Cr [25–30], Cu [25,31–34], Pb [25,31,32,35–37], As [32,38], Au and Pd [39] or U [28]. GO-CH was also applied to remove Hg[40], although only in deionized water, and for relatively high concentrations of material (1 $g \cdot L^{-1}$) and Hg (up to 500 $mg \cdot L^{-1}$), which in addition to not being environmentally friendly, are not representative of real cases.

An easy and environmentally-friendly way to obtain GO-CH would be by the formation of hydrogels by self-assembly, which was already reported by recent works in the literature [31,33,41]. In this case, CH acts as a crosslinking agent, and the presence of amine groups in the positively charged CH strongly attract the negatively charged GO through electrostatic interactions. Additionally, hydrogen bonds should also occur between both GO and CH, creating stable hydrogels converted into aerogels by freeze drying. Nowadays, most of the reports in literature are restricted to explore graphene-chitosan nanocomposite materials for heavy metals adsorption in batch studies with ultrapure water. Evaluation of these graphene-based sorbents under real wastewater conditions is thus needed, to provide critical information regarding their real applicability on water remediation.

The aim of the study was the use of a simple, eco-friendly, and easily scalable preparation of a GO-CH nanocomposite and its applicability in Hg removal from different natural water matrices, starting at more realistic relatively low concentration of Hg (50 $\mu g \cdot L^{-1}$), which corresponds to the maximum allowable limit in wastewater discharges from industry in Europe [42]. GO-CH nanocomposites showed an excellent adsorption performance and efficiency for Hg in ultrapure water and tap water (q_e = 4554 and 4700 $\mu g\ g^{-1}$, respectively). However, in other natural waters, where the complexity of the matrices is much higher, a significant decrease on the adsorption ability of the nanocomposite material was observed, particularly seawater assays.

3.3 Materials and methods

3.3.1. Materials synthesis

Chitosan (CH) with M.W. 310000 – 375000 (Sigma Aldrich) solution with a concentration of 5 mg mL^{-1} was prepared in distilled water and acetic acid (1% v/v). Graphene oxide (GO) water dispersion (0.4 wt% concentration from Graphenea-Spain) was added to the polymer solution with a targeted ratio of 24 % v/v (GO-CH). This ratio was optimized in order to achieve the most stable hydrogel. The pH of both GO and CH solutions were modified to 2 before mixing, using 0.1 $mol \cdot dm^{-3}$ NaOH (Sigma Aldrich) or

HCl (Sigma Aldrich) solutions. After the mixture, the resulting solution was quickly shaken for 10 s to form the hydrogel, which was subsequently freeze-dried (Telstar LyoQuest HT-40, Beijer Electronics Products AB, Malmoe, Sweden) at -80 ºC, obtaining 3D porous structures. The lyophilized samples were then washed in MQ water (ultrapure water from Milli-Q®, USA; 18 MΩ cm^{-1}) for 12 h to remove acidic residues. Finally, the washed sample was freeze-dried once more and stored until the adsorption experiments.

3.3.2. Materials characterization

XPS spectra were obtained in an ultra-high vacuum (UHV from SPECS, Berlin, Germany) system with a base pressure of $2x10^{-10}$ mbar. The high-resolution spectra were taken at normal emission take-off angle and with a pass-energy of 20 eV, which provides a global instrumental peak broadening of about 0.5 eV. The spectra were rectified in binding energy by referencing to the first component of the C1s core level at 284.5 eV (Csp^2). The chemical structure of the GO-CH aerogels, GO and CH were analysed via Attenuated Total Reflectance Fourier Transform Infrared (ATR-FTIR) in a Bruker Tensor 27 FT-IR spectrometer (Bruker Corporation, Massachusetts, USA). The spectra were obtained between 4000 and 400 cm^{-1}, using a resolution of 4 cm^{-1} and 256 scans. The microstructure of the GO-CH scaffolds was observed using scanning electron microscope (SEM) in a Hitachi SU-70 (Tokyo, Japan) operating at 15 kV. The zeta potential was measured, at different pH, in a Malvern Panalytical Nano-ZS Zetasizer (Malvern, United Kingdom). The specific surface area of the GO-CH aerogel was determined by means of N_2 sorption isotherms, using the Brunauer Emmett Teller (BET) method, in a Gemini Micromeritics device (Norcross, USA). The results of the BET study are presented in the SI section.

3.3.3 Water collection and characterization

For this work, different types of waters (MQ, tap, river and sea) were used to evaluate the efficiency of Hg removal by GO-CH in natural conditions. The Vouga river was the source for the river water (40°40′42″ N, 08°22′18″ W) whereas the seawater was collected at the beach in Vagueira, near Aveiro (40°32′58″ N 8°46′31″ W). Tap water was sourced at the University of Aveiro. The full physicochemical characterization of the

waters used where already reported elsewhere [43,44]. After being filtered (0.45 μm pore size filter), all the waters used in this work where left for at least 24 h to pre-equilibrate after spiking with Hg, before joining the sorbent. The pH of the contaminated solutions was ~ 4.0, 7.1, 4.3 and 7.8 for MQ, tap, river, and sea waters, respectively. The elemental composition of the major and minor elements of the untapped matrix was determined by Inductively Coupled Plasma (ICP, Jobin–Yvon JY70 Plus Spectrometer, New Jersey, USA).

3.3.4 Mercury sorption studies

The study of the sorption of Hg onto GO-CH was executed in lot experiments, where ~10 mg of CO-CH was added to 1 L of Hg spiked water for up to 24 h contact, in Schott glass bottles, under consistent magnetic stirring (700 rpm). A certified standard Hg solution (1001 ± 2 mg L^{-1} of Hg(II) in HNO_3 0.5 mol L^{-1}, from Merck) was used to spike the ultra-pure (MQ), tap, river, and sea water with a concentration of 50 μg L^{-1}, which matches the maximum value allowed for Hg in discharges (Directive 84/156/EEC) [42]. It should be noted that European Union imposed that Hg emissions, discharges and losses to water cease or be phased out by 2021 (Directive 2013/39/EU 2013) [45]. The sorption kinetics was evaluated by removing 5 to 10 mL of water at pre-determined periods of time, followed by centrifugation at 5000 rpm for 3 min. The supernatant liquid was the transferred to a small Schott glass bottle (25 mL) and acidified to pH ≤ 2 using Suprapur© HNO_3 (65%v/v). The amount of Hg was quantified using cold vapour atomic fluorescence spectroscopy (CV-AFS), in a PSA 10.025 Millennium Merlin Hg analyser (Orpington, UK) with $SnCl_2$ (2% m/v in HCl 10% v/v) as a reducing agent. All tests were made in duplicate and a control experiment, consisting in Hg contaminated water without GO-CH, was always running simultaneously.

3.3.4.1 Analysis of sorption data

The performance of a removal process (R%) was evaluated by calculating the percentage of sorbate (Hg) removed from the solution by the sorbent (GO-CH) using the following mathematical expression:

$$R(\%) = \frac{C_0 - C_t}{C_0} \times 100 \quad (1)$$

where C_0 represents the original Hg concentration in solution (μg L^{-1}) and C_t is the Hg concentration at a given time t (μg L^{-1}). Presuming that all the removed Hg remained in the sorbent, one can estimate the concentration of Hg in the material at time t, qt (μg g^{-1}) using:

$$q_t = \frac{(C_0 - C_t)}{m} \times V \quad (2)$$

where V (L) is the volume of the solution and m (g) the mass of sorbent. When an equilibrium situation is reached, equation 2 can be rewritten taking into account $t = t_e$, $q_t = q_e$ and $C_t = C_e$ [22]. In most cases the actual initial concentration of the spiked solutions shows small deviations from the nominal initial concentration, thus, in order to compare results between trials, the analysis of the results was presented in terms of standard concentrations C_t/C_0.

3.3.4.2 Kinetics and equilibrium models

In this study, the kinetics of Hg uptake by GO-CH was followed by using three reaction models in their non-linear form to fit the experimental data [46], specifically Lagergren pseudo-first-order model [47], Ho's pseudo-second-order model [48] and the Elovich model [49] (Table S3.1). For a more detailed study, two diffusion-based models were also applied, namely Boyd's film-diffusion [50] and Weber's pore-diffusion [51] models (details in SI).

3.4 Results and discussion

3.4.1 Chemical and structural analysis

The synthesis of the nanostructured composite GO-CH was completed by simply shaking the mixture of the GO and CH solutions. The strong electrostatic attraction among

the two components of the mixture leads to the formation of stable gels at room temperature. After gelation, GO-CH was lyophilized to obtain the respective foams in dry state, as an aerogel. Figure 15 depicts SEM images of GO-CH nanocomposite at different magnifications, detailing the typical structural macroporosity of these aerogels, which has an alveolar-like microstructure.

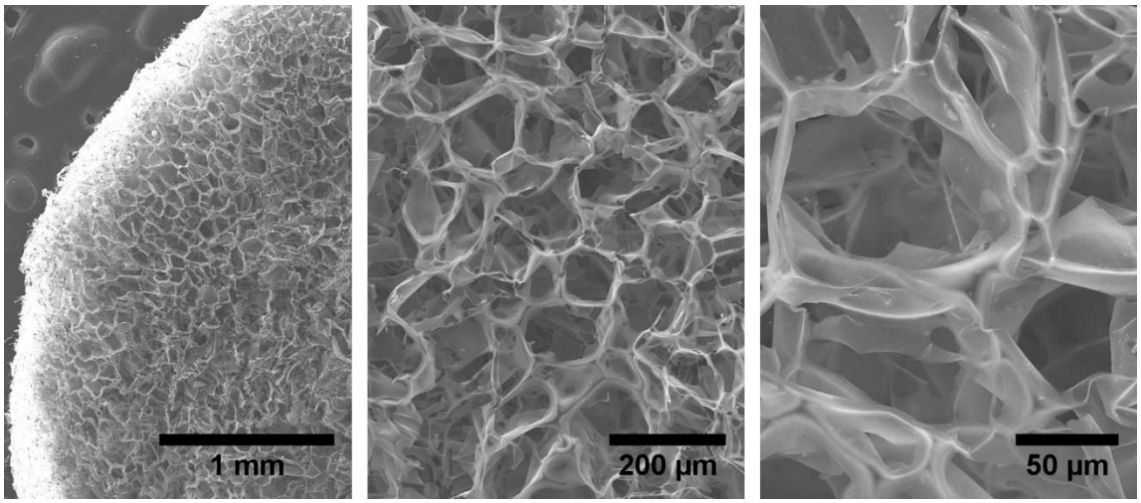

Figure 15 Details of SEM micrographs at different magnifications of the prepared GO-CH aerogels.

Figure 16 compares the FTIR spectra for GO, CH and GO-CH, showing only the details below 2000 cm^{-1}, for greater clarity. The GO exhibits the typical hydroxyl peak at 3440 cm^{-1} (O-H stretch), 1402 cm^{-1} (CO-H symmetry stretch), carboxyl peaks at 1722 cm^{-1} (C=O stretch) and 1037 cm^{-1} (C-O stretch), and the peak at 1607 cm^{-1}, which can be attributed to the epoxy group (COOH asymmetry stretch) and also to sp^2 carbon skeletal network (C=C stretch) [52,53]. The spectra for CH exhibits a broad peak centred at ~ 3257 cm^{-1} (-NH_2 extension, -OH stretching and inter hydrogen bonds), a peak at 2868 cm^{-1} (-CH stretch), a peak at 1631 cm^{-1}, which corresponds to the NHCO group (C=O stretch), at 1543 cm^{-1}, which can be attributed to NH_2 bending mode. The peak at 1405 cm^{-1} can be assigned to -CH bend, while the one at 1150 cm^{-1} can be assigned to C-O-C asymmetric stretching. The bands at 1062 cm^{-1} and 1026 cm^{-1} can be attributed to skeletal vibrations of C-O (stretching) while the peak at 897 cm^{-1} corresponds to the pyranoid ring stretching mode [26,52,54]. In the case of the GO-CH nanocomposites it is possible to observe that the band corresponding to C-O stretching mode is relatively more intense than for the GO due to the presence of -OH groups from chitosan. The lower relative intensity of the peak

at 1717 cm^{-1} (C=O stretching) than for GO confirms the interaction, at least partial, of the carboxylic groups of GO with amine group of chitosan [52].

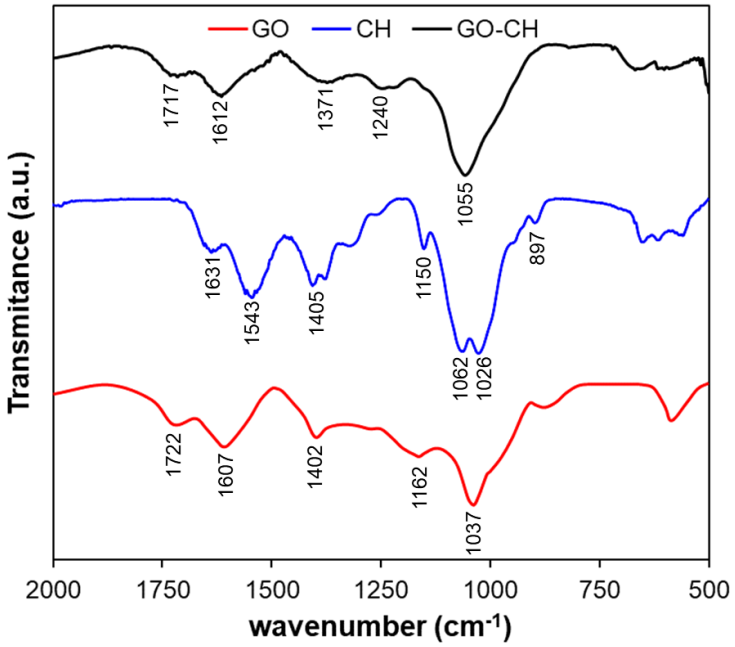

Figure 16 FTIR spectra for GO, CH and the GO-CH nanocomposite.

3.4.2 Mercury sorption studies

The reduction of Hg concentration as a function of time was followed in 4 distinct water matrixes (MQ, tap, river and sea water) in the presence or absence (control) of GO-CH, as depicted in Figure 17. The concentrations of Hg in the control solution were observed to be relatively constant over the whole test period, which indicates that a possible loss of Hg due to the adsorption in the glass walls or due to volatilization were insignificant. Under the presence of GO-CH sorbents, there was an evident decrease in the concentrations of Hg, C_t/C_0, from 1.0 to < 0.1 in MQ water, and from 1.0 to 0.2 in tap water (Figure 17). The results suggest a strong interaction between the active sites at the surface of the nanocomposite and the Hg ions. At the beginning of the experiments the surface of the sorbent material is free of metal, thus inducing a high concentration gradient between the solution and the nanocomposite. In MQ water, after the initial rapid descent, the sorption equilibrium is reached at t = 2 h. In tap water, Hg sorption rate is slower,

reaching the equilibrium at t = 4 h, as the driving force decreases. In the case of river and sea waters (Figure 17), GO-CH was not efficient in reducing the Hg contamination. This observation emphasizes the importance of studying metal adsorption in real waters, which is overlooked in most of the studies, leading to potentially misleading affirmations as for the real potential of the studied materials.

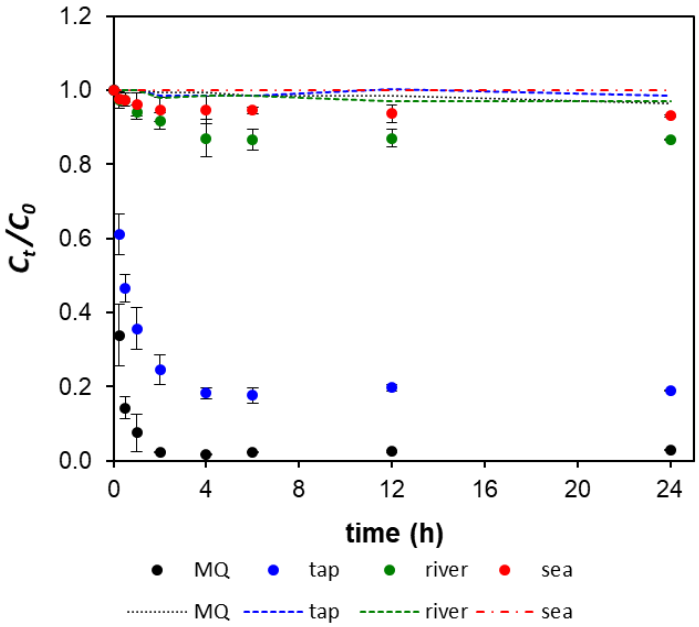

Figure 17 Evolution of the normalized concentration of Hg in solution (Ct/C0) as a function of time (h) for ~10 mg L-1 of GO-CH nanocomposite in different water matrixes contaminated with Hg. The dotted lines represent the control Hg spiked waters. Initial concentration of Hg where ~50 µg L^{-1}. The results correspond to mean ± standard deviation of 2 replicates.

Figure 18 depicts the efficiency of GO-CH in the Hg decontamination process, in terms of maximum removal percentage (% R) and the time needed to reach equilibrium, which was contrasted to the legal values for the presence of Hg in water [45,55,56]. In MQ and tap water, the sorption kinetics showed to be very fast, which is promising in view of a practical application [57].

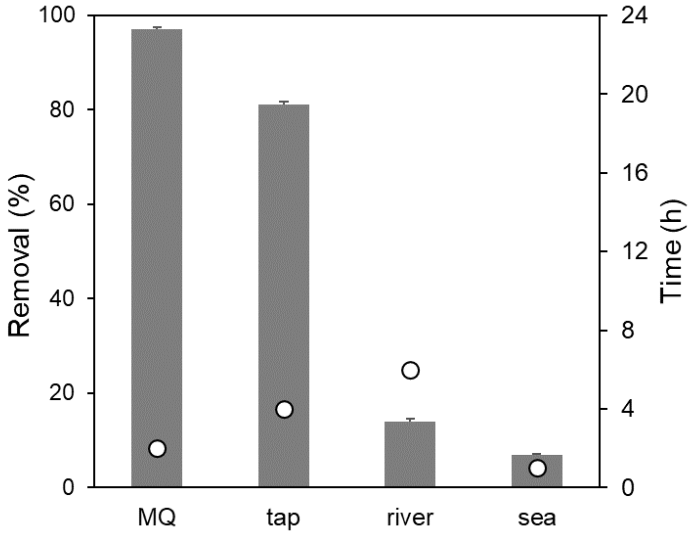

Figure 18 Efficiency of GO-CH in the removal of Hg from contaminated MQ, tap, river and sea waters: (bars) percentage of Hg removed at equilibrium and (circles) time for equilibrium. The original concentration of Hg was 50 μg L^{-1}; the amount of GO-CH used was 10 mg L^{-1}. The results are a mean values of 2 replicates.

The equilibrium, after only 2 h, the remaining Hg in the liquid phase for the system with GO-CH in MQ water was 1.3 μg L^{-1} (in line with the European guideline for drinking water quality of 1 μg L^{-1}) [45]. Kysas *et al.* [40] also used a GO-CH composite to remove Hg from MQ water and showed similar efficiency (~95 %R) and equilibrium time, but starting from a much higher metal concentration (100 mg L^{-1}) which corresponds to a much higher residual Hg concentration after the equilibrium was reached (~5 mg L^{-1}). In the case of tap water, the residual Hg concentration was 9.5 μg L^{-1}, but this value was, nevertheless, attained after only 4 h of contact time. This value is closer to the World Health Organization (WHO), of 6 μg L^{-1} for inorganic mercury for the case of a 60-kg adult consuming 2 L of water a day and distributing 10% of the total daily intake (TDI) to drinking-water [58].

However, for river and sea water, GO-CH revealed to be inefficient in removing Hg from such matrices, with concentrations at equilibrium of 43.5 and 46.5 μg L^{-1}, respectively.

3.4.3 Kinetic modelling

Represented in Figure 19 are the experimental values of Hg sorbed onto GO-CH as μg of Hg adsorbed per g of GO-CH over a period of time (24h) or q_t (μg g^{-1}), as well as the adjustments made by the kinetic models of pseudo-first order (PFO), pseudo-second order (PSO) and Elovich.

The quality of the fits and the values of the kinetic parameters resulting from the modelling are shown in Table 8. In general, for MQ and tap water, the models used were deemed suitable to describe the kinetics of Hg sorption on GO-CH ($0.9379< R^2 <0.996$). In the case of river and sea water, the low removal values and the high variability in the results led to poor fitting parameters ($R^2< 0.8289$). For GO-CH in MQ water, the model that fits the most is the PFO model, which can be confirmed by the higher values of R^2 (0.996) and low Sy.x values (139). Nevertheless, this model slightly underestimated the value of q_e (PFO = 4544 and exp.= 4554).

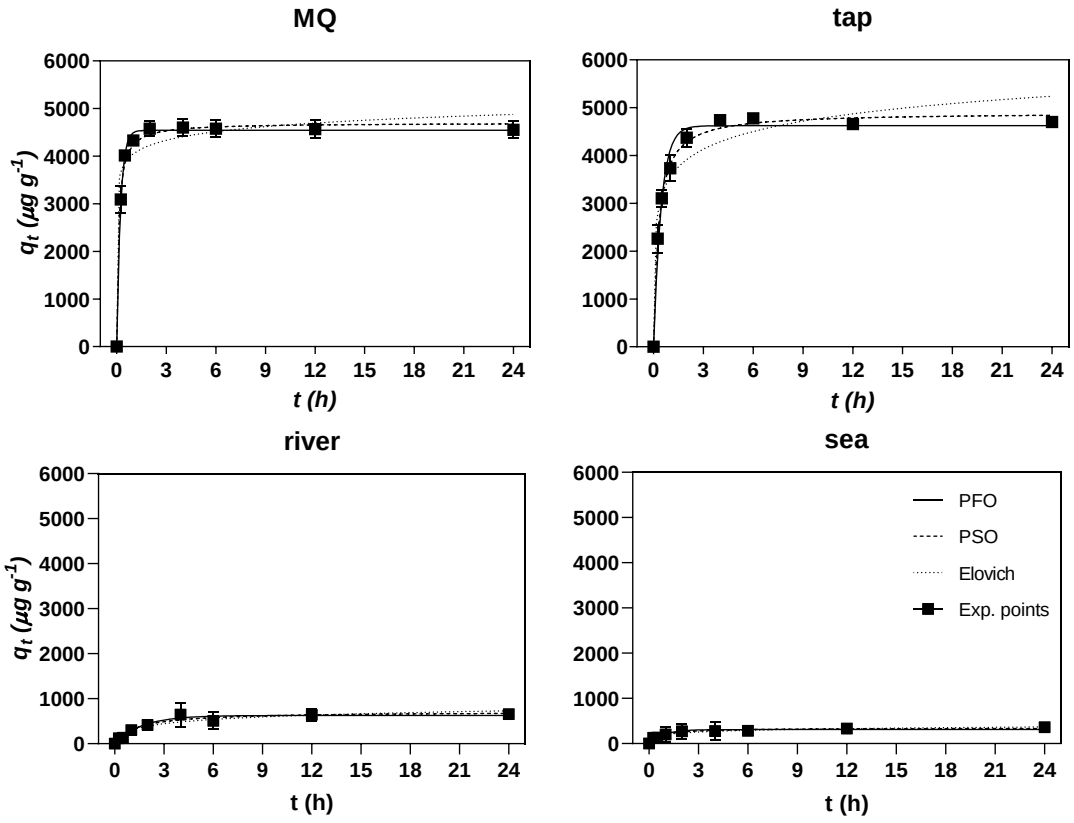

Figure 19 Experimental points of the PFO, PSO and Elovich models to experimental data regarding the sorption of Hg onto GO-CH over time. The concentration of GO-CH and Hg(II) in the matrices were of ~10 mg L^{-1} and ~50 μg L^{-1}, respectively.

On the contrary, the kinetic model with the worst performance in the adjustments was the Elovich model (with values of R_2 = 0.9533 and Sy.x = 328). When PFO represents the experimental points better, the surface of the sorbent is deemed to be homogeneous, and in theory, only one binding mechanism is possible [59]. Therefore, it is proposed that, in the process of Hg adsorption onto GO-CH in MQ water, there is no restriction of surface area and binding sites, and thus the adsorption process resembles an homogeneous one. In the case of tap water, the model that most closely fits the data is PSO, with R^2 = 0.99 and Sy.x = 161, but PFO (R^2 = 0.9789 and Sy.x = 234) shows a closer q_e value to the experimental values than PSO (PFO = 4623, PSO = 4899 and exp.= 4700).

Table 10 Fitting parameters for the several reaction models applied to the adsorption of Hg on GO-CH for the water matrices in this study. Experimental qe were also added for comparison**.**

Models	**Water matrices**			
	MQ	**tap**	**river**	**sea**
q_e1 exp ± SD (μg g^{-1})	4554 ± 180	4700 ± 66	656 ± 16	360 ± 19
Pseudo First Order				
q_e1 ± SD (μg g^{-1})	4544 ± 40	4623 ± 74	627 ± 47	310 ± 32
k_1 ± SD (h^{-1})	4.44 ± 0.24	2.20 ± 0.16	0.61 ± 0.17	1.19 ± 0.49
R^2	0.9960	0.9789	0.8289	0.5973
Sy.x	139	234	113	91.1
Pseudo Second Order				
q_e2 ± SD (μg g^{-1})	4698 ± 58	4899 ±6 3	711 ± 67	342 ± 41
k_2 ± SD (h^{-1})	0.0019 ± 0.0002	0.0007 ± 0.00005	0.001 ± 0.0004	0.0045 ± 0.003
R^2	0.9877	0.9900	0.8256	0.6217
Sy.x	168	161	114	88.3
Elovich				
ß ± SD (g μg^{-1})	0.0038 ± 0.0008	0.0019 ± 0.0002	0.0071 ± 0.002	0.019 ± 0.006
α ± SD (μg g^{-1} h^{-1})	$1.36x10^9$ ± 4.49 $x10^9$	413852 ± 360766	1069 ± 640	2046 ± 2505
R^2	0.9533	0.9379	0.7928	0.6279
Sy.x	328	401	124	87.6

To gather more information on the Hg sorption mechanism onto GO-CH, namely on most probable rate-controlling steps, a Piecewise Linear Regression (PLR) [60] of the adsorption data was performed based on the film-diffusion model proposed by Boyd [50] and the intraparticle-diffusion model, proposed by Weber [51]. In all the water matrices, Boyd's method showed a first linear segment that included the origin, which is a sign that film-diffusion is not the rate-defining step in this sorption process [61,62]. In the case of

Weber's model, the Akaike Information Criteria (AIC) was used to compare the fits (to determine the most probable number of segments), indicating a two-step fitting as the more likelihood, for all the water matrices. Therefore, the postulation that the sorption takes place in two diffusion steps is the most likely to be correct. Figure 20 shows the experimental (exp.) points (full symbols) overlapped by the estimated (est.) values (lines) and the kinetics parameters are presented in Table 9, for all the water matrices. The first linear segment corresponds to a step where the diffusion is faster due to higher concentration gradient, which can correspond to the diffusion in the larger pores. The second segment can be ascribed to the equilibrium stage with a much less marked slope, which is an indication that the intra-particle diffusion is reduced as the concentration gradient decreases.

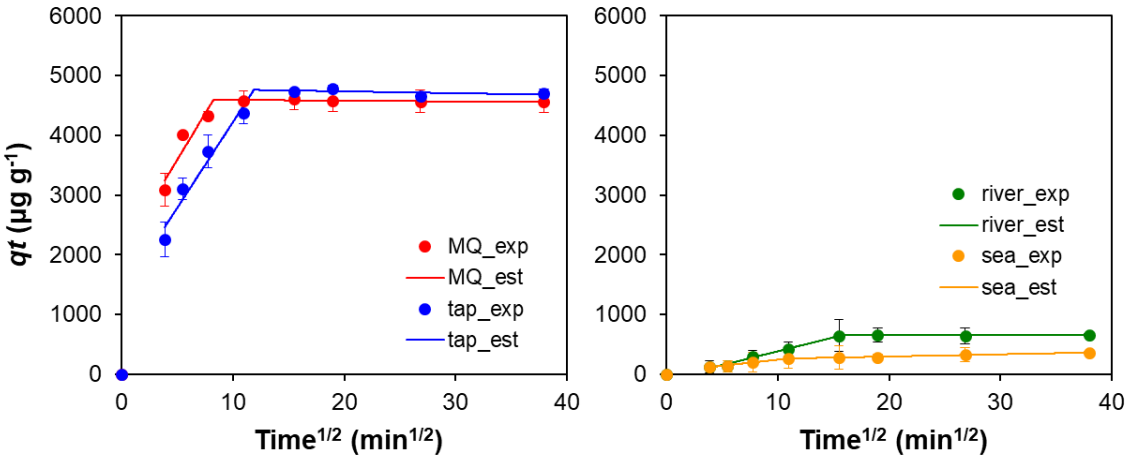

Figure 20 Best-fit results for the kinetic modeling of Hg sorption onto CO-CH using Weber's intraparticle-diffusion model, for all the matrices used in this work. Full symbols represent the experimental data while the segmented lines represent the estimated values

Table 11 Kinetic parameters resulting from the use of Weber's intraparticle-diffusion model to fit the experimental sorption data of Hg onto GO-CH.

Matrix	stage	Breakpoint (min)	K_i (µg g^{-1} $h^{-1/2}$)	R^2
MQ	1	68	307.7	0.8647 (n=4)
2	2	-	-1.285	0.6257 (n=5)
tap	1	141	286.7	0.9534 (n=5)
2	2	-	-3.062	0.3554 (n=4)
river	1	247	46.45	0.9854 (n=5)

2	2	-	0.1609	0.0467 (n=4)
sea	1	120	20.53	0.8743 (n=4)
	2	-	3.663	0.9536 (n=5)

3.4.4 Removal mechanism

To study the sorbents surface charge, the zeta potential of GO-CH in MQ water was measured in different pH (2-12) and the results are shown on Figure 21. GO-CH zeta potential shows that is has an amphoteric nature, with a point zero charge (pzc) of 6.7, where the CH primary amines are protonated for lower pH. This trend is in accordance to previous reports for similar materials [30,34,63].

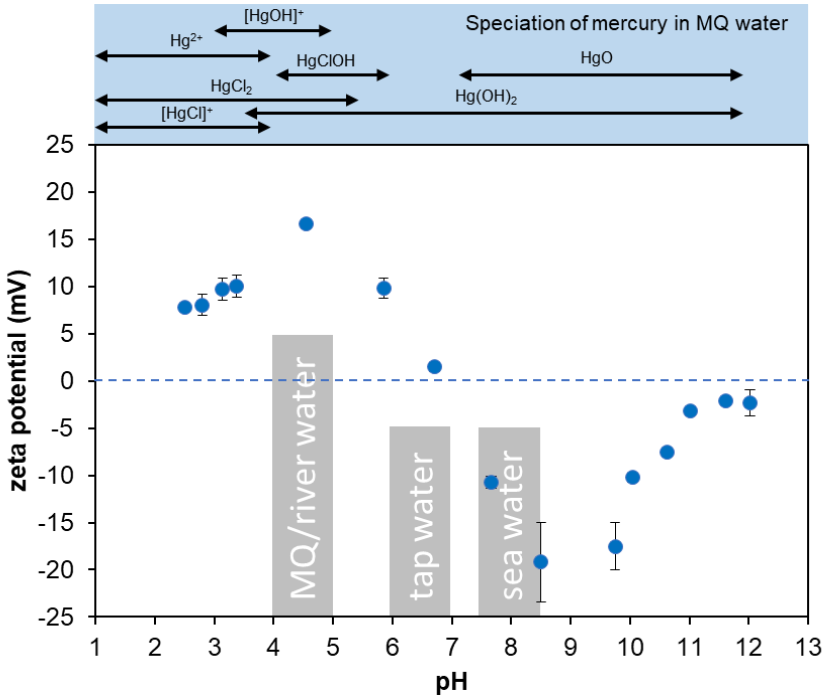

Figure 21 Zeta potential for the GO-CH aerogels at different pH. The grey boxes represent the pH of each type of water at which the experiment was conducted. At the top, one can find the speciation for Hg in MQ water as a function of pH.

Speciation studies in ultrapure water (pH = 4) suggested that Hg in solution is mainly present in the neutral form: 93.0% $Hg(OH)_2$, and as diminute contribution of positive ions 5.5% $Hg(OH)^+$ and 1.5% Hg^{2+} (determined by Visual MINTEQ 3.1). Interestingly, for GO-CH in MQ (pH 4.0) or tap water (pH 7.1) the removal efficiency is

quite high, even if the surface is mostly protonated, as shown by the zeta-potential study (Figure 21). Thus, it is anticipated that, for these waters, and accordingly to the kinetic study, the removal mechanism of these GO-based macrostructures is mainly governed by physical sorption where intermolecular attractions such as induced dipole-dipole interactions should be predominant. In the case of river water (pH 4.3) the removal efficiency drops, which can be linked to the presence of different ions (see Table S3.2), which may compete directly with Hg for the sorbents active sites, together with the existence of some organic matter which can interact with the Hg ions. At the pH of sea water (pH 7.8), GO-CH does not adsorb much Hg, in spite of showing a negative zeta-potential, although the formation of Hg chloro-complexes must be considered in this process. With this respect, further tests were conducted for interpretation of the experimental data observed for seawater solutions (see section 3.5).

The XPS survey spectra of the GO-CH nanocomposites are shown in Figure 22, before (black line) and after (red line) the contact with Hg solution, in MQ water. Figure 22a shows the anticipated peaks for O1s, C1s and N1s, attributed to the structural composition of the two components in the nanocomposite materials. A residual S2s peak can also be detected, most probably a remaining from the synthesis of GO. While the oxygen and carbon peaks result from the contribution of both GO and CH, naturally, the nitrogen peaks are attributed only to the structural contribution of the CH. The high-resolution XPS spectra (HR-XPS) with curve fitting for C1s of GO-CH nanocomposites (Figure 22b) shows the presence of the C=C groups at 284.5 eV and C-O/C-N functional groups at 286.4 eV. The HR-XPS spectra with curve fitting for N1s (Figure 22c) displays peaks at 398.8 eV, that corresponds to the presence of the free amine groups of the polymer, and at 401.3 eV, that corresponds to N^+ species, suggesting the formation of weak electrostatic interactions between the primary amines of the polymers and oxygen functionals groups of GO [64,65]. After the exposure GO-CH to the Hg solution, the strong interactions of the amine groups with Hg can be witnessed in the HR-XPS for N1s (Figure 22c), where one can observe the reduction in the relative intensity of the peak at 401.3 eV with a simultaneous increase of the peak at 398.8 eV [66], and also a slight positive shift of the peaks by 0.5 eV [67]. These indications imply that the sorption process occurs primarily by a charge transfer from N to Hg, making N groups the main sorption sites and that the efficiency of the sorption is controlled by its protonation [68]. According

to the Hard Soft Acid Base (HSAB) theory, the softer acid mercury ions should have strong affinity to softer bases like amines, resulting in the formation of metal-chelate complexes[69].

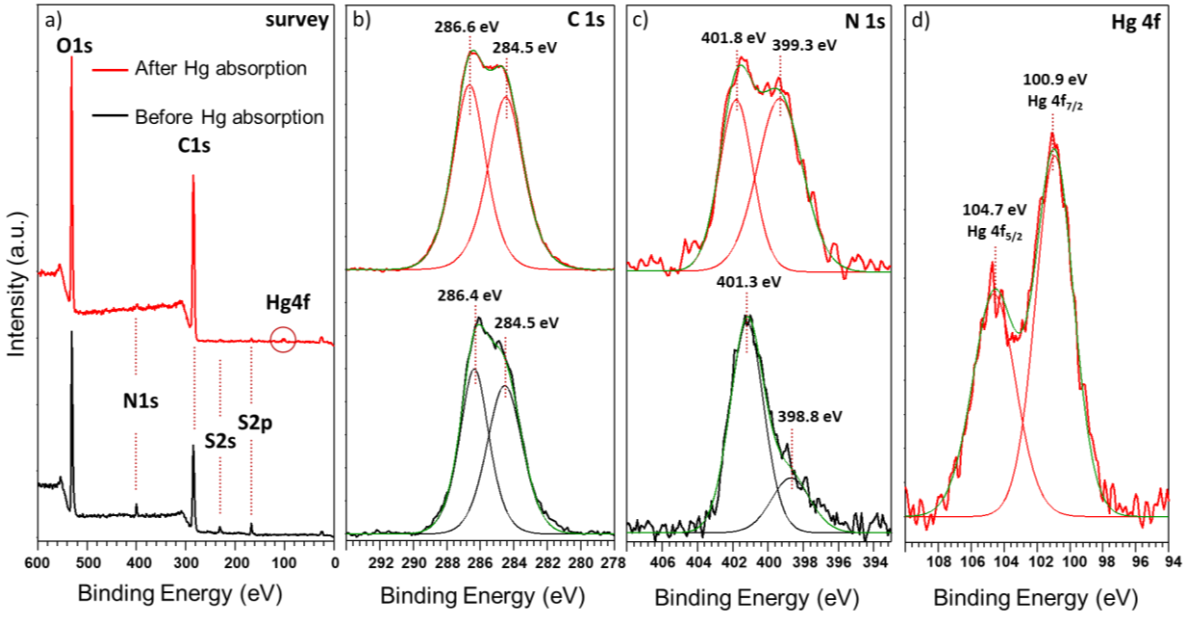

Figure 22 a) XPS Survey spectra of GO-CH before and after contact with Hg(II) solution (MQ water), HR-XPS of the a) C1s, b) N1s and Hg 4f peaks and respective deconvolutions.

The XPS survey of the composite materials (Figure 22a) after the contact with Hg clearly show the presence of the characteristic Hg peak at ~100 eV. The HR-XPS (Figure 22d) shows peaks at 100.9 eV ($Hg4f_{7/2}$) and 104.7 eV ($Hg4f_{5/2}$), which can be attributed to the oxidized state of Hg [22,70], which can be confirmed by the predominance of $Hg(OH)_2$ and $Hg(OH)^+$ at pH 4.0 (Figure 21).

C1s and O1s peaks shows much higher relative intensity (Figure 8a), which represent the majority of the components of GO-CH and no significant changes before and after the contact with Hg solution was detected. Nevertheless, the influence of these elements on the whole sorption process should not be ignored. In fact, in a previous publication by this group, it was shown that the oxygen functional groups have an important contribution to the adsorption mechanism of Hg species in MQ matrix [22].

3.4.5 Influence of co-existing ions in natural waters

ICP was used to characterize the elemental composition of the natural waters spiked with Hg, before and after contact with GO-CH (Table S3.2). The major elements detected in the waters (Ca, Na, K and Mg) presented similar values before and after Hg sorption experiments. In terms of minor elements, in tap water, the most expressive reduction due to the presence of GO-CH occurred for Al, Fe and Zn, whereas in river water only Fe and Pb concentrations were significantly reduced. In sea water, only Al was reduced to half its initial concentration and the remaining elements remained virtually the same.

The removal of Hg by GO-CH in river and sea water was strongly inhibited, which cannot be explained through ζ potential. The pH of the sea water spiked with Hg was 7.8, above the pzc of GO-CH of 6.7, turning the surface of the macrostructure negatively charged, which in theory should favour the removal of Hg cations, unfortunately not observed. In sea water there is a higher presence of cations, principally Na, Mg, K and Ca, as well as a higher concentration of Cl^-, which may hinder the ability of GO-CH to adsorb Hg due to an increased competition for the binding sites at the surface of the macrostructure, or mainly due to changes in the mobility and speciation of Hg (formation of negatively charged chloro-complexes). To clarify this point, experiments conducted in 0.5 M NaCl and 0.5 M $NaNO_3$ (Figure 23), mimicking the ionic strength of sea water, showed that the removal of Hg by GO-CH is practically unaffected by the presence of NO_3^- and Na^+ (93% R of Hg in 0.5 M $NaNO_3$ vs 98% R of Hg in MQ water), the latest being the major cation in sea water. On the other hand, in the presence of Cl^- the removal was virtually non-existent (1% R of Hg) most likely because the formation of very stable chloro-complexes of Hg with less affinity towards GO-CH.

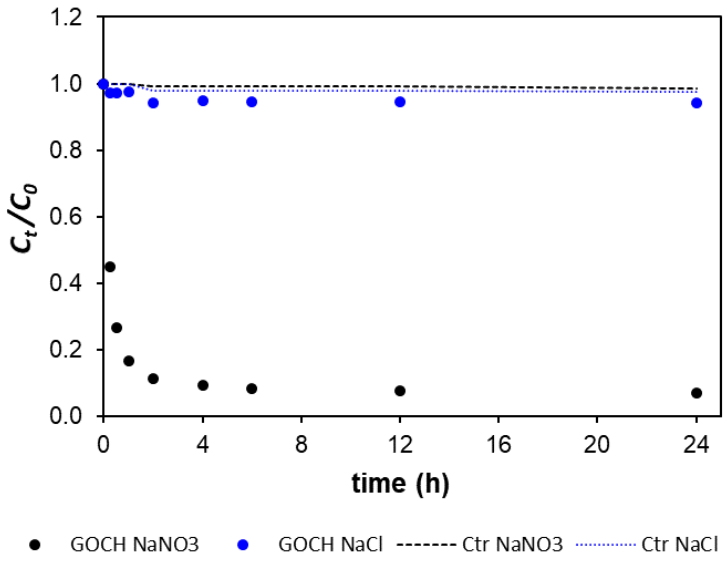

Figure 23 Variation of the normalized concentration of Hg in solution (Ct/C0) as a function of contact time (h), with ~10 mg L-1 of GO-CH in 0.5 M NaCl and 0.5 M NaNO3 solutions. Controls correspond to the absence of sorbent. The original concentration of Hg(II) ~50 µg L^{-1}.

3.6 Conclusion

This study focuses on a simple and eco-friendly synthesis of a GO-CH nanocomposite to obtain an aerogel (after lyophilization) and use it to remove Hg in ultrapure (MQ) and natural waters (tap, river and sea water). Starting at a concentration of Hg 50 µg L^{-1}, which matches to the maximum permissible wastewaters discharges values for Hg, 10 mg L^{-1} of the material was able to reduce the level of this contaminant down to 1.3 µg L^{-1} in MQ, and 9.5 µg L^{-1} in tap water. The equilibrium was achieved after 2 h for MQ water and after 4 h for tap water. However, for river and sea water, the GO-CH nanocomposite was not efficient in removing Hg. It was confirmed that the higher concentration of Cl^- in aqueous medium can lead to the formation of chloro-complexes with reduced affinity to GO-CH. Nevertheless, GO-CH shows a good potential as sorbent for mercury in MQ and tap water, and the insights revealed in this study for the remaining water matrices should be considered for future rational design of nanocomposite materials for natural water remediation.

3.7 References

[1] M. Lahsen, R. Sanchez-rodriguez, P. R. Lankao, P. Dube, R. Leemans, O. Gaffney, M. Mirza, P. Pinho, B. Osman-elasha, M.S. Smith, Impacts, adaptation and vulnerability to global environmental change: challenges and pathways for an action-oriented research agenda for middle-income and low-income countries, Curr. Opin. Environ. Sustain. 2 (2010) 364–374. doi:10.1016/j.cosust.2010.10.009.

[2] J. Lubchenco, Entering the Century of the Environment: A New Social Contract for Science, Science (80). 279 (2004) 1–16. doi:10.1126/science.279.5350.491.

[3] S. Chowdhury, M. A. J. Mazumder, O. Al-Attas, T. Husain, Heavy metals in drinking water: Occurrences, implications, and future needs in developing countries, Sci. Total Environ. 569–570 (2016) 476–488. doi:10.1016/j.scitotenv.2016.06.166.

[4] L. Therese, L. Casteleyn, Science of the total environment mercury pollution in modern times and its socio-medical consequences, Sci. Total Environ. 654 (2019) 720–734. doi:10.1016/j.scitotenv.2018.10.408.

[5] C. T. Driscoll, R. P. Mason, H. M. Chan, D. J. Jacob, N. Pirrone, Mercury as a global pollutant: Sources, pathways, and effects, (2013).

[6] P. Govind, S. Madhuri, Heavy metals causing toxicity in animals and fishes, (2014).

[7] G. Bjørklund, M. Dadar, J. Mutter, J. Aaseth, The toxicology of mercury: Current research and emerging trends, Environ. Res. 159 (2017) 545–554. doi:10.1016/j.envres.2017.08.051.

[8] European Environment Agency, Mercury in Europe's environment, Copenhagen, 2018. doi:10.2800/558803.

[9] A. S. Adeleye, J. R. Conway, K. Garner, Y. Huang, Y. Su, A. A. Keller, Engineered nanomaterials for water treatment and remediation: Costs , benefits , and applicability, 286 (2016) 640–662. doi:10.1016/j.cej.2015.10.105.

[10] X. Qu, P. J. J. Alvarez, Q. Li, Applications of nanotechnology in water and wastewater treatment, Water Res. 47 (2013) 3931–3946. doi:10.1016/j.watres.2012.09.058.

[11] I. Anastopoulos, A. Robalds, H. N. Tran, D. Mitrogiannis, D. A. Giannakoudakis, A. Hosseini-Bandegharaei, G. L. Dotto, Removal of heavy metals by leaves-derived biosorbents, Environ. Chem. Lett. 17 (2019) 755–766. doi:10.1007/s10311-018-00829-x.

[12] I. Anastopoulos, I. Pashalidis, A. Hosseini-Bandegharaei, D.A. Giannakoudakis, A. Robalds, M. Usman, L. B. Escudero, Y. Zhou, J. C. Colmenares, A. Núñez-Delgado, É. C. Lima, Agricultural biomass/waste as adsorbents for toxic metal decontamination of aqueous solutions, J. Mol. Liq. 295 (2019) 111684. doi:10.1016/j.molliq.2019.111684.

[13] E. Fabre, C. B. Lopes, C. Vale, E. Pereira, C. M. Silva, Valuation of banana peels as an effective biosorbent for mercury removal under low environmental concentrations, Sci. Total Environ. 709 (2020) 135883. doi:10.1016/j.scitotenv.2019.135883.

[14] S. I. Siddiqui, S. A. Chaudhry, A review on graphene oxide and its composites preparation and their use for the removal of As^{3+} and As^{5+} from water under the effect of various parameters: Application of isotherm, kinetic and thermodynamics, Process Saf. Environ. Prot. 119 (2018) 138–163. doi:10.1016/j.psep.2018.07.020.

[15] J. Xu, Z. Cao, Y. Zhang, Z. Yuan, Z. Lou, X. Xu, X. Wang, Chemosphere A review of functionalized carbon nanotubes and graphene for heavy metal adsorption from water: Preparation, application, and mechanism, Chemosphere. 195 (2018) 351–364. doi:10.1016/j.chemosphere.2017.12.061.

[16] K. Yang, J. Wang, X. Chen, Q. Zhao, A. Ghaffar, B. Chen, Application of graphene-based materials in water purification: from the nanoscale to specific devices, Environ. Sci. Nano. 5 (2018) 1264–1297. doi:10.1039/C8EN00194D.

[17] Z. Niu, L. Liu, L. Zhang, X. Chen, Porous Graphene Materials for Water Remediation, (2014) 3434–3441. doi:10.1002/smll.201400128.

[18] N. Yousefi, X. Lu, M. Elimelech, N. Tufenkji, Environmental performance of graphene-based 3D macrostructures, Nat. Nanotechnol. (n.d.). doi:10.1038/s41565-018-0325-6.

[19] G. Goncalves, P. A. A. P. Marques, C. M. Granadeiro, H. I. S. Nogueira, M. K. Singh, J. Gr, Surface Modification of Graphene Nanosheets with Gold

Nanoparticles: The Role of Oxygen Moieties at Graphene Surface on Gold Nucleation and Growth, (2009) 4796–4802. doi:10.1021/cm901052s.

[20] D. R. Dreyer, S. Park, W. Bielawski, R. S. Ruoff, The chemistry of graphene oxide, (2010). doi:10.1039/b917103g.

[21] J. Shao, W. Lv, Q. Yang, Self-Assembly of Graphene Oxide at Interfaces, (2014) 5586–5612. doi:10.1002/adma.201400267.

[22] B. Henriques, G. Gonçalves, N. Emami, E. Pereira, M. Vila, P. A .A. P. Marques, Optimized graphene oxide foam with enhanced performance and high selectivity for mercury removal from water, J. Hazard. Mater. 301 (2016) 453–461. doi:10.1016/j.jhazmat.2015.09.028.

[23] Y. Li, L. Yang, X. Zhu, J. Hu, H. Liu, Post-synthesis modification of porous organic polymers with amine: a task-specific microenvironment for CO_2 capture, Int. J. Coal Sci. Technol. 4 (2017) 50–59. doi:10.1007/s40789-016-0148-8.

[24] Q. Zhang, Q. Hou, G. Huang, Q. Fan, Removal of heavy metals in aquatic environment by graphene oxide composites: a review, Environ. Sci. Pollut. Res. 27 (2020) 190–209. doi:10.1007/s11356-019-06683-w.

[25] H. Hadi Najafabadi, M. Irani, L. Roshanfekr Rad, A. Heydari Haratameh, I. Haririan, Removal of Cu^{2+}, Pb^{2+} and Cr^{6+} from aqueous solutions using a chitosan/graphene oxide composite nanofibrous adsorbent, RSC Adv. 5 (2015) 16532–16539. doi:10.1039/c5ra01500f.

[26] H. Ge, Z. Ma, Microwave preparation of triethylenetetramine modified graphene oxide/chitosan composite for adsorption of Cr(VI), Carbohydr. Polym. 131 (2015) 280–287. doi:10.1016/j.carbpol.2015.06.025.

[27] L. Zhang, H. Luo, P. Liu, W. Fang, J. Geng, A novel modified graphene oxide/chitosan composite used as an adsorbent for Cr(VI) in aqueous solutions, Int. J. Biol. Macromol. 87 (2016) 586–596. doi:10.1016/j.ijbiomac.2016.03.027.

[28] Y. Cai, C. Wu, Z. Liu, L. Zhang, L. Chen, J. Wang, X. Wang, S. Yang, S. Wang, Fabrication of a phosphorylated graphene oxide-chitosan composite for highly effective and selective capture of U(VI), 2017. doi:10.1039/c7en00412e.

[29] Ş. Parlayıcı, A. Avcı, E. Pehlivan, Fabrication of novel chitosan-humic acid-graphene oxide composite to improve adsorption properties for Cr(VI), Arab. J. Geosci. 12 (2019). doi:10.1007/s12517-019-4828-8.

[30] B. Zhang, R. Hu, D. Sun, T. Wu, Y. Li, Fabrication of chitosan/magnetite-graphene oxide composites as a novel bioadsorbent for adsorption and detoxification of Cr(VI) from aqueous solution, Sci. Rep. 8 (2018) 1–12. doi:10.1038/s41598-018-33925-7.

[31] L. L. Yunqiang Chen, Libin Chen, Hua Bai, Graphene oxide–chitosan composite hydrogels as broad-spectrum adsorbents for water purification, J. Mater. Chem. A. 1 (2013) 1992–2001. doi:10.1039/c2ta00406b.

[32] A. Shahzad, W. Miran, K. Rasool, M. Nawaz, J. Jang, S.-R. Lim, D.S. Lee, Heavy metals removal by EDTA-functionalized chitosan graphene oxide nanocomposites, RSC Adv. 7 (2017) 9764–9771. doi:10.1039/C6RA28406J.

[33] Y. Yang, W. Q. Wu, H. H. Zhou, Z. Y. Huang, T. T. Ye, R. Liu, Y. F. Kuang, Adsorption behavior of cross-linked chitosan modified by graphene oxide for Cu(II) removal, J. Cent. South Univ. 21 (2014) 2826–2831. doi:10.1007/s11771-014-2246-3.

[34] H. Yan, H. Yang, A. Li, R. Cheng, pH-tunable surface charge of chitosan / graphene oxide composite adsorbent for efficient removal of multiple pollutants from water, 284 (2016) 1397–1405. doi:10.1016/j.cej.2015.06.030.

[35] S. Satapathi, Graphene-based 3D xerogel as adsorbent for removal of heavy metal ions from industrial wastewater purnendu, J. Renew. Mater. 5 (2017) 96–102. doi:10.7569/JRM.2016.634134.

[36] P. Sharma, A.K. Singh, V.K. Shahi, Selective Adsorption of Pb(II) from Aqueous Medium by Cross-Linked Chitosan-Functionalized Graphene Oxide Adsorbent, 2019. doi:10.1021/acssuschemeng.8b05138.

[37] L. T. M. Thy, N.H. Thuong, T. H. Tu, H. M. Nam, N. H. Hieu, M.T. Phong, Synthesis of magnetic iron oxide/graphene oxide nanocomposites for removal of cadmium ions from water, Adv. Nat. Sci. Nanosci. Nanotechnol. 10 (2019). doi:10.1088/2043-6254/ab1b79.

[38] A. I. A. Sherlala, A. A. A. Raman, M. M. Bello, A. Buthiyappan, Adsorption of arsenic using chitosan magnetic graphene oxide nanocomposite, J. Environ. Manage. 246 (2019) 547–556. doi:10.1016/j.jenvman.2019.05.117.

[39] L. Liu, C. Li, C. Bao, Q. Jia, P. Xiao, X. Liu, Q. Zhang, Preparation and characterization of chitosan/graphene oxide composites for the adsorption of Au(III) and Pd(II), Talanta. 93 (2012) 350–357. doi:10.1016/j.talanta.2012.02.051.

[40] G. Z. Kyzas, N. A. Travlou, E. A. Deliyanni, The role of chitosan as nanofiller of graphite oxide for the removal of toxic mercury ions, Colloids Surfaces B Biointerfaces. 113 (2014) 467–476. doi:10.1016/j.colsurfb.2013.07.055.

[41] C. Qi, L. Zhao, Y. Lin, D. Wu, Journal of Colloid and Interface Science Graphene oxide / chitosan sponge as a novel filtering material for the removal of dye from water, 517 (2018) 18–27. doi:10.1016/j.jcis.2018.01.089.

[42] Commission regulation, Directive 84/156/EEC (1984). Council Directive 84/156/EEC of 8 March 1984 on limit values and quality objectives for mercury discharges by sectors other than the chlor- alkali electrolysis industry, Off. J. Eur. Communities. 74 (1984) 29.

[43] C. B. Lopes, P. Figueira, D. S. Tavares, Z. Lin, A. L. Daniel-da-Silva, A. C. Duarte, J. Rocha, T. Trindade, E. Pereira, Core-shell magnetite-silica dithiocarbamate-derivatised particles achieve the Water Framework Directive quality criteria for mercury in surface waters, Environ. Sci. Pollut. Res. 20 (2013). doi:10.1007/s11356-013-1615-z.

[44] C. B. Lopes, J. R. Oliveira, L. S. Rocha, D. S. Tavares, C. M. Silva, S. P. Silva, N. Hartog, A. C. Duarte, E. Pereira, Cork stoppers as an effective sorbent for water treatment: the removal of mercury at environmentally relevant concentrations and conditions, Environ. Sci. Pollut. Res. Int. 21 (2014) 2108–21. doi:10.1007/s11356-013-2104-0.

[45] Council of the European Union, E. Parliament, Directive 2013/39/EU of the European Parliament and of the Council of 12 August 2013 amending Directives 2000/60/EC and 2008/105/EC as regards priority substances in the field of water policy, Official Journal of the European Union, 2013.

[46] M.I. El-Khaiary, G. F. Malash, Common data analysis errors in batch adsorption studies, Hydrometallurgy. 105 (2011) 314–320. doi:DOI 10.1016/j.hydromet.2010.11.005.

[47] S. Lagergren, About the theory of so-called adsorption of soluble substances, K. Sven Veten Hand. 24 (1898) 1–39.

[48] Y. S. Ho, G. McKay, Pseudo-second order model for sorption processes, Process Biochem. 34 (1999) 451–465. doi:Doi 10.1016/S0032-9592(98)00112-5.

[49] M. J. D. Low, Kinetics of Chemisorption of Gases on Solids, Chem. Rev. 60 (1960) 267–312. doi:Doi 10.1021/Cr60205a003.

[50] G. E. Boyd, A. W. Adamson, L. S. Myers, The Exchange Adsorption of Ions from Aqueous Solutions by Organic Zeolites .2., J. Am. Chem. Soc. 69 (1947) 2836–2848. doi:Doi 10.1021/Ja01203a066.

[51] W. J. Weber, J. C. Morris, Kinetics of adsorption on carbon from solution, Kinet. Adsorpt. Carbon from Solut. (1963).

[52] N. A. Travlou, G. Z. Kyzas, N. K. Lazaridis, E. A. Deliyanni, Graphite oxide/chitosan composite for reactive dye removal, Chem. Eng. J. 217 (2013) 256–265. doi:10.1016/j.cej.2012.12.008.

[53] L. Fan, C. Luo, X. Li, F. Lu, H. Qiu, M. Sun, Fabrication of novel magnetic chitosan grafted with graphene oxide to enhance adsorption properties for methyl blue, J. Hazard. Mater. 215–216 (2012) 272–279. doi:10.1016/j.jhazmat.2012.02.068.

[54] N. K. Lazaridis, G. Z. Kyzas, A. A. Vassiliou, D. N. Bikiaris, Chitosan derivatives as biosorbents for basic dyes, Langmuir. 23 (2007) 7634–7643. doi:10.1021/la700423j.

[55] Council of the European Union, Council Directive 98/83/EC of 3 November 1998 on the quality of water intended for human consumption., 1998.

[56] Decree-Law No. 236/98, Decree-Law No. 236/98 of the Portuguese Ministry of the Environment of 1 August establishing water quality standards, Diário da República : I Série, 1998.

[57] N .K. Gupta, A. Gupta, 2D and 3D carbon-based adsorbents for an efficient removal of HgII ions: A review, FlatChem. 11 (2018) 1–14. doi:10.1016/J.FLATC.2018.11.002.

[58] B. Yan, Z. Hiew, L. Yee, X. Jiat, S. Thangalazhy-gopakumar, S. Gan, S. Shee, G. Pan, T.C. Yang, Review on synthesis of 3D graphene-based configurations and their adsorption performance for hazardous water pollutants, Process Saf. Environ. Prot. 116 (2018) 262–286. doi:10.1016/j.psep.2018.02.010.

[59] H. Qiu, L. Lv, B. Pan, Q. Zhang, W. Zhang, Q. Zhang, Critical review in adsorption kinetic models, J. Zhejiang Univ. Sci. A. 10 (2009) 716–724. doi:10.1631/jzus.A0820524.

[60] G. F. Malash, M. I. El-Khaiary, Piecewise linear regression: A statistical method for the analysis of experimental adsorption data by the intraparticle-diffusion models, Chem. Eng. J. 163 (2010) 256–263. doi:http://dx.doi.org/10.1016/j.cej.2010.07.059.

[61] C. W. Cheung, J. F. Porter, G. McKay, Sorption kinetics for the removal of copper and zinc from effluents using bone char, Sep. Purif. Technol. 19 (2000) 55–64. doi:http://dx.doi.org/10.1016/S1383-5866(99)00073-8.

[62] L. S. Rocha, C. B. Lopes, J. A. Borges, A. C. Duarte, E. Pereira, Valuation of Unmodified Rice Husk Waste as an Eco-Friendly Sorbent to Remove Mercury: A Study Using Environmental Realistic Concentrations, Water. Air. Soil Pollut. 224 (2013). doi:10.1007/s11270-013-1599-9.

[63] P. M. Pakdel, S.J. Peighambardoust, Review on recent progress in chitosan-based hydrogels for wastewater treatment application, Carbohydr. Polym. 201 (2018) 264–279. doi:10.1016/j.carbpol.2018.08.070.

[64] H. Guo, T. Jiao, Q. Zhang, W. Guo, Q. Peng, X. Yan, Preparation of Graphene Oxide-Based Hydrogels as Efficient Dye Adsorbents for Wastewater Treatment, Nanoscale Res. Lett. (2015) 0–9. doi:10.1186/s11671-015-0931-2.

[65] Z. Sui, Y. Cui, J. Zhu, B. Han, Preparation of Three-Dimensional Graphene Oxide – Polyethylenimine Porous Materials as Dye and Gas Adsorbents, 5 (2013) 9172–9179. doi:10.1021/am402661t.

[66] J. Geng, Y. Yin, Q. Liang, Z. Zhu, H. Luo, Polyethyleneimine cross-linked graphene oxide for removing hazardous hexavalent chromium: Adsorption performance and mechanism, Chem. Eng. J. (2018) 0–1. doi:10.1016/j.cej.2018.10.141.

[67] P. L. Yap, S. Kabiri, D. N. H. Tran, Multifunctional binding chemistry on modified graphene composite for selective and highly efficient adsorption of mercury, Appl. Mater. Interfaces. (2018). doi:10.1021/acsami.8b17131.

[68] L. Dambies, C. Guimon, S. Yiacoumi, E. Guibal, Characterization of metal ion interactions with chitosan by X-ray photoelectron spectroscopy, Colloids Surfaces A. 177 (2001) 203–214.

[69] F. S. Awad, K. M. Abouzeid, W. M. A. El-maaty, A.M. El-wakil, Efficient Removal of Heavy Metals from Polluted Water with High Selectivity for Mercury (II) by 2-Imino-4-Thiobiuret Partially Reduced Graphene Oxide (IT-PRGO), ACS Appl. Mater. Interfaces. 9 (2017) 34230−34242. doi:10.1021/acsami.7b10021.

[70] E. Sasmaz, A. Kirchofer, A.D. Jew, A. Saha, D. Abram, T.F. Jaramillo, J. Wilcox, Mercury chemistry on brominated activated carbon, Fuel. 99 (2012) 188–196. doi:10.1016/j.fuel.2012.04.036.

3.8 A.1 Supplementary material of chapter 3

BET analysis of GO-CH aerogel

The result for the specific surface area (S_{BET}) of the GO-CH aerogel was very low (9.06 m^2 g^{-1}, with a pore volume of 0.016 cm^3 g^{-1}). This is not uncommon, as the S_{BET} of graphene-based aerogels is normally substantially lower than the expected value for the single-sheet graphene (~2600 m^2 g^{-1}) [1]. The determination of S_{BET} for GO-based aerogels is generally quite challenging and is normally largely underestimated. The possible overlapping of graphene sheets, high degree of oxidation and the presence of water molecules at the surface may difficult the access of N_2 molecules, thus triggering such low S_{BET} values.[2] In a previous study of GO aerogels, we observed H3-type hysteresis loop, which can be assigned to the presence of plate-like particle aggregates and slit-shaped pores. The plateau was not reached even in saturation conditions, which can be a result of unrestricted multilayer adsorption in large mesopores and macropores, which can ultimately hinder a accurate estimation of the real pore volume.[3]

Tables

Table S3.2 Sorption reaction kinetic models.

Kinetic model	Equation	References
Pseudo-first-order (Lagergren)	$q_t = q_e(1-e^{-k_1 t})$	[4]
Adsorption capacity Pseudo-second-order (Ho)	$q_t = \frac{q_e^2 k_2 t}{1+q_e k_2 t}$	[5]
Elovich	$q_t = \frac{1}{\beta}\ln(1+\alpha\beta t)$	[6]

q_t is the amount of metal sorbed per gram of at time t (μmol g^{-1}), q_e amount of metal adsorbed per gram of materials at equilibrium (μmol g^{-1}), k_1 rate constant of pseudo-first order (h^{-1}), k_2 rate constant of pseudo-second order (g μmol^{-1} h^{-1}), α initial sorption rate (μmol g^{-1} h^{-1}), β desorption constant (g μmol^{-1}).

In addition to the reaction models, two widely known diffusion-based models, Boyd's film-diffusion [7] and Webber's pore-diffusion [8], were used in order to analyse the sorption mechanism and the rate-controlling step involved in the sorption process.

Boyd's film-diffusion model presumes that the main resistance to diffusion is in the boundary layer surrounding the adsorbent particle[9,10] and it is expressed as:

$$F = 1 - \frac{6}{\pi^2}\sum_{n=1}^{\infty}\left(\frac{1}{n^2}\right)\exp\left(-n^2 Bt\right) \tag{4}$$

where F is the fractional attainment of equilibrium, at different times, t, and Bt is a function of F:

$$F = \frac{q_t}{q_e} \tag{5}$$

Bt can be calculated as:

For F values > 0.85 $\quad Bt = -0.4977 - \ln\left(1 - F\right)$ (6)

For F values < 0.85 $\quad Bt = \left(\sqrt{\pi} - \sqrt{\pi - \frac{\pi^2 F}{3}}\right)^2$ (7)

If the plot Bt vs t (Boyd's plot) excludes the origin, on can conclude that film diffusion or chemical reaction is the rate-controlling step. If the plot is linear and passes through the origin the intra-particle diffusion controls the rate of mass transfer.

Weber's intraparticle-diffusion model is defined by the following equation [9,10] :

$$q_t = k_i t^{1/2} \tag{8}$$

Where ki is the intraparticle-diffusion parameter (mg g^{-1} $h^{-1/2}$). If intraparticle-diffusion is the rate-limiting step, then a plot of qt vs t will give a straight line with a slope that equals ki and an intercept equal to zero. If not, some other mechanism along with intraparticle diffusion must also be involved. The analysis of the experimental data using film-diffusion and the intraparticle-diffusion models, as well as the prediction of the diffusion coefficients, was performed following the piecewise linear regression methodology (PLR) proposed by Malash *et al.* [9] using a Microsoft® Excel™ worksheet developed by these authors.

Table S3.2 Elemental analysis of natural waters before and after Hg removal studies by GO-CH.

Water source	**Tap**		**River** **σ = 33.1 µS/m**		**Sea** **Sal. = 34.7**	
	Initial	GOCH	Initial	GOCH	Initial	GOCH
pH	7.13	7.45	4.30	4.32	7.80	7.69
Major elements ($mg\ L^{-1}$)						
Ca	33	33	1.3	1.3	411	399
Na	8.5	8.3	5.5	4.9	> 1000	> 1000
K	1.9	1.9	0.5	0.5	> 500	> 500
Mg	2.0	2.0	0.5	0.5	> 2000	> 2000
Minor elements ($\mu\ L^{-1}$)						
B	10	7.5	4.3	4.3	5346	5340
Al	34	< 5	54	54	178	86
Cr	0.7	< 0.5	< 0.5	< 0.5	16.8	16.8
Fe	54	< 10	12	< 5	351	351
Co	< 0.1	< 0.1	< 0.1	< 0.2	< 40	< 40
Ni	< 1	< 1	< 1	< 1	< 20	< 20
Cu	2.7	< 1	< 1	< 1	< 20	< 20
Zn	76	31	7.8	5	1120	1000
As	< 2	< 2	< 2	< 2	< 100	< 100
Se	< 2	< 2	< 2	< 2	185	185
Sr	21	21	7	7	9338	9338
Cd	<0.1	<0.1	0.21	<0.1	< 40	< 40
Sb	< 0.1	< 0.1	< 0.1	< 0.1	< 2	< 2
Ba	6.1	5.3	2.3	2.0	160	158
Pb	< 0.1	< 0.1	2.2	< 0.2	< 80	< 80

3.8.1 References

[1] C. N .R. Rao, A. K. Sood, K. S. Subrahmanyam, A. Govindaraj, Graphene: The new two-dimensional nanomaterial, Angew. Chemie - Int. Ed. 48 (2009) 7752–7777. doi:10.1002/anie.200901678.

[2] M. A. Worsley, P. J. Pauzauskie, T. Y. Olson, J. Biener, J. H. Satcher, T. F. Baumann, Synthesis of graphene aerogel with high electrical conductivity, J. Am. Chem. Soc. 132 (2010) 14067–14069. doi:10.1021/ja1072299.

[3] A. Borrás, G. Gonçalves, G. Marbán, S. Sandoval, S. Pinto, P.A.A.P. Marques, J. Fraile, G. Tobias, A.M. López-Periago, C. Domingo, Preparation and Characterization of Graphene Oxide Aerogels: Exploring the Limits of Supercritical CO_2 Fabrication Methods, Chem. - A Eur. J. 24 (2018) 15903–15911. doi:10.1002/chem.201803368.

[4] S. Lagergren, About the theory of so-called adsorption of soluble substances, K. Sven Veten Hand. 24 (1898) 1–39.

[5] Y. S. Ho, G. McKay, Pseudo-second order model for sorption processes, Process Biochem. 34 (1999) 451–465. doi:Doi 10.1016/S0032-9592(98)00112-5.

[6] M. J. D. Low, Kinetics of Chemisorption of Gases on Solids, Chem. Rev. 60 (1960) 267–312. doi:Doi 10.1021/Cr60205a003.

[7] G. E. Boyd, A. W. Adamson, L. S. Myers, The Exchange Adsorption of Ions from Aqueous Solutions by Organic Zeolites .2., J. Am. Chem. Soc. 69 (1947) 2836–2848. doi:Doi 10.1021/Ja01203a066.

[8] W. J. Weber, J. C. Morris, Kinetics of adsorption on carbon from solution, Kinet. Adsorpt. Carbon from Solut. (1963).

[9] G. F. Malash, M. I. El-Khaiary, Piecewise linear regression: A statistical method for the analysis of experimental adsorption data by the intraparticle-diffusion models, Chem. Eng. J. 163 (2010) 256–263. doi:http://dx.doi.org/10.1016/j.cej.2010.07.059.

[10] Y. S. Ho, J. C. Y. Ng, G. Mckay, Kinetics of pollutant sorption by biosorbents: Review, Sep. Purif. Methods. 29 (2000) 189–232. doi:Doi 10.1081/Spm-100100009.

Chapter 4

4. General discussion

Despite results already have been discussed in each chapter of this thesis, a brief general discussion of the most relevant results is presented in this section. The points discussed below include: the role of graphene oxide in the composite materials prepared, a general comparison between the efficiency of the different materials for Hg removal from the different waters under study and finally a discussion of the potential environmental impact of these graphene-based materials, founded on work still being developed in the research group.

The physical-chemical methodologies currently available for the removal of PTEs from contaminated water, such as coagulation and flocculation, precipitation, activated carbon sorption or electrochemical techniques present several drawbacks (e.g., generation of toxic sludge requiring adequate disposal, high operating cost and low efficiency). It is therefore imperative to develop more efficient and cost-effective alternative technologies.

To achieve this goal, one of the most promising approaches followed by the research community is the development and application of new highly efficient and selective synthetic materials. Expanding nanotechnology and surprising advances in research into three-dimensional graphene macrostructures (3DGM) have been a great promise to its broad applications, notably as environmental matters. The assembly of 2D graphene in hierarchical 3D architectures has been recognized as one of the most promising strategies for "bottom-up" nanotechnology and has become one of the most active research fields of recent years. The 3D ensures mass transport, thereby improving performance, offsetting the main disadvantage of nanoparticles in practical application. Different 3DGM have been explored for water purification, mainly for sorption and degradation of organic contaminants. However, the removal of potential toxic trace metal from contaminated waters using 3DGM is still being investigated.

This work was focused on the development of a controlled preparation of 3DGM and its application for the removal of mercury from various types of contaminated water under realistic conditions.

GO nanosheets are heavily oxygenated, with hydroxyl and epoxy functional groups on the basal plane and carbonyl/carboxylic acids groups on the plane edges. These functional groups are responsible for making the GO surface highly hydrophilic, which facilitates the formation of stable aqueous colloids. This property offers the possibility of combining those oxygen-containing groups with specific functional groups of a great variety of polymers in order to promote the self-assembly into a variety of 3D macrostructures. This can be achieved via either covalent (*e.g.* nucleophilic substitution) or non-covalent (e.g. Van der Waals forces, electrostatic interaction, hydrogen bonding) bonds and can be used to adapt and improve materials. The GOPEI and GOCH hydrogels, reported respectively on Chapter 2 and 3, took benefit from this. These physically cross-linked aerogels are particularly appealing because of their simple synthesis and absence of potentially toxic chemical crosslinking agents or organic solvents. Therefore, the experimental approaches followed to prepare GOPEI and GOCH can be considered eco-friendly.

Amine rich polymers were a natural choice due to the high affinity between amine groups and the oxygen functional groups of GO, enabling this combination with a synergistic performance for sorption of several contaminants from water. For this reason, PEI and CH were selected for the preparation of GO-polymer aerogels. From the results obtained, GOPEI showed to be much more effective for Hg removal from waters than GOCH. This can be easily justified by the higher number of nitrogen groups in the hyperbranched PEI structure than in the CH polymer. Additionally, GOPEI showed the particularity of owing negative ζ potential values all over the working pH range, displaying a point of zero charge (pzc) at ~ pH 2.6, while GO-CH showed an amphoteric nature, with a pzc of 6.7, where the CH primary amines are protonated at lower pH values. These properties, together with others already discussed in the respective chapters, resulted in an excellent sorption capacity of Hg (II), using very small doses (10 mg L^{-1}) of GO-CH in ultrapure water with a removal percentage of 97 % after only two hours of contact time. In the case of tap water, the % R was 81.4% after four hours of contact time. In the case of river and seawater, the GO-CH nanocomposite showed a limited performance due the high complexity of the water

matrixes, leading to a residual removal of Hg(II). The efficiency of Hg(II) removal at equilibrium in river and seawater for GO-CH was 13% R and 7% R, respectively. Interestingly, GOPEI proved to have a high efficiency for Hg removal from natural waters (tap (91%), river (90%) and sea (81%)) also under realistic discharged concentrations (50 μg L^{-1}) and low dosage (10 mg L^{-1}), where the existence of co-ions and different Hg-speciation are usually inhibitory factors of a good removal efficiency. Given the higher potential of GOPEI to be applied under real remediation conditions, the scale-up of its production was explored. This goal was successfully accomplished using higher vessels while keeping the initial pH of the precursor solutions lower than 2. Its reproducibility towards Hg removal ability was also proved.

Figure 24 shows the comparative performance in terms of %R of the new graphene-based materials with the respective equilibrium time in MQ water, alongside activated carbon (Act-C), under the same experimental conditions.

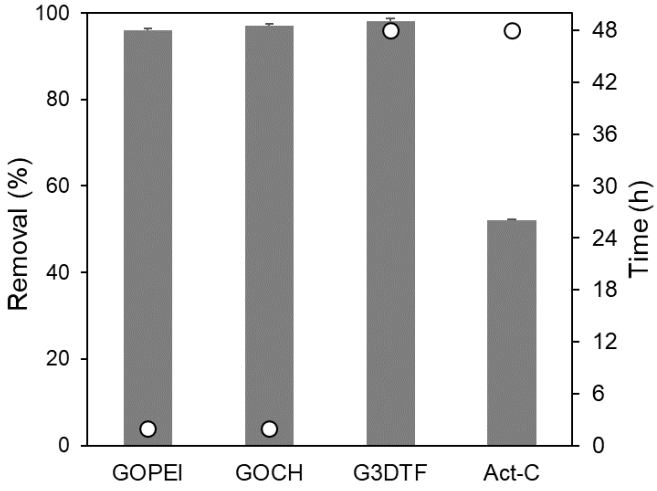

Figure 24 Efficiency of GOPEI, GOCH, G3DTF and Act-C in the removal of Hg from contaminated MQ: (bars) percentage of Hg removed at equilibrium and (circles) time for equilibrium. The original concentration of Hg was 50 μg L-1; the amount of material used was 10 m L^{-1}. The results are a mean value of 2 replicates.

Moreover, and not less important, is to test whether the water treated with these graphene-based materials is effectively acceptable to be released in the aquatic medium (river, basin, sea). That is, if the developed new materials, despite its highly efficient Hg removal, do not release into the water, elements that may, at some level of, present environmental toxicity. Due to their unique chemical and nanotoxicological properties,

nanomaterials have been worldwide used in different fields, constituting potential threats to the environment. Having in mind these considerations, the comparative evaluation of the GO-based nanocomposites was performed taken in consideration the ecological risks and the remediation performance.

Therefore, in parallel with the work performed in this Thesis and in the scope of other PhD student program, the environmental risks related to the application of GOPEI (selected due to its good performance for Hg removal in seawater and also due to the time schedule of the experimental work realized) was evaluated. The safety of GOPEI was explored through the oxidative stress, metabolic and histopathological alterations in mussels exposed to GOPEI remediated seawater, after contamination with Hg [1]. The study evaluated the impacts of such potential stressors, on benthic species, which can be a good model as they are affected by several environmental constraints. Particularly, the mussel *Mytilus galloprovincialis* has been identified by several authors as a bioindicator that responds quickly to environmental disturbances, with a wide spatial distribution and economic relevance. Thus, the impacts caused in *M. galloprovincialis* by seawater previously contaminated by Hg and decontaminated using GOPEI was evaluated. For this, histopathological and biochemical alterations were examined. This study demonstrated that mussels exposed to the contaminant (Hg), the decontaminant (GOPEI) and the combination of both (Hg + GOPEI) presented an increment of histopathological, oxidative stress and metabolic alterations when compared to organisms exposed to remediated seawater and control conditions. The present findings highlight the possibility to remediate seawater with GO-based materials for environmental safety purposes. In other study, the alterations of clam species *Ruditapes philippinarum,* were also assessed, when exposed to GOPEI remediated seawater to actual and predicted increased temperature conditions due to the global warming [2]. The results obtained demonstrated that seawater contaminated with Hg and/or Hg+GOPEI induced higher toxicity in clams exposed to 17 and 22 ºC compared to organisms exposed to remediated seawater at the same temperatures. Moreover, similar histological and biochemical results were observed between organisms exposed to control and remediated seawater, independently of the temperatures (17 and 21 ºC), highlighting the potential use of GOPEI to remediate Hg from seawater without significant toxicity issues to the selected marine species.

4.1 References

[1] F. Coppola, A. Bessa, B. Henriques, T. Russo, A. M. V. M. Soares, E. Figueira, P. A. A. P. Marques, G. Polese, A. Di Cosmo, E. Pereira, R. Freitas, Oxidative stress, metabolic and histopathological alterations in mussels exposed to remediated seawater by GO-PEI after contamination with mercury, Comp. Biochem. Physiol. -Part A Mol. Integr. Physiol. 243 (2020) 110674. doi:10.1016/j.cbpa.2020.110674.

[2] F. Coppola, A. Bessa, B. Henriques, T. Russo, A. M. V. M. Soares, E. Figueira, E. Pereira, P. Marques, G. Polese, R. Freitas, The role of temperature on the impact of remediated water towards marine organisms, Water (Switzerland). 12 (2020) 2148. doi:10.3390/W12082148.